AN ABSTRACT OF THE DISSERTATION OF

Ricardo A. González Pinzón for the degree of Doctor of Philosophy in Water Resources Engineering presented on May 31, 2013.

Title: Integrating Solute Transport, Metabolism and Processing in Stream Ecosystems.

Abstract approved:

Roy D. Haggerty

After three decades of active research coupling hydrology and stream ecology, the connection among solute transport, metabolism and processing is still unresolved. These knowledge gaps obscure the functioning of stream ecosystems and how those ecosystems interact with other landscape processes. We must resolve these challenges to wisely manage water resources, because there is a need to understand controls on stream ecosystems at local, regional and continental scales, and because we need to predict in-stream biogeochemical processes in environments and conditions that do not have supporting data. More robust methods are required to deconvolve signal imprints of solute transport, metabolism and processing, thus allowing the development and implementation of improved decision-making approaches for stream management.

Recognizing that uncertainty and equifinality are ubiquitous issues in hydrologic problems, this dissertation focuses on the development of parsimonious methods to couple solute transport, metabolism and processing in stream ecosystems. These methods consist of scaling and predicting relationships for solute transport, efficient modeling frameworks to estimate processing rates in streams, and the use of the smart tracer resazurin to estimate stream metabolism at different spatial scales. This dissertation is the

result of lab and field experiments, meta-analyses, and mathematical, statistical and computational modeling.

The most significant contributions of this dissertation to the hydrological and biogeosciences are: (1) there are scaling relationships in stream solute transport. We found that the coefficient of skewness (CSK) of conservative tracer breakthrough curves is statistically constant over time and this result can be used to predict solute transport. (2) The CSK of all commonly used solute transport models decreases over time. This shows that current theory is inconsistent with experimental data and suggests that a revised theory of solute transport is needed. (3) Simple algebraic relationships can be used to estimate processing rates in streams. This eliminates the need to calibrate highly uncertain (and intermediate) parameters. (4) Under some common stream transport conditions dispersion does not play an important role in the estimation of processing rates and, therefore, can be neglected. Under such conditions, no computer modeling is needed to estimate processing rates. (5) Even if the reactions of target and proxy tracers happen in exactly the same locations at rates that are linearly proportional, the exact relationship between the two volume-averaged rates can be nonlinear and a function of transport conditions. However, the uncertainty in the estimation of the target processing rate is linearly proportional to the proxy-tracer processing rate. (6) The transformation of resazurin is nearly perfectly, positively correlated with aerobic microbial respiration. Therefore, resazurin can be used as a surrogate to measure respiration *in situ* and *in vivo* at different spatial scales (this is an extension of (5)). (7) Community respiration rates in streams may not need to be “corrected” for temperature between daytime and nighttime, because even when photosynthetically active radiation and stream water temperature are different, respiration rates might not be different across nighttime and daytime conditions.

Integrating Solute Transport, Metabolism and Processing in Stream Ecosystems

by

Ricardo A. González Pinzón

A DISSERTATION

submitted to

Oregon State University

in partial fulfillment of

the requirements for the

degree of

Doctor of Philosophy

Presented May 31, 2013

Commencement June 2013

Doctor of Philosophy dissertation of Ricardo A. González Pinzón presented on May 31, 2013.

APPROVED:

Major Professor, representing Water Resources Engineering

Director of the Water Resources Graduate Program

Dean of the Graduate School

I understand that my dissertation will become part of the permanent collection of Oregon State University libraries. My signature below authorizes release of my dissertation to any reader upon request.

Ricardo A. González Pinzón, Author

ACKNOWLEDGMENTS

The pursuit of my doctoral degree and the completion of this dissertation would not have been possible without the support of many people and institutions. I want to especially thank my wife, Paula, and my daughter, Silvia, for their continuous support.

My Ph.D. marathon actually started with the support of the U.S. Department of State, Education USA's Opportunity Grant program, administered by the Centro Colombo Americano in Bogotá, Colombia. I am particularly thankful to Omayra Marroquín and Doris Fonseca.

I am infinitely thankful to my advisor, Roy Haggerty, who always helped me go smoothly through the Ph.D. program, and made sure I was enjoying life outside of graduate school. He encouraged me to attend national and international conferences to present my research with high-quality standards and to develop my own academic and professional network. Roy supported my applications for external research funds, and advised me with his expertise as grant reviewer. He always supported my external research projects and that gave me the unique opportunity to conduct lab and field work in Wyoming, Oregon, Pennsylvania, Virginia and Spain. These were life changing experiences for me and I will strive to offer my students these types of possibilities when I start my new job as tenure-track Assistant Professor at University of New Mexico. I thank Roy for being not only my advisor, but also my friend.

I am very thankful to my committee members for their support. Thanks to Eugènia Martí, David M. Myrold and Judson W. Harvey for their guidance during my field and lab research work. I thank my graduate council representative, Dr. Willie E. Rochefort, and Dr. Brian D. Wood for their generous service.

I want to thank all of my collaborators for their advice on academic, professional and personal issues: Dr. Alba Argerich (Oregon St. Univ.); Dr. Kamini Singha (Colorado School of Mines.); Dr. Sherri L. Johnson (Oregon St. Univ.); Dr. Laura Lautz (Syracuse Univ.); Dr. Laurel Larsen (Univ. of California – Berkeley); Dr. Christine Hatch (Univ. Massachusetts – Amherst); Jennifer Drummond (Northwestern University); Dr. Mike

Gooseff (Colorado St. Univ.); Dr. Olaf Cirpka (Univ. of Tübingen); Dr. Marco Dentz (Institute of Environmental Assessment and Water Research); Dr. Adam Ward (Univ. of Iowa); Dr. Aaron Packman (Northwestern Univ.); Marc Peipoch (CEAB); Dennis Lemke (Univ. of Tübingen); Dr. Jan H. Fleckenstein (UFZ- Helmholtz Centre for Environmental Research); Dr. Martin Briggs (USGS); and Dr. Jay Zarnetske (Yale Univ.).

Main funding was made available by the U.S. National Science Foundation through the research grant EAR 08-38338. Funding for work in WS01 and WS03 was provided by the HJ Andrews Experimental Forest research program, funded by the National Science Foundation’s Long-Term Ecological Research Program (DEB 08-23380), US Forest Service Pacific Northwest Research Station, and Oregon State University. Funding was also available from the Consortium of Universities for the Advancement of Hydrologic Science CUAHSI, Pathfinder Graduate Student Fellowships to Support Multi-site Research in Hydrology, and from the OSU Graduate School and the Geography program at OSU.

CONTRIBUTION OF AUTHORS

Chapter 2: Dr. Marco Dentz assisted with the analysis of the decoupled continuous time random walk and Levy-Flight models, and with editorial advice.

Chapter 4: Dr. David M. Myrold assisted with the collection and interpretation of the data. He also assisted with editorial advice.

Chapter 5: Dr. Alba Argerich assisted with the interpretation of the data and editorial advice.

Chapter 6: Marc Peipoch and Dr. Eugènia Martí assisted with the collection and interpretation of the data. Dr. Jan H. Fleckenstein assisted with the collection of data. All coauthors will assist with editorial advice.

TABLE OF CONTENTS

Page

1. General Introduction 2
2. Scaling and predicting solute transport processes in streams 7
   - 2.1. Introduction 8
   - 2.2. Methodology 11
     - 2.2.1. Temporal moments from time-series 11
     - 2.2.2 Experimental database 13
   - 2.3. Results and Discussion 14
     - 2.3.1. Statistical relationships derived from temporal moment analysis 14
     - 2.3.2. Observed scale-invariance in streams and solute transport models 15
     - 2.3.3. Use of moments scaling properties to predict solute transport 22
     - 2.3.4. Implications for scale-invariant patterns 27
   - 2.4. Conclusions 29
   - APPENDICES 40
   - References 48
3. An efficient method to estimate processing rates in streams 55
   - 3.1. Introduction 56
   - 3.2. Processing Rates in Streams 57
   - 3.3. Relationship between Processing Rates of Two Solutes 59
   - 3.4. Conclusions 63
   - References 65
4. Measuring aerobic respiration in stream ecosystems using the resazurin-resorufin system 67
   - 4.1. Introduction 68
   - 4.2. Materials and Methods 71
     - 4.2.1 Pure culture experiments: 71

TABLE OF CONTENTS (continued)

Page

4.3. Results and Discussion 76
4.3.1 CO_2 production and cell growth in pure culture experiments 76
4.3.2 Raz transformation and DO consumption 77
4.3.3 Implications of hydrologic processes on field-scale use of Raz for measuring respiration 78
4.4. Conclusions 81
References 89
5. Quantifying spatial differences in metabolism in headwater streams 93
5.1. Introduction 94
5.2. Estimating Rates and Fluxes of Metabolism from the Transformation of Raz 97
5.2.1. Estimating rates of respiration 98
5.2.2. Estimating rates of reaeration and primary production 99
5.2.3. Estimating fluxes of metabolism 101
5.2.4. Estimating oxygen longitudinal profiles 102
5.3. Methodology 103
5.3.1. Research sites 103
5.3.2. Stream tracer injections and solute transport modeling 104
5.3.3. Calibration of the molar processing ratio $\boldsymbol{K}_{DO}^{Raz}$ at the field sites 105
5.3.4. Two-station diel technique to estimate stream metabolism 105
5.4. Results 106
5.4.1. Stream solute transport 106
5.4.2. Stream metabolism from the transformation of Raz 106
5.5. Discussion 107
5.5.1. Spatial variability of respiration rates 107
5.5.2. Reaeration and primary production rates 108
5.5.3. Oxygen profiles 108
5.5.4. Comparing stream metabolism estimates 109

TABLE OF CONTENTS (continued)

Page

5.6. Conclusions 110

References 119

6. Diel fluctuations of respiration in a headwater stream 124

6.1. Introduction 125

6.2. Methodology 127

6.2.1. Study Sites 127

6.2.2. PAR and Stream Temperature Records 128

6.2.3. Stream Tracer Experiments 128

6.2.4. Estimating Respiration Rates with Raz 129

6.2.5. Raz and DO Uptake Relationships in Stream Sediments 130

6.3. Results and discussion 130

6.3.1. Differences in Incoming PAR between Open and Shaded Reaches 130

6.3.2. Differences in Night and Day Time Stream Water Temperatures 131

6.3.3. Raz and DO Uptake Rates as a Function of Stream Bedforms 131

6.3.4. Differences in Respiration Rates 132

References 140

7. General conclusions 142

LIST OF FIGURES

Figure Page

2.1. Meta-analysis (n=384 BTCs) of conservative solute transport experiments in streams demonstrates the general occurrence of non-Fickian dispersion processes. (a) The growth rate of the variance is non-linear (therefore non-Fickian) with respect to the mean travel time; the thick dashed line represents the slope pattern of Fickian dispersion. (b) Skewness as a function of the mean travel time. Coefficients were fitted with 95% confidence bounds. Thin dashed lines represent 95% prediction bounds ………………………………………………………………………. 34

2.2. a) Meta-analysis (n=384 BTCs) of conservative solute transport experiments from contrasting stream ecosystems suggests that the coefficient of skewness holds statistically constant. Fitted coefficients defined $CSK = 1.18 \pm 0.08$. b) The factor $[m_1 \; m_2]$ is a quasi-linear estimator of m_3. However, using m_1 to define the ratio $[m_3 / m_2]$ yields an $R^2 = 0.66$, showing that a satisfactory bottom-up estimation of normalized central moments is restricted to one level, at most. Coefficients were fitted with 95% confidence bounds. Thin dashed lines represent 95% prediction bounds ……………………………………………………………………………….. 35

2.3. Predicted results using empirical relationships derived from normalized central moment meta-analysis (n=384 BTCs) and the moment matching technique for the TSM. The known variables were L, Q and $m_{1\,est.}$, and all others were predicted from 1000 Monte Carlo simulations. The effects of uncertainty in estimating m_1 (i.e., $m_{1\,est.} = \phi m_{1\,obs.}$, with $\phi = [0.8 - 1.2]$), the parameters of the TSM and the fitting coefficients from our meta-analysis are shown as uncertainty bounds. a) River Brock, b) River Conder, c) River Dunsop, d) River Ou Beck. Experimental observations from *Young and Wallis* [1993]. The best parameter sets from the simulations are presented in Table 2.3. Goodness of fit was estimated with the Nash–Sutcliffe model efficiency coefficient (E) ………………………….................... 36

2.4. Predicted results using empirical relationships derived from normalized central moment meta-analysis (n=384 BTCs) and the moment matching technique for the ADZM. The known variable was m_1 (or $\bar{t}$), and τ_{ADZ} was predicted from 1000 Monte Carlo simulations. The effects of uncertainty in m_1 (i.e., $m_{1\,est.} = \phi m_{1\,obs.}$, with $\phi = [0.8 - 1.2]$) and the fitting coefficients from our meta-analysis are shown as uncertainty bounds. a) River Brock, b) River Conder, c) River Dunsop, d) River Ou Beck. Experimental observations from *Young and Wallis* [1993]. The best parameter sets from the simulations are presented in Table 2.3. Goodness of fit was estimated with the Nash–Sutcliffe model efficiency coefficient (E)……………… 37

LIST OF FIGURES (continued)

Figure Page

2.5. Predicted results using empirical relationships derived from normalized central moment meta-analysis (n=384 BTCs) and the Gumbel distribution, which has a constant $CSK_{Gumbel} = 1.1395$. Uncertainty bounds represent 1000 Monte Carlo simulations where $m_{1\,est.} = \phi\, m_{1\,obs.}$, with $\phi = [0.8 - 1.2]$, and $m_{2\,est.} = \left(m_{1\,est.}\right)^{\theta}$, with $\theta = [1.601 - 1.629]$. The "Gumbel=f(Obs.)" simulation uses the actual m_1 and m_2 moments derived from the observed data. a) River Brock, b) River Conder, c) River Dunsop, d) River Ou Beck. Experimental observations from *Young and Wallis* [1993]. Goodness of fit was estimated with the Nash–Sutcliffe model efficiency coefficient (E)………………………………………………………………….. 38

2.6. Predicted results using empirical relationships derived from normalized central moment meta-analysis (n=384 BTCs) and the log-normal distribution. Uncertainty bounds represent 1000 Monte Carlo simulations where $m_{1\,est.} = \phi\, m_{1\,obs.}$, with $\phi = [0.8 - 1.2]$, and $m_{2\,est.} = \left(m_{1\,est.}\right)^{\theta}$, with $\theta = [1.601 - 1.629]$. The "L-N=f(Obs.)" simulation uses the actual m_1 and m_2 moments derived from the observed data. a) River Brock, b) River Conder, c) River Dunsop, d) River Ou Beck. Experimental observations from *Young and Wallis* [1993]. Goodness of fit was estimated with the Nash–Sutcliffe model efficiency coefficient (E)…………………........................... 39

3.1. The scaling factor ω to estimate processing rates of a target solute ($\lambda_{\theta,\,sz}^{\text{target}}$) from a proxy-tracer ($\lambda_{\theta,\,sz}^{\text{proxy}}$) is a function of the molar uptake ratio $K_{\text{target}}^{\text{proxy}}$ and the Da. The Da defines three characteristic regions under which solute transport and processing reactions operate. When the system is transport-limited, $\omega \to 1$, and $\lambda_{\theta,\,sz}^{\text{target}} \approx \lambda_{\theta,\,sz}^{\text{proxy}}$. When the system is reaction-limited, $\omega \to K_{\text{target}}^{\text{proxy}}$, and $\lambda_{\theta,\,sz}^{\text{target}} \approx \lambda_{\theta,\,sz}^{\text{proxy}}\, K_{\text{target}}^{\text{proxy}}$. Under 'dynamic-equilibrium' conditions, both hydrology and reactivity define the scaling factor ω, and $\lambda_{\theta,\,sz}^{\text{target}} \approx \lambda_{\theta,\,sz}^{\text{proxy}}\ \omega$ ………………………… 64

4.1. Resazurin (Raz) is irreversibly transformed to resorufin (Rru) by aerobic metabolism. The figure shows Raz being transformed by *Sinorhizobium meliloti* 1021……………………………………………………………………………... 84

4.2. The resazurin-resorufin (Raz-Rru) system can be used to estimate aerobic respiration in stream ecosystems. Raz is transformed to Rru in surface and hyporheic metabolically active zones………………………………………………... 85

LIST OF FIGURES (continued)

Figure Page

4.3. Respiration chamber experiments conducted at the H.J. Andrews Experimental Forest to test the correlation between ΔRru and ΔDO. Left) fiberglass incubation meshes. Right) recirculating chamber with incubated sediments………………………………………………………………………… 85

4.4. At the 95% confidence level, respiration is not a function of Raz at concentrations < 300 μg L^{-1}. The figure shows normalized cellular CO_2 production rates (R_N) relative to the control, for two species of bacteria and three different concentrations of Raz (cf. Table 4.1). a) *A. chlorophenolicus* A6. b) *P. putida KT2440*. Left) temporal variations with respect to the control bioreactor (dashed-line). Right) box-and-whisker plots of the same data……………………………… 86

4.5. Correlation between CO_2 production and cell growth for *P. putida* (*Pp*), *A. chlorophenolicus* (*Ac*) and *B. subtilis* (*Bs*). Data from the four bioreactors are included for each species……………………………………………………….. 87

4.6. Raz transformation is linearly proportional to aerobic respiration in pure cultures. The figures show correlations between Raz transformation (as ΔRru) and cellular respiration (ΔDO) in pure culture experiments. Linear trend-lines, valid over the entire range of *DO*, are presented to facilitate the discussion. Power-law trend-lines with exponents between 1 and 1.3 also fit the data, and such behavior was previously discussed by *Haggerty et al.* [2009, cf. eqn. 5-7]…………………. 88

4.7. Raz transformation is linearly proportional to aerobic respiration in stream sediments. The figure shows a reach-scale experimental correlation between Raz transformation (as ΔRru) and cellular respiration (ΔDO). Left) regressions for experiments in two streams. Right) regression including both streams…………… 88

5.1. Respiration ($\lambda_{resp.}$) and reaeration ($\lambda_{reae.}$) rates estimated from the Raz-Rru system for different subreaches in a) WS01 and b) WS03. Rates were computed using night-time oxygen histories. Lower and upper bounds describe the uncertainty in the estimates (cf. (2))……………………………………………….. 113

5.2. Gross primary production ($\lambda_{PP.}$) and net input oxygen ($\lambda_{input.} = \lambda_{PP} + \lambda_{reae.}$) rates estimated from the Raz-Rru system for different subreaches in a) WS01 and b) WS03. Rates were computed using day-time and night-time oxygen histories. Lower and upper bounds describe the uncertainty in the estimates (cf. (2))………………………... 114

LIST OF FIGURES (continued)

Figure Page

5.3. Longitudinal profile for DO concentrations in a) WS01, b) WS03; night-time conditions. Markers indicate the location of stations SA – SF. Concentrations have been estimated solving eqn. (11). Lower and upper bounds describe the uncertainty in the estimates (cf. (2))…………………………………………….. 115

5.4. Longitudinal profiles for DO concentrations in a) WS01, b) WS03; day-time conditions. Markers indicate the location of stations SA – SF. Concentrations have been estimated solving eqn. (11). Lower and upper bounds describe the uncertainty in the estimates (cf. (2))………………………………………………... 116

5.5. The largest respiration and reaeration rates estimated with the Raz-Rru system were obtained for subreaches with observable optimum conditions for such processes. Largest respiration rates: a) WS03 subreach SC-SD was characterized by step-pool and pool-riffle bedforms, with stream water flowing through large woody debris which are known to increase retention times, microbial colonization and hyporheic exchange. b) WS03 subreach SE-SF was characterized by complete subsurface (hyporheic) flow with stream water reemerging only at the end of the reach. Largest reaeration rates: c) WS01 subreach SD-SE and SE-SF were characterized by sequences of pools and riffles formed over a bedrock outcrop…………………………………………………………………........... 117

5.6. Comparison of reaeration rates estimated with the Raz-Rru system and the propane evasion and night-time regression techniques for sites with comparable information. Lower and upper bounds describe the uncertainty in the estimates (cf. (2))……………………………………………………………………………….. 118

5.7. Comparison of net metabolism fluxes (per unit depth) estimated with the Raz-Rru system, and the propane evasion and night-time regression techniques for sites with comparable information. Lower and upper bounds describe the uncertainty in the estimates (cf. (2))……………………………………………………….. 118

6.1. Size distribution of the sediments used in the closed chamber experiments. Colors in the bars represent different sieve diameters and percentages reflect the fraction of mass retained by the sieves…………………………………………….. 136

6.2. Photosynthetically active radiation (PAR) recorded at representative sites during daytime injections. Top panel shows values recorded in the shaded reach; bottom panel in the open reach. Labels in boxes (e.g., S1) indicate the nearest sampling station. Mean and median PAR values in both reaches are significantly different at the 95.0% confidence level (Fisher's LSD and Mood’s median test)…. 136

LIST OF FIGURES (continued)

Figure Page

6.3. Stream water temperature recorded at representative sites during night and daytime (d) consecutive injections. Recording time spans from the beginning of the injection up to 8 h later. Day and night mean and median temperatures are significantly different at the 95.0% confidence level (Fisher's LSD and Mood’s median test). P: pool; R: riffle; d: day………………………………………………… 137

6.4. Molar uptake ratio of DO consumed to Raz consumed, K_{DO}^{Raz}. Sediment samples were taken in pools and riffles. Top panel shows results with sediments from the shaded reach; bottom panel from the open reach………………………... 138

6.5. Respiration rates estimated from the Raz-Rru system. Upper and bottom whiskers represent the uncertainty in $\lambda_{resp.}$ considering only K_{DO}^{Raz} from experiments in each of the respective reaches. Circles represent $\lambda_{\theta,\,sz}^{Raz}$…………… 139

LIST OF TABLES

Table Page

2.1. Conservative solute transport database. A total of 98 tracer experiments with 384 BTCs were used in this meta-analysis………………………………………. 31

2.2. Conservative solute transport database grouped by the orders of magnitude of discharge. The regressions presented in Figures 2.1-2.2 were labeled as described hereafter………………………………………………………………………. 32

2.3. Best parameter sets from 1000 Monte Carlo simulations using empirical relationships derived from normalized central moment meta-analysis (n=384 BTCs) and the moment matching technique. Study case of four rivers located in the UK [*Young and Wallis*, 1993; pp. 160-165]. Goodness of fit was estimated with the Nash–Sutcliffe model efficiency coefficient (E)……………………………………………………………………………….. 32

2.4. List of estimated parameters and prediction efficiencies for each predictive model explored. 1000 Monte Carlo simulations were run per model using empirical relationships derived from normalized central moment meta-analysis (n=384 BTCs). Study case of four rivers located in the UK [*Young and Wallis*, 1993; pp. 160-165]. $m_{2\,est.} = (m_{1\,est.})^{\theta}$, with $\theta = [1.601 - 1.629]$…………………… 33

4.1. Experimental configuration to determine the relationship between Raz and oxygen uptake in pure culture experiments……………………………………….. 83

4.2. Statistical results from *ΔRru* vs. *ΔDO* linear regressions in pure culture and field experiments. All regressions have a *p*-value < 0.001………………………… 83

4.3. Quantitative analysis of rate-control on effective respiration rates in stream ecosystems……………………………………………………………………….. 84

5.1. Geomorphic characteristics of the subreaches studied in WS01 and WS03, H.J. Andrews Experimental Forest (OR, USA)…………………………………… 112

5.2. Conservative and reactive solute transport characteristics…………………...... 112

6.1. Sampling locations and type of subreach bedforms…………………………… 134

6.2. Stream metabolism sampling scheme……………………………………...... 134

LIST OF TABLES (continued)

Table Page

6.3. Chamber experiments with sediments from different bedforms in open and shaded subreaches………………………………………………………………... 135

6.4. PAR and stream water temperature values recorded during each of the experiments in both reaches…………………………………………………………… 135

DEDICATION

Para mi hija Silvia y mi siempre amada esposa Paula. Ustedes dos son lo único que siempre necesitaré para ser feliz.

Integrating Solute Transport, Metabolism and Processing in Stream Ecosystem

1. GENERAL INTRODUCTION

1.1. Context

Headwater streams drain 60 – 80% of the terrestrial landscape [*Benda et al.*, 2005], play an important role in global carbon and nutrient cycles [*Triska et al.*, 1989; *Dent et al.*, 2001; *Battin et al.*, 2009; *Zarnetske et al.*, 2012] and provide ecosystem services such as water supply, flood control and recreation [*Lowe and Likens*, 2005]. Headwater streams continuously exchange nutrients, substrates, heat and oxygen with aquifers and with the atmosphere, primarily due to large topographic gradients and coarse sediments [*Elliott and Brooks*, 1997; *Morrice et al.*, 1997; *Peterson et al.*, 2001; *Alexander et al.*, 2007; *MacDonald and Coe*, 2007; *Meyer et al.*, 2007]. These interactions enhance the development of a wide range of microbial communities that, according to recent estimates, maintain the largest biofilm density associated with streambed surfaces and the highest rate of metabolic processing of all lotic systems in the whole river continuum [*Battin et al.*, 2003, 2008; *Bottacin-Busolin et al.*, 2009].

The same biogeochemical properties that make headwater streams highly valuable challenge us when quantifying mass and heat budgets. Headwater streams are characterized by heterogeneous geomorphic and biochemical properties. Because the classic hydrodynamics theory (developed for alluvial channels) is not directly applicable in headwater streams, in the last three decades many researchers have worked on new methods and techniques to model the flow of water through these systems [*Bathurst*, 1985; *Thome and Zevenbergen*, 1985; *Jarrett*, 1990; *Stone and Hotchkiss*, 2007; *Baki et al.*, 2012]. Advances also have taken place in stream solute transport theory [*Beer and Young*, 1983; *Bencala and Walters*, 1983; *Haggerty et al.*, 2002; *Boano et al.*, 2007]. Even after the advent of remote sensing and progress in computing, most of the challenges of studying headwater streams are linked to the difficulty of measuring their geomorphic properties, which are characterized by large-scale heterogeneities (e.g., boulders and large woody debris), high canopy densities which limit the use of remote sensing, irregular bank delineations, and even complete subsurface (hyporheic) flows nearby topographic breakpoints [*Montgomery and Buffington*, 1997; *Adams and Spotila*, 2005; *Wörman et al.*, 2007; *Jiménez and Wohl*, 2013].

After three decades of active research coupling hydrology and stream ecology, the connection among stream solute transport, metabolism and processing is still unresolved. These knowledge gaps obscure the functioning of stream ecosystems and how those ecosystems interact with other landscape processes. We must resolve these challenges to wisely manage water resources, because there is a need to understand controls on stream ecosystems at local, regional and continental scales, and because we need to predict in-stream biogeochemical processes in environments and conditions that do not have supporting data. Therefore, more robust methods are required to deconvolve signal imprints of solute transport, metabolism and processing, allowing the development and implementation of improved decision-making approaches for stream management.

Recognizing that uncertainty and equifinality are ubiquitous issues in hydrologic problems, this dissertation focuses on the development of parsimonious methods to couple solute transport, metabolism and processing in stream ecosystems. To accomplish this, I worked on: 1) scaling and predicting relationships for solute transport, 2) the development of an efficient method to estimate processing rates in streams, and 3) the use of the tracer resazurin [*Haggerty et al.*, 2008, 2009] to estimate stream metabolism. This dissertation was developed through lab and field experiments, meta-analyses, and mathematical, statistical and computational modeling.

1.2. Objectives

- To investigate the existence of patterns that can be used to scale and predict solute transport and nutrient processing in streams.
- To derive an efficient method to estimate processing rates in streams, considering model uncertainty and equifinality issues.
- To determine the quantitative relationship between the transformation of the smart tracer resazurin and oxygen consumption by microorganisms.

- To develop a mathematical framework for the use of the smart tracer resazurin in the analysis of stream metabolism.
- To apply the resazurin-resorufin system to test the hypothesis that hypothesis that community respiration is constant across nighttime and daytime.

1.3. Summary of content

This dissertation is the result of the compilation of five manuscripts that are (or will be) published in the following journals: Water Resources Research, Journal of Geophysical Research – Biogeosciences, Freshwater Biology and Environmental Science and Technology.

Chapter 2, *Scaling and Predicting Solute Transport Processes in Streams*, discusses the existence of temporal patterns that can be used to scale and predict solute transport processes, through the analysis of an extensive database of tracer experiments that span 7 orders of magnitude in discharge, 5 orders of magnitude in longitudinal scale, and sample different lotic environments on 5 continents‐ forested headwater streams, hyporheic zones, desert streams, major rivers and an urban manmade channel. From this meta-analysis, which is only implicitly dependent on hydrogeomorphic characteristics, we proposed an approach to perform uncertainty analysis on solute transport processes, and discussed some inconsistencies of the classic solute transport theory.

In chapter 3, we provide *An Efficient Method to Estimate Processing Rates in Streams* through simple algebraic relationships derived from the transient storage model equations. The method is based on the transport equations, but eliminates the need to calibrate highly uncertain (and intermediate) parameters. We demonstrate that under some common stream transport conditions dispersion does not play an important role in the estimation of processing rates and, therefore, can be neglected. Under such conditions, no computer modeling is needed to estimate processing rates. We also derive algebraic equations to estimate processing rates of target solutes (such as dissolved oxygen) with proxy-tracers (such as resazurin), and show that even if both the target and proxy reactions happen in exactly the same locations at rates that are linearly proportional, the exact relationship between the two volume-averaged rates can be nonlinear and a function of transport. However, the uncertainty in the estimation of the target processing rate is linearly proportional to the proxy-tracer processing rate.

In chapter 4, *Measuring Aerobic Respiration in Stream Ecosystems using the Resazurin-Resorufin System*, we quantify the relationship between the transformation of resazurin and aerobic bacterial respiration in pure culture experiments. We show that the transformation of resazurin to resorufin is nearly perfectly, positively correlated with aerobic microbial respiration. These results suggest that resazurin can be used as a surrogate to measure respiration *in situ* and *in vivo* at different spatial scales, thus providing an alternative to investigate mechanistic controls of solute transport and stream metabolism on nutrient processing.

In chapter 5, *Quantifying Spatial Differences in Metabolism in Headwater Streams*, we use the resazurin-resorufin system to estimate metabolism at different spatial scales (habitat, subreach and reach) in two headwater streams of the H. J. Andrews Experimental Forest (Oregon, USA), and present a mathematical framework for its application. We investigate the relationship between metabolism and hydrodynamics, i.e., geomorphic units (e.g., pool-riffle, pool-cascade), bed materials (i.e., alluvium vs. bedrock channels) and type of transient storage (i.e., pure hyporheic exchange, pure surface transient storage and a combination of both). We show that the resazurin-resorufin system is a good integrator of solute transport and stream metabolism processes.

Finally, in chapter 6, *Diel Fluctuations of Respiration in a Headwater Stream*, we investigate temperature controls on respiration rates and test the hypothesis that community respiration is constant across nighttime and daytime. We conducted consecutive nighttime and daytime experiments in two stream reaches (with different canopy densities) using the resazurin-resorufin system to compare respiration rates. We found that even though photosynthetically active radiation and stream water temperature were different across the reaches, respiration rates were not different across nighttime and daytime conditions. This result suggests that community respiration rates in streams may not need to be “corrected” for temperature between daytime and nighttime.

2. SCALING AND PREDICTING SOLUTE TRANSPORT PROCESSES IN STREAMS

Ricardo González-Pinzón, Roy Haggerty, and Marco Dentz

Water Resources Research
DOI: 10.1002/wrcr.20280

ABSTRACT

We investigated scaling of conservative solute transport using temporal moment analysis of 98 tracer experiments (384 breakthrough curves) conducted in 44 streams located on 5 continents. The experiments span 7 orders of magnitude in discharge (10^{-3} – 10^{3} m^3/s), span 5 orders of magnitude in longitudinal scale (10^{1} – 10^{5} m), and sample different lotic environments – forested headwater streams, hyporheic zones, desert streams, major rivers, and an urban manmade channel. Our meta-analysis of these data reveals that the coefficient of skewness is constant over time ($CSK = 1.18 \pm 0.08$, $R^2 > 0.98$). In contrast, the CSK of all commonly used solute transport models decreases over time. This shows that current theory is inconsistent with experimental data and suggests that a revised theory of solute transport is needed. Our meta-analysis also shows that the variance (second normalized central moment) is correlated with the mean travel time ($R^2 > 0.86$), and the third normalized central moment and the product of the first two are very strongly correlated ($R^2 > 0.96$). These correlations were applied in four different streams to predict transport based on the transient storage and the aggregated dead zone models, and two probability distributions (Gumbel and log-normal).

2.1. Introduction

Two of the most challenging problems in surface hydrology are scaling and predicting solute transport in streams [*Young and Wallis*, 1993; *Jobson* 1997; *Wörman*, 2000, *O'Connor et al*., 2010]. We must resolve these challenges to wisely manage water resources because there is a need to understand controls on stream ecosystems at local, regional and continental scales, and because we need to predict transport in environments and conditions that do not have supporting tracer test data.

Quantitative representations of hydrobiogeochemical processes are based on mathematical and numerical simplifications. Each simplification, the need to parameterize and integrate spatial and temporal processes, and the limitation of available observations to constrain models introduce structural errors and uncertainty in the predictions derived from such models [*Beven*, 1993; *Wagener*, 2004]. On the other hand, the transferability of empirical relationships from intensely instrumented catchments (mainly located in developed countries) to ungauged catchments relies on the similarity of hydrobiogeochemical characteristics [*Sivapalan*, 2003], thus limiting their practical application in regions where they are more needed.

Solute transport and nutrient processing have been analyzed from different modeling perspectives, i.e., physically-based, stochastic [*Botter et al.*, 2010; *Cvetkovic et al.*, 2012] and data-based mechanistic approaches [*Young and Wallis*, 1993; *Young* 1998; *Ratto et al.*, 2007]. Although these approaches have increased our awareness about key compartments and hydrologic conditions that exert important influence on biogeochemical processes, i.e., identification of hot spots and hot moments [*McClain et al.*, 2003], there is not yet a unified approach that has proven successful to scale and predict solute transport and nutrient processing.

In the last three decades, research on solute transport and nutrient processing has revealed complex interactions between landscape and stream ecosystems, and attempts to scale and predict these processes have been limited by the difficulty of measuring and extrapolating hydrodynamic and geomorphic characteristics [*Scordo and Moore*, 2009; *O'Connor and Harvey*, 2008; *O'Connor et al.*, 2010], and by the qualitatively confusing analyses derived from poorly constrained parametric interpretations of model-based approaches. A literature review presented hereafter (chronologically organized) shows contradictory evidence about the relationship between transient storage (TS) [*Bencala and Walters*, 1983; *Beer and Young*, 1983], the theory most frequently used to explain solute transport, and in-stream processing. *Valett et al.* [1996] found a strong correlation ($R^2 = 0.77$) between TS and NO_3 retention in 3 first-order streams in New Mexico. *Mulholland et al*. [1997] found larger PO_4 uptake rates in a stream with higher TS, when they compared 2 forested streams. *Martí et al*. [1997] found no correlation between NH_3 uptake length and A_s/A (TS to main channel sizing ratio) in a desert stream. *Hall et al*. [2002] found a very weak correlation ($R^2 = 0.14 - 0.35$) between TS parameters and NH_4 demand in Hubbard Brook streams. In the 11-stream LINX-I dataset, *Webster et al*. [2003] found no statistically significant relationship between NH_4 uptake and TS.

Thomas et al. [2003] showed that TS accounted for 44% to 49% of NO_3 retention measured by ^{15}N in a small headwater stream in North Carolina. *Niyogi et al*. [2004] did not find significant correlations among soluble reactive phosphorous (P-SRP) and NO_3 uptake velocities, and TS parameters. *Ensign and Doyle* [2005] found an increase of A_s/A and the uptake velocities for NH_4 and PO_4, after the addition of flow baffles to the streams studied. *Ryan et al*. [2007] found strong relationships in 2 urban streams between P-SRP retention and TS when the variables were measured at different regimes in the same stream. *Lautz and Siegel* [2007] found a modest correlation ($R^2 = 0.44$) between NO_3 retention efficiency and TS in the Red Canyon Creek watershed (WY). *Bukaveckas* [2007] reported an indefinite relationship between TS and NO_3 and P-SRP retention efficiencies. Lastly, the LINX-II dataset from ^{15}N-NO_3 injections in 72 streams showed no relationship between NO_3 uptake and TS [*Hall et al*., 2009].

One factor that might contribute to the absence of strong relationships between TS and nutrient processing is the use of metrics that obscure the importance of TS across study sites [see discussions by *Runkel*, 2002 and 2007]. Also, it has become apparent that there are important limitations to identifying TS parameters with current techniques [*Wagener et al*., 2002; *Schmid*, 2003; *Camacho and González-Pinzón*, 2008], i.e., multiple sets of parameters might represent field observations ‘equally-well’ [*Beven and Binley*, 1992], and choosing a unique set of parameters to describe the behavior of a system might lead to misinterpretations of their physical meaning (if any), especially when those parameter sets are used to compare streams from different ecosystems and/or hydrologic conditions.

In spite of the observed complexity of solute transport processes in streams, it is surprising that systems governed by physical processes that are considered ‘well-understood’ and by reasonably predictable biochemical interactions, behave so unpredictably when combined. More robust methods are required to deconvolve signal imprints of solute transport and nutrient processing, thus allowing the development and implementation of improved decision-making approaches for stream management.

In this paper we investigated the existence of temporal patterns that can be used to scale and predict solute transport processes using an extensive database of tracer experiments that span 7 orders of magnitude in discharge, 5 orders of magnitude in longitudinal scale, and sample different lotic environments on 5 continents- forested headwater streams, hyporheic zones, desert streams, major rivers and an urban manmade channel. From this meta-analysis, which is only implicitly dependent on hydrogeomorphic characteristics, we have proposed an approach to perform uncertainty analysis on solute transport processes, and discussed some inconsistencies of the classic solute transport theory.

2.2. Methodology

2.2.1. Temporal moments from time-series

We investigated conservative solute transport using temporal moments of the histories of multiple conservative tracer tests. Our analysis is based on an Eulerian approach, where the time-series have been collected at different fixed spatial locations in each stream. Temporal moments have been widely used in the study of solute transport and biochemical transformations. *Das et al.* [2002] and *Govindaraju and Das* [2007] presented an extensive review of the theory and applications of temporal moment analysis to study the fate of conservative and reactive solutes. Recently, *Leube et al.* [2012] discussed the efficiency and accuracy of using temporal moments for the physically-based model reduction of hydrogeological problems.

Moments of distributions are commonly expressed as measures of central tendency. The n^{th} absolute moment (also referred to as the n^{th} raw moment, or n^{th} moment about 0), μ_n, of a concentration time-series, $C(t)$, is defined as:

$$\mu_n = \int_0^\infty t^n \; C(t) \, dt \,. \tag{1}$$

The n^{th} normalized absolute moment (also referred to as the n^{th} normalized raw moment, or n^{th} normalized moment about 0), μ_n^*, is defined as:

$$\mu_n^* = \frac{\mu_n}{\mu_0} , \tag{2}$$

and the n^{th} normalized central moment (also referred to as the n^{th} normalized moment about the mean), m_n, is defined as:

$$m_n = \frac{1}{\mu_0} \int_0^\infty \left(t - \mu_1^*\right)^n \, C(t) \, dt , \tag{3}$$

$$m_n = \sum_{i=0}^{n} \binom{n}{i} \mu_{n-i}^* \left(-\mu_1^*\right)^i , \tag{4}$$

where i is an index. Note that (4) is an inverse binomial transform that can be easily used to calculate the normalized central moments of order 1 (mean travel time), 2 (variance) and 3 (skewness):

$$\begin{aligned} m_1 &= \mu_1^* \\ m_2 &= \mu_2^* - \mu_1^{*2} \\ m_3 &= \mu_3^* - 3\mu_1^* \, \mu_2^* + 2\mu_1^{*3} \end{aligned} \quad . \tag{5}$$

Temporal moments are also related to residence time distributions and transfer functions of linear dynamic systems [*Jury and Roth*, 1990; *Sardin et al.*, 1991]. *Aris* [1958] developed a method to compute the theoretical temporal moments of linear functions, thus allowing the use of experimental temporal moments (i.e., those estimated from observed time-series) to estimate the parameters of linear dynamic models, i.e.,

$$\mu_n = (-1)^n \, \lim_{s \to 0} \left\{ \frac{d^n}{ds^n} \left[\overline{C}(x, s) \right] \right\} , \tag{6}$$

where $\overline{C}(x,s)$ is the Laplace transform of $C(x,t)$, and x is the longitudinal distance in one-dimensional approximations.

Theoretical temporal moments for most solute transport models have been estimated for different types of boundary conditions. A few examples of the progress on this topic are the development of temporal moment-generating equations to model transport and mass transfer [*Harvey and Gorelick*, 1995; *Luo et al.*, 2008], and the calculation of temporal moments for the transient storage model [*Czernuszenko and Rowinski*, 1997; *Schmid*, 2003], equilibrium and nonequilibrium sorption models [*Goltz and Roberts*, 1987; *Cunningham and Roberts*, 1998], the aggregated dead zone model [*Lees et al.*, 2000], and the metabolically active transient storage model [*Argerich et al.*, 2011].

Matching (or equating) experimental and theoretical temporal moments is a useful technique to parameterize linear models [*Nash*, 1959]. The advantages of using experimental moments to match theoretical moments come with the challenge to completely recover the tracer experiment signals, as it has been shown that truncation errors affect the estimation of higher-order temporal moments. Using experimental data *Das et al.* [2002] and *Govindaraju and Das* [2007] showed that when the error in mass recovery is 16%, the errors in absolute n^{th} moments can be as high as approximately $(n+1)\cdot 16\%$ for $n=0$ through $n=4$. This problem is related to the early cut-off of data measurement or the lack of instrumental resolution to detect low concentrations of tracers, and is not related to the apparent incomplete mass recovery due to dilution effects (e.g., groundwater contributions). Note that correcting the observed breakthrough curves uniformly (with a steady-state gain factor) for dilution only affects the magnitude of the absolute moments, but does not modify the magnitude of the normalized absolute moments, or that of the normalized central moments.

2.2.2 Experimental database

We created a database that includes 384 concentration time-series, or breakthrough curves (BTCs), from 98 conservative tracer experiments conducted in 44 streams under different quasi-steady hydrologic conditions (10^{-3} to 10^{3} m^3/s), different experimental conditions (BTCs observed from 10^1 to 10^5 m downstream the injection point), and different types of lotic environments (Table 2.1). We grouped the database by the orders of magnitude of discharge (Table 2.2) to facilitate the analysis and presentation of the statistical regressions in Figures 2.1 - 2.2. All BTCs were zeroed to background concentrations and corrected by discharge changes during the experiments as specified in the references or recorded in experimental notes.

2.3. Results and Discussion

2.3.1. Statistical relationships derived from temporal moment analysis

Information regarding longitudinal mixing and exchange processes can be found in the normalized central moments (moments about the mean). Figure 2.1a shows that the variance scales in a non-linear (non-Fickian) form with the mean travel time. If dispersion processes in streams were Fickian, the regression presented in Figure 2.1a would have a slope of ~1.0, still preserving a scatter pattern which would be associated with the magnitudes of the dispersion coefficient for each experiment (i.e., different intercepts). Non-Fickian dispersion processes have been widely observed in stream ecosystems [e.g., *Fischer*, 1967; *Nordin and Sabol*, 1974; *Nordin and Troutman*, 1980; *Bencala and Walters*, 1983, and citations therein], and in heterogeneous porous media [e.g., *Rao et al.*, 1980; *Haggerty and Gorelick*, 1995; *Dentz and Tartakovsky*, 2006]. A non-Fickian behavior is, broadly defined, the result of the presence of multi-scale heterogeneities that cannot be integrated into a singular dispersion coefficient [*Neuman and Tartakovsky*, 2009]. To date, several approaches have been proposed to better represent non-Fickian transport, which are largely based on the conceptualization of TS processes and/or the definition of smaller representative elementary volumes, where local homogeneities can be integrated in space and time.

We also correlated m_3 vs. m_2 and m_3 vs. $f(m_1, m_2)$. Figure 2.2a suggests that solute transport data have a small range in their coefficient of skewness (CSK , eqn.7). The coefficient of skewness is a measure of asymmetry, i.e., when $CSK = 0$ the data is perfectly symmetrical (no tailing), but it is known that solute transport experiences tailing effects due to surface and hyporheic TS, regardless of the type of stream ecosystem. For the 98 tracer tests (384 BTCs), $CSK = 1.18 \pm 0.08$ (95% confidence bounds). In Figure 2.2b we show that the product $m_1 \cdot m_2$ is a quasi-linear estimator of m_3 ($R^2 = 0.96$). This result, although not representing a pre-defined statistical descriptor on its own, will be later used to define objective functions for predictive solute transport models (see section 2.3.3.). Not unexpectedly, based on the results from Figure 2.1, m_1 is a much weaker predictor of the ratio m_3/m_2 ($R^2 = 0.66$, results not shown), suggesting that a satisfactory bottom-up estimation of normalized central moments is restricted to one level, at most.

$$\begin{aligned} CSK &= \frac{m_3}{(m_2)^{3/2}} \\ \ln(m_3) &= \frac{3}{2}\ln(m_2) + \ln(CSK) \end{aligned} \quad . \tag{7}$$

2.3.2. Observed scale-invariance in streams and solute transport models

Nordin and Sabol [1974] first reported observations revealing persistent skewness (longitudinally) from Eulerian observations of solute transport time distributions. *Nordin and Troutman* [1980] investigated the performance of the Fickian-type diffusion equation (advection dispersion equation, ADE), and the inclusion of dead zone processes (i.e., TS model - TSM) to account for the persistence of skewness, concluding that "…the observed data deviate consistently from the theory in that the skewness of the observed concentration distributions decreases much more slowly than the Fickian theory predicts", and that although the inclusion of dead zones "…yields a theoretical skewness coefficient [CSK] considerably larger than that given by the ordinary Fickian diffusion equation", "…the skewness of the observed concentrations does not appear to be decreasing as rapidly as the theory predicts". The skewness of BTCs also do not begin with values as high as those predicted by the TSM (cf. Figure 3 in *Nordin and Troutman*, 1980).

Mazijk [2002] reported that tracer experiments conducted to develop the River Rhine alarm model also showed time distributions with persistent CSK along the extensive reach studied ($100\,km < L < 1000\,km$; $Q = 1170\ m^3/s$; cf. Figure 6 in *Mazijk*, 2002), i.e., $0.93 \le CSK \le 1.24$. These observations justified the use of the Chatwin-approximation (Edgeworth series) [*Chatwin*, 1980] to predict solute concentrations in space and time, by fixing $CSK = 1$ for the whole river. Further tracer experiments in the River Rhine ($Q = 663\,m^3/s$, $Q = 1820\ m^3/s$) supported the existence of a persistent CSK [*Mazijk and Veling*, 2005].

Schmid [2002] investigated the conditions under which the TSM could represent the persistence of skewness in solute transport processes. *Schmid* examined the case of a slug injection into a uniform channel and concluded that a small parametric region (a loop right-bounded by $A_s/A < 0.008$; cf. *Schmid* [2002, Figure 1]) could generate a non-decreasing CSK. However, this condition was hypothetical and does not play a major role in practice. Such conditions, if they exist, would be logically inconsistent because tailing effects would be inversely proportional to transient storage. *Schmid* also examined a more general scenario with a time-varying concentration distribution as an upstream boundary condition, the division of long reaches into hydraulically uniform subreaches and a routing procedure to link temporal moments at both ends of the subreaches. This analysis suggested that "…the TS model has the potential to explain persistent or growing temporal skewness coefficients, if applied to a sequence of subreaches with respective parameter sets different from each other". However, predicting solute transport meeting these conditions is rather impractical.

If a transport theory is to be capable of scaling and predicting solute transport processes, it will have a persistent and statistically constant CSK. Our observations of CSK being statistically constant for widely different hydrodynamic conditions suggest that CSK is not only persistent for a given stream (with distance traveled downstream), but can also be used to scale and predict solute transport processes across ecosystems. At a minimum, a persistent value of CSK is a test that a theory of solute transport must pass.

We used the theoretical temporal moments of three models commonly used for the analysis of in-stream solute transport (ADE, TSM and the aggregated dead zone model ADZM) to calculate their theoretical CSK. If these models were systematically capable of representing the scale-invariant patterns observed in our meta-analysis, the parameters would be self-consistent when describing CSK. The model equations, and the theoretical temporal moments and CSKs (calculated for an impulse-type boundary condition, e.g., *Cunningham and Roberts* [1998]) are shown below, along with the consequences of the invariance of CSK on the model parameters. We also included in our analysis (see section 2.3.2.4) three additional transport models less commonly used to describe solute transport in streams, but that have been used in groundwater systems.

2.3.2.1. Advection Dispersion Equation (ADE)

$$\frac{dC}{dt} = -\frac{Q}{A}\frac{dC}{dx} + D\frac{d^2C}{dx^2} \ , \tag{8}$$

$$\begin{aligned} m_1 &= \tau \\ m_2 &= 2\tau^2 / Pe \\ m_3 &= 12\tau^3 / Pe^2 \\ CSK_{ADE} &= 3\sqrt{2}\big/\sqrt{Pe} \end{aligned} \ , \tag{9}$$

where C [ML^{-3}] is the concentration of the solute in the main channel; Q [L^{3}T^{-1}] the discharge; A [L^2] the cross-sectional area of the main channel; D [LT^{-2}] the dispersion coefficient; x [L] the reach length; t [T] time; $\tau = x/u$ [T] is the conservative mean travel time; $Pe = x\,u/D$ [-] the Peclet number; and $u = Q/A$ the mean velocity in the main channel [LT^{-1}].

Eqn. (9) suggests that if CSK_{ADE} is constant, the Peclet number should also be constant. This implies that, under steady-state flow conditions, the dispersion coefficient must scale linearly with the distance traveled. This violates the assumption of spatially uniform coefficients. Therefore, the ADE with spatially uniform coefficients is incapable of representing the experimental observations. Dispersion coefficients scaling with distance have been widely observed in porous media [e.g., *Pickens and Grisak*, 1981; *Silliman and Simpson*, 1987, *Pachepsky*, 2000, and references therein]. Note that the ADE with constant coefficients predicts BTCs with longitudinally decreasing skewness ($CSK_{ADE} \sim x^{-1/2}$), becoming asymptotically Gaussian (i.e., $CSK_{ADE(x\to\infty)} = 0$).

2.3.2.2. Transient Storage Model (TSM)

$$\frac{\partial C}{\partial t} = -\frac{Q}{A}\frac{\partial C}{\partial x} + D\frac{\partial^2 C}{\partial x^2} - \frac{A_s}{A}\alpha_2\left(C - C_s\right), \qquad \text{(10a)}$$

$$\frac{\partial C_s}{\partial t} = \alpha_2\left(C - C_s\right), \qquad \text{(10b)}$$

$$\begin{aligned}
m_1 &= \tau\left(1+\beta\right)\\
m_2 &= \frac{2\left(1+\beta\right)^2\tau^2}{Pe} + \frac{2\beta\tau}{\alpha_2}\\
m_3 &= \frac{12\left(1+\beta\right)^3\tau^3}{Pe^2} + \frac{12\,\tau^2\,\beta\left(1+\beta\right)}{\alpha_2\,Pe} + \frac{6\beta\tau}{\left(\alpha_2\right)^2}\\
CSK_{TSM} &= \frac{3\tau\left(Pe^2\,\beta + 2\alpha_2\,\tau\,Pe\,\beta\left(1+\beta\right) + 2{\alpha_2}^2\,\tau^2\left(1+\beta\right)^3\right)}{\sqrt{2}\,{\alpha_2}^2\,Pe^2\left(\dfrac{\beta\tau}{\alpha_2} + \dfrac{\left(1+\beta\right)^2\tau^2}{Pe}\right)^{3/2}}
\end{aligned}, \qquad \text{(11)}$$

where C_s [ML^{-3}] is the concentration of the solute in the storage zone; A_s [L^2] the cross-sectional area of the storage zone; α_2 [T^{-1}] the mass-exchange rate coefficient between the main channel and the storage zone; and $\beta = A_s/A$ [-]. Other variables are as defined for the ADE. The TSM in eqn. (10) is the same presented by *Bencala and Walters* [1983] and *Runkel* [1998] for a reach without lateral inputs, with a slightly different definition of $\alpha_2 = \alpha/\beta$. Note that $CSK_{TSM} = CSK_{ADE}$ when $\beta = 0$.

If dispersion effects were assumed negligible [e.g., *Wörman*, 2000; *Schmid*, 2002], CSK_{TSM} in eqn. (11) would simplify to:

$$CSK_{TSM:(D=0)} = \frac{3}{\sqrt{2\alpha_2\ \beta\ \tau}} = \frac{3}{\sqrt{2\alpha\tau}} \ . \qquad (12)$$

Using the CSK value found in our meta-analysis, the mean residence time in the storage zones ($t_s = 1/\alpha_2$) normalized by β scale linearly with travel time (τ), i.e.:

$$\frac{t_s}{\beta} = \tau\frac{2}{9}(CSK)^2 \Rightarrow \frac{t_s}{\beta} \approx \frac{\tau}{(3.23 \pm 0.4)} \ . \qquad (13)$$

Eqns. (11) and (12) suggest that the standard TSM generates BTCs with longitudinally decreasing skewness ($CSK_{TSM} \sim x^{-1/2}$), becoming asymptotically Gaussian (i.e., $CSK_{TSM\,(x\to\infty)} = 0$). The physical meaning of the parameters describing $CSK_{TSM} = \text{constant}$ is unclear unless dispersion is assumed negligible ($D = 0$). In this case, eqn. (13) suggests that the TSM model parameters are not independent and that their ratio grows with distance traveled. This analysis supports the results of other studies showing problems of equifinality for the TSM [e.g., *Wagner and Harvey, 1997*; *Wagener et al.*, 2002; *Camacho and González-Pinzón*, 2008; *Kelleher et al.*, 2012]. Equations (11) and (13) suggest that the physical meaning of the TSM parameters is limited, and that relationships between TSM parameters and biogeochemical processing may be site-dependent (as was discussed in the introduction) or even experiment-dependent.

2.3.2.3. Aggregated Dead Zone model (ADZM)

$$\frac{dC}{dt} = \frac{1}{T_r}\left[C_u(t-\tau_{ADZ}) - C(t)\right], \qquad (14)$$

$$\begin{aligned} m_1 &= n(\tau_{ADZ} + T_r) \\ m_2 &= nT_r^{\ 2} \\ m_3 &= 2nT_r^{\ 3} \\ CSK_{ADZM} &= 2/\sqrt{n} \end{aligned} \ , \qquad (15)$$

where T_r [T] is the lumped ADZ residence time parameter representing the component of the overall reach travel time associated with dispersion; C_u [ML^{-3}] is the known concentration at the input or upstream location; and τ_{ADZ} [T] is the time delay describing solute advection due to bulk flow movement.

Equation (14) describes the mass balance of an imperfectly mixed system (ADZ representative volume), where a solute undergoes pure advection, followed by dispersion in a lumped active mixing volume [*Lees et al.*, 2000]. In the ADZM, the distance x implicitly appears in the model description through the time parameters. Note that when $n=1$, the mean travel time (m_1) could be written as $m_1 = x/u$. In equation (15), the parameter n [-] represents the number of identical ADZ elements serially connected ($n=1$ for a single ADZ representative volume) to route the upstream boundary condition. The serial ADZM, although capable of representing a persistent CSK, would require the specification of the non-physical parameter n. More complex ADZM structures can be defined under the data-base mechanistic approach [e.g., *Young*, 1998], but we restricted our discussion to those that have been more commonly used in stream solute transport modeling [*Young and Wallis*, 1993; *Lees et al.*, 2000; *Camacho and González-Pinzón*, 2008; *Romanowicz*, 2013].

2.3.2.4. Alternative solute transport models

Similar sets of calculations also show that the multi-rate mass transfer (MRMT) model [*Haggerty and Gorelick*, 1995; *Haggerty et al.*, 2002] (Appendix A) and a decoupled continuous time random walk (dCTRW) model [e.g., *Dentz and Berkowitz*, 2003; *Dentz et al.*, 2004; *Boano et al.*, 2007] (Appendix B) are equally incompatible with observations of persistent skewness. The CSK in both of these models also scales as $CSK \sim x^{-1/2}$.

We also explored a Lévy-flight dynamics model (LFDM) (Appendix C) [e.g., *Shlesinger et al.*, 1982; *Pachepsky*, 1997, 2000; *Sokolov*, 2000;], which describes the motion of particles behaving similarly to Brownian motion, but allowing occasional clusters of large jumps (significant deviations from the mean). Lévy-flight models have constant transition times, combined with transition length distributions that are characterized by power-law behaviors for large distances. Therefore, such models represent processes characterized by large velocities for long transitions and low velocities for short transitions, and would account for transport in the continuum of river and storage, with the high velocities present in the stream. We were able to generate a LDFM with persistent CSK for a Lévy distribution parameter $\alpha = 1$ (this α is different from the mass-exchange rate coefficient used in the TSM and MRMT model, (cf. (C2) and (C31)). However, $\alpha = 1$ gives an inconsistent scaling of the variance with distance, i.e., $m_2 \sim x^2$ (cf. (C25)). Furthermore, this distribution parameter would imply a velocity distribution in the stream that scales as $p(u) \sim u^{-2}$ at large velocities, which does not appear realistic.

2.3.2.5. Remarks on existent solute transport models

To preserve CSK, the parameters in the solute transport models, including common versions of the CTRW and MRMT, must change with travel distance. Solute transport parameters therefore have some degree of scale-dependence (and arbitrariness) imposed by the constant CSK. Furthermore, these parameters have scaling patterns that are unrelated to anything that can currently be measured in the field. These inconsistencies might be because (1) the common solute transport models and assumptions are partly incorrect, or (2) we (the stream research community) have collected erroneous observations for decades. The latter condition is possible, but is not likely the explanation for a problem that has been observed across so many data sets. The worst-case scenario in our meta-analysis is that all BTCs were truncated prematurely, due to lack of instrument sensitivity or other reasons. However, this would generate BTCs with larger CSK and would contradict the asymptotic behavior shown for CSK in the transport models discussed above. Consequently, we suspect that our models do not correctly represent one or more aspects of solute transport processes from the field.

2.3.3. Use of moments scaling properties to predict solute transport

While the models contain an error that needs correction, it may be possible (in the meantime) to adjust the parameters in a way that is predictive of field behavior. In this section we use the regressions from the temporal moment analysis (section 2.3.1.) to predict solute transport. We provide the parameterization of the TSM, ADZM, and two probability distributions. We then provide an example using data from tracer experiments that were conducted in the River Brock, River Conder, River Dunsop and River Ou Beck in the UK [*Young and Wallis,* 1993 pp. 160-165]. The first three rivers are natural and River Ou Beck is a concrete urban channel.

The methodology requires an independent estimation of the mean travel time (m_1). One way to do this is to regress m_1 against discharge (Q) using a power-law or an inverse relationship in Q [*Young and Wallis,* 1993; *Wallis et al.*, 1989; *Pilgrim,* 1977; *Calkins and Dunne*, 1970]. Once m_1 is estimated, the results from our temporal moment analysis can be used to constrain predictive (forward) simulations of solute transport models. We exemplify this methodology using the experiments by *Young and Wallis* [1993], which were not used in the previous moment analysis, because they show the technique to estimate mean travel times from discharge.

2.3.3.1. Predicted solute transport with classic solute transport models

The parameters of solute transport models can be determined by matching theoretical and experimental moments. Here, we show how the empirical scaling relationships described in section 2.3.1. can be used to direct the search of the parameters of the TSM and the ADZM in predictive simulations.

Predicted solute transport with the TSM

We used the empirical relationships derived for m_3 vs. m_2 and m_3 vs. $f(m_1, m_2)$ (Figure 2.2) to match the theoretical moment equations presented by *Czernuszenko and Rowinski* [1997]. These theoretical equations have been developed for a general upstream boundary condition with tracer distribution $C(t)$. The parameters for the TSM are those defined by *Bencala and Walters* [1983] and *Runkel* [1998]:

$$m_1 = \frac{2D}{u^2} + \frac{L}{u}(1+\beta), \tag{16}$$

$$m_2 = \frac{8D^2}{u^4} + \frac{L}{u}\frac{2D}{u^2}(1+\beta) + \frac{2L}{u}\frac{\beta^2}{\alpha}, \tag{17}$$

$$\begin{aligned} m_3 &= \frac{2L^2}{u^2}\frac{D}{u^2}(1+\beta)^2\,\beta + \frac{64D^3}{u^6} \\ &+ \frac{L}{u}\left[\frac{12D^2}{u^4}(1+\beta)^2 + \frac{4D}{u^2}\frac{\beta^2}{\alpha}(\beta+2) + \frac{6\beta^3}{\alpha^2}\right]. \end{aligned} \tag{18}$$

We have 8 variables, i.e., the dispersion coefficient D, β ($\beta = A_s/A$), the mass-transfer rate α, the length of the reach L, the discharge Q ($u = Q/A$), and the normalized central moments m_1, m_2, m_3. We have 5 equations: 3 for the theoretical moments (eqns. 16–18) and 2 empirical relationships (derived from Figure 2.2). To balance the degrees of freedom ($n = 8$), we therefore need to specify 3 ($3 = 8 - 5$) variables, namely L, Q and m_1. We used a Newton-Raphson algorithm to solve for the 5 unknowns by minimizing the objective function OF shown in eqn. (19). We estimated the mean travel time as: $m_{1\,est.} = \phi\, m_{1\,obs.}$, with $\phi = [0.8 - 1.2]$, and randomly varied the regression coefficients of our meta-analysis within the 95% confidence bounds.

$$\begin{aligned} O.F_1 &= abs\left[1 - \frac{CSK_{theor.}}{CSK_{empirical}}\right] = abs\left[1 - \frac{CSK_{theor.}}{1.18(\pm 0.08)}\right] \\ O.F_2 &= abs\left[1 - \frac{\ln[m_{3\,theor.}]}{\ln[m_{3\,empirical}]}\right] = abs\left[1 - \frac{\ln[m_{3\,theor.}]}{0.932(\pm 0.04)\,\ln[m_{1\,est.}\,m_2]}\right]. \\ O.F_3^* &= abs\left[1 - \frac{m_{1\,theor.}}{m_{1\,est.}}\right] \\ O.F &= O.F_1 + O.F_2 + O.F_3^* \end{aligned} \tag{19}$$

In the optimization routine, we allowed the TSM parameters to vary within ranges typically found in similar streams, i.e., $D = [10^{-3}, 10^{1}]$ [m^2/s], $A_s = [10^{-5}, 10^{1}]$ [m^2], $A = [10^{-3}, 10^{1}]$ [m^2], $\alpha = [10^{-7}, 10^{-4}]$ [s^{-1}]. Once the system of equations was optimized for each random set of estimated mean travel time and fitting coefficients (n=1000), we ran a forward simulation using the optimum parameters. Results from the Monte Carlo simulations are presented in Figure 2.3 and Tables 2.3−2.4. We used the Nash–Sutcliffe model efficiency coefficient (E) [*Nash and Sutcliffle*, 1970] to estimate the goodness of fit of the predictions, i.e., how well the plot of observed versus simulated data fits a 1:1 line.

Predicted solute transport with the ADZM

The two parameters of this model are the advection time delay, τ_{ADZ}, and the residence time, $T_r = \bar{t} - \tau_{ADZ}$, where $\bar{t}$ is the mean travel time (m_1). The theoretical moments of the ADZM for one first-order ADZ element ($n = 1$) were presented in eqn. (15). Since the mean travel time is a measured or estimated quantity, we only need to solve for the advection time delay, τ_{ADZ}. We applied the same optimization routine described for the TSM, and the results obtained are presented in Figure 2.4 and Tables 2.3 − 2.4.

2.3.3.2. Predicted solute transport with probability distributions

Time series described by probability distributions can be used to predict solute transport processes. Here, we show how the empirical scaling relationships described in section 2.3.1. can be used to estimate the temporal moments of two probability distributions, and then to perform predictive simulations.

Predicted solute transport with the Gumbel distribution

We chose the Gumbel (Extreme Value I) probability distribution because of its constant $CSK_{Gumbel} = 1.1395$, which closely agrees with the empirical relationships derived from our meta-analysis ($CSK = 1.18 \pm 0.08$). This distribution is typically used to describe hydrologic events pertaining to extremes [*Brutsaert*, 2005]. The concentration distribution of a solute BTC using this distribution takes the form:

$$\begin{aligned} C(t) &= m_0 \frac{\exp(-z(t)) \cdot \exp(-\exp(-z(t)))}{\beta} \\ z(t) &= \frac{t-\mu}{\beta} \\ \mu &= m_1 - \beta \cdot 0.5772 \\ \beta &= \sqrt{\frac{6\, m_2}{\pi^2}} \end{aligned} \quad , \qquad (20)$$

where μ and β are the location (mode) and scale parameters, respectively. Note that these parameters, and those of any other probability distribution, have no direct physical interpretation.

The use of probability distributions requires the explicit definition of moments beyond the mean travel time, i.e., variance and in some cases the skewness. Therefore, we would need to use empirical relationships such as those derived in Figure 2.1, even though $R^2 < 0.9$. In our predictive analysis we used $m_{1\,est.} = \phi\, m_{1\,obs.}$, with $\phi = [0.8 - 1.2]$ to estimate the uncertainty of $m_{1\,est.}$, and $m_{2\ est.} = \left(m_{1\ est.}\right)^{\theta}$, with $\theta = [1.601 - 1.629]$, as it was suggested by our meta-analysis (i.e., $\ln m_2 = 1.615(1.601, 1.629) \cdot \ln m_1$, $R^2 = 0.86$, regression not shown in Figure 2.1). The results obtained are presented in Figure 2.5 and Table 2.4.

Predicted solute transport with the log-normal distribution

A random variable described by a log-normal distribution comes from the product of *n* variables, each with its own arbitrary density function with finite mean and variance. This distribution has been widely used in hydrologic modeling of flood volumes and peak discharges, duration curves for daily streamflow, and rainfall intensity-duration data [*Chow*, 1954; *Stedinger*, 1980]. Applications in solute transport suggested that the solute velocity, saturated hydraulic conductivity, and dispersion coefficient are log-normally distributed [*Rogowski*, 1972; *Van De Pol et al.*, 1977; *Russo and Bresler*, 1981]. The concentration distribution of a solute BTC with this distribution takes the form:

$$\begin{aligned} C(t) &= \frac{m_0}{\sigma_n\ t\ \sqrt{2\pi}} \exp\left[-\frac{1}{2}\left(\frac{\ln(t)-\mu_n}{\sigma_n}\right)^2\right] \\ m_1 &= \exp\left(\mu_n+\sigma_n^2/2\right) \\ m_2 &= m_1^2\left[\exp\left(\sigma_n^2\right)-1\right] \end{aligned} \quad , \qquad (21)$$

where μ_n and σ_n are the mean and the standard deviation of $\ln(t)$. In our predictive analysis we followed the same procedure described for the Gumbel distribution. The results obtained are presented in Figure 2.6 and Table 2.4.

2.3.3.3. Analysis of predictive solute transport modeling

In our predictive analyses we used two classic models (TSM and ADZM) and hypothesized that these models could adequately predict solute transport if the results of our meta-analysis were defined as objective functions to minimize the differences between the theoretical and empirical temporal moments. Our main goal therefore was to fix a constant CSK, regardless of the longitudinal positioning. The predictive results presented in Figures 2.3 – 2.4 and Tables 2.3 – 2.4 show that this approach required only basic information (i.e., Q, L and an estimation of the mean travel time) to adequately predict the behavior of the solute plumes traveling downstream. For the TSM (4 parameters), the best predictions in the uncertainty analysis had $E > 0.96$ for the four rivers. For the ADZM (2 parameters), the best predictions had $E > 0.97$ for all natural rivers, and $E = 0.76$ for the concrete channel. Although satisfactory results can be achieved with this predictive methodology, it is important to bear in mind that good fittings do not necessarily come from adequate interpretations of mechanistic processes and, therefore, the physical meaning of the parameters should not be taken literally in both inverse (used for calibration) and forward (predictive) simulations.

Besides from predicting solute transport with classic models, we explored the use of probability distributions. We developed predictive models through the parameterization of the Gumbel and log-normal probability distributions, using the results from our meta-analyses and performing uncertainty estimations. The results of our predictive simulations can be summarized as (Table 2.4): 1) the Gumbel distribution ($CSK_{Gumbel} = 1.1395$) yielded better predictions when the distributions were parameterized with the observed m_1 and m_2, suggesting that $CSK = 1.18 \pm 0.08$ is a consistent pattern derived from our meta-analysis, and 2) estimating the variance (m_2) of the distributions from the mean travel time (m_1) can be highly uncertain and it is explicitly required for using probability distributions in predictive mode; therefore, uncertainty analysis must be always included. Importantly, the parameters of these distributions do not have direct physical meaning and this has two main consequences: 1) solute transport understanding cannot be mechanistically advanced, and 2) erroneous parametric interpretations from physically-based, but poorly constrained models are explicitly avoided.

In summary, we found that the regressions from our meta-analysis can be used to adequately predict solute transport processes using either transport models (fixing CSK) or probability distributions. We consider this a transitional methodology ("a patch solution") between our current understanding and an improved transport theory that better represents the experimental results.

2.3.4. Implications for scale-invariant patterns

Other experimental findings reveal intriguing similarities to the scale-invariant patterns that we have highlighted here. These include the linear relationship between cross-sectional maximum and mean velocities [*Chiu and Said*, 1995; *Xia*, 1997; *Chiu and Tung*, 2002], and the relatively constant behavior of the dispersive fraction (a parameter derived from the ADZM) in alluvial and headwater streams [*Young and Wallis*, 1993; *González-Pinzón*, 2008]. These observations suggest that stream cross-sections establish and tend to maintain a quasi-equilibrium entropic state by adjusting the channel characteristics, i.e., erodible channels adjust their geomorphic characteristics with discharge (bedform and type of sediment transported, slope, alignment, etc.) and nonerodible channels adjust their velocity distributions by changing the maximum velocity and flow depths [*Chiu and Said*, 1995; *Chiu and Tung*, 2002]. An improved solute transport theory should address these observed scale-invariant hydrodynamic patterns and explore the physical meaning of the persistence of skewness, which perhaps could be based on principles of thermodynamics and fluid dynamics.

The coefficient of skewness of the classic solute transport models discussed in section 2.3.2. shows that Fickian dispersion is inconsistent with the experimental results. The inclusion of macroscopic Fickian dispersion generates a system where the variance of a dispersing solute grows linearly with the distance traveled, generating skewed distributions that later become asymptotically Gaussian [*Fisher et al.*, 1979; *Nordin and Troutman*, 1980]. This behavior is independent of the assumption of hydraulically uniform stream reaches, suggesting that a revised dispersion approach would be needed unless other mechanisms included in the transport theory (e.g., transient storage) were capable of counteracting the ever decreasing skewness represented by Fickian dispersion.

Although we have not yet investigated scale-invariant behaviors of temporal distributions in processes other than solute transport, we predict that similar patterns can be derived from meta-analysis of flow routing BTCs. We ground this prediction in the fact that the conservative tracers used in our analyses have marked up how water flowed through the different stream ecosystems considered, experiencing similar physical characteristics and processes involved in flow routing (i.e., shear effects, heterogeneity and anisotropy, and dual-domain mass transfer). Regardless of the adequacy of current transport and flow routing modeling approaches, clear similarities appear when comparing the BTCs of these hydrologic processes, and the temporal moments of (for example) the ADZM and those of the Nash cascade [*Nash*, 1960] and the Linear (and Multilinear) Discrete (Lag) Cascade channel routing models [*O'Connor*, 1976; *Perumal*, 1994; *Camacho and Lees*, 1999]. If similar patterns were found with respect to the persistence of skewness in solute transport and flow routing, this could be advantageously used to better understand, scale and predict solute transport processes under flow dynamic conditions, which is a problem that still remains largely unresolved [*Runkel and Restrepo*, 1993; Graf, 1995; *Zhang and Aral*, 2004].

2.4. Conclusions

Despite numerous detailed studies of in-stream transport processes [e.g., *Bencala and Walters*, 1983; *Harvey and Bencala*, 1993; *Elliott and Brooks*, 1997a,b; *Gooseff et al*., 2005; *Wondzell*, 2006; *Cardenas et al.*, 2008], scaling and predicting solute transport can be highly uncertain. This is primarily due to the difficulties of measuring and incorporating stream hydrodynamic and geomorphic characteristics into models. A consequence of these simplifications is that parameters cannot be obtained uniquely from physical attributes. The parameters are functions of a combination of several processes and physical attributes. Therefore, model parameters interact with each other, and the overall model response to different parameter sets might be numerically 'equal' and mechanistically misleading.

Our (model-free) meta-analysis of the BTCs from conservative tracer experiments conducted in a wide range of locations and hydrodynamic conditions suggests that the coefficient of skewness (CSK) is scale-invariant and equal to approximately 1.18. Considering the limited information that is currently available on solute transport processes in different catchments around the world, this methodology is perhaps the least biased (different personnel and instrumentation were used to collect the data) and most informative (BTCs sampled a wide range of multi-scale heterogeneities) to investigate scaling patterns in stream ecosystems. The self-consistent relationships derived from our extensive database for normalized central temporal moments can be used to adequately predict solute transport. Such relationships also revealed systematic limitations of the solute transport models currently used in hydrology and suggest that we need a revised solute transport theory that is capable of representing the observed scaling patterns.

Because solute transport is the foundation of biogeochemical models, if transport models with unidentifiable parameters are used to investigate the coupling between transient storage and biochemical reactions across ecosystems, it is not unexpected that the relationships derived are inconclusive, as it has been extensively shown to date. Ultimately, model structural errors generate equifinal systems that can lead to biased conclusions with respect to the nature of mechanistic relationships.

Acknowledgments

This work was funded by NSF grant EAR 08-38338. Funding was also available from the HJ Andrews Experimental Forest research program, funded by the National Science Foundation's Long-Term Ecological Research Program (DEB 08-23380), US Forest Service Pacific Northwest Research Station, and Oregon State University. We thank the AE, Olaf Cirpka, Adam Wlostowski and an anonymous reviewer for providing insightful comments that helped to improve this manuscript.

Table 2.1. Conservative solute transport database. A total of 98 tracer experiments with 384 BTCs were used in this meta-analysis.

Stream	Reach length (km)	Discharge (m^3/s)	State, Country, (Continent**)	References
Canal Molinos	0.2	0.2-0.4	Colombia (SA)	As referenced by *González-Pinzón* [2008]
Quebrada Lejía	0.3	0.1-0.5	Colombia (SA)	
Subachoque 1	0.3-0.4	0.2-1.3	Colombia (SA)	*González-Pinzón* [2008] and *Camacho and González-Pinzón* [2008]
Subachoque 2	0.1-0.2	0.3-1.9	Colombia (SA)	
Teusacá 1	0.1-0.2	0.3-0.4	Colombia (SA)	
Teusacá 2	0.3-0.4	0.2-1.4	Colombia (SA)	
Rio Magdalena	36-207	1200-1390	Colombia (SA)	*Torres-Quintero et al.* [2006]
Shaver's Cr.	0.1-0.4	0.2	PA, USA (NA)	Unpublished data
Cherry Cr.	0.7-1.3	0.2	WY, USA (NA)	*Briggs et al.* [2013]
Oak Cr.	0.04-0.3	0.02	OR, USA (NA)	Experiments conducted during the Ph.D. dissertation of the first author.
Fuirosos 1	0.2-0.3	0.01	Spain (EU)	
Fuirosos 2	0.2-0.3	0.01	Spain (EU)	
Antietam Cr.	2.6-67	1.2-12.7	MD, USA (NA)	As referenced by *Nordin and Sabol* [1974, Appendix A].
Monocacy River	7.5-34	12.7-22.1	MD, USA (NA)	
Conococheague Cr.	4.4-34	2.6-30.6	MD, USA (NA)	
Chattahoochee River	10.5-104	108-180	GA, USA (NA)	
Salt Cr.	9.3-52	2.5-4.1	NE, USA (NA)	
Difficult Run	0.6-2	0.9-1.1	VA, USA (NA)	
Bear Cr.	1.1-10.9	10.2-10.5	CO, USA (NA)	
Little Piney Cr.	0.6-7.3	1.4-1.6	MO, USA (NA)	
Bayou Anacoco	11-38	2.0-2.7	LA, USA (NA)	
Comite River	6.8-79	0.8-1.0	LA, USA (NA)	
Bayou Bartholomew	3.2-117	4.1-8.1	LA, USA (NA)	
Amite River	10-148	5.7-8.9	LA, USA (NA)	
Tickfau River	6.4-50	2.0-2.9	LA, USA (NA)	
Tangipahoa River	8.2-94	3.5-18.7	LA, USA (NA)	
Red River	5.7-199	108-249	LA, USA (NA)	
Sabine River	7.9-209	127-433	LA, USA (NA)	
Sabine River	17-121	0.7-9.5	TX, USA (NA)	
Mississippi River	35-294	1495-6824	LA, USA (NA)	
Wind/Bighorn River	9.1-181	55-255	WY, USA (NA)	
Copper Cr.	0.2-8.4	1.0-8.7	VA, USA (NA)	
Clinch River	0.7-6.6	5.7-110	VA, USA (NA)	
Powell River	1.0-7.1	3.9-4.1	TN, USA (NA)	
Coachella Canal	0.3-5.5	25.4-26.9	CA, USA (NA)	
Missouri River	66-227	883-977	IA, USA (NA)	
WS1	0.02-0.3	1 l/s-0.06	OR, USA (NA)	*Gooseff et al.* [2003, 2005]; *Haggerty et al.* [2002], unpub.
WS3	0.04-0.7	1 l/s-0.03	OR, USA (NA)	
Lookout Cr.	0.2-0.4	0.3	OR, USA (NA)	*Gooseff et al.* [2003]
Huey Cr.	0.5-1.0	0.1	AN	*Runkel et al.* [1998]
Swamp Oak Cr.	0.1-0.3	0.1	AUS	*Lamontagne and Cook* [2007]
Clackamas River	9.3	36.8	OR, USA (NA)	*Lee* [1995]
Uvas Cr.	0.04-0.4	0.01	CA, USA (NA)	*Bencala and Walters* [1983]
River Mimram	0.1-0.2	0.3	UK (EU)	*Lees et al.* [2000]

** SA: South America; NA: North America; EU: Europe; AUS: Australia; AN: Antarctica.

Table 2.2. Conservative solute transport database grouped by the orders of magnitude of discharge. The regressions presented in Figures 2.1-2.2 were labeled as described hereafter.

Discharge group Q Gr.	Discharge order of magnitude (m^3/s)	Number of experiments
1	10^{-3}	19
2	10^{-2}	37
3	10^{-1}	68
4	10^{0}	131
5	10^{1}	59
6	10^{2}	53
7	10^{3}	17

Table 2.3. Best parameter sets from 1000 Monte Carlo simulations using empirical relationships derived from normalized central moment meta-analysis (n=384 BTCs) and the moment matching technique. Study case of four rivers located in the UK [*Young and Wallis*, 1993; pp. 160-165]. Goodness of fit was estimated with the Nash–Sutcliffe model efficiency coefficient (*E*).

			TSM				ADZM	
River	**Q [m^3/s]**	**L [m]**	**D [m^2/s]**	**β [-]**	**α x10^5 [s^{-1}]**	**E [-]**	**τ_{ADZ} [s]**	**E [-]**
Brock	4.5×10^{-1}	128	2.33	1.31×10^{-2}	9.77	0.96	218.01	0.98
Conder	1.0	116	2.20	8.12×10^{-3}	8.08	0.99	151.95	0.97
Dunsop	5.4×10^{-1}	130	1.33	1.45×10^{-2}	7.89	0.98	332.55	1.00
Ou Beck	3.5×10^{-2}	127	0.67	4.40×10^{-3}	8.92	1.00	135.95	0.76

Table 2.4. List of estimated parameters and prediction efficiencies for each predictive model explored. 1000 Monte Carlo simulations were run per model using empirical relationships derived from normalized central moment meta-analysis (n=384 BTCs). Study case of four rivers located in the UK [*Young and Wallis*, 1993; pp. 160-165]. $m_{2\,est.} = (m_{1\,est.})^{\theta}$**, with** $\theta = [1.601 - 1.629]$**.**

Predictive model	**Estimated pars. besides** $m_{1\,est.} = [0.8 - 1.2] \cdot m_{1\,obs.}$	**Prediction efficiency (** E **)**			
		R. Brock	**R. Conder**	**R. Dunsop**	**R. Ou Beck**
TSM	A_s/A, α, D, Q†, L†	0.74 – 0.96	0.71 – 0.99	0.39 – 0.99	0.26 – 1.00
ADZM	τ_{ADZ}	0.50 – 0.98	0.21 – 0.97	0.48 – 1.00	-0.26 – 0.76
Gumbel dist.	m_2	0.39 – 0.96	0.45 – 0.95	0.38 – 0.99	0.18 – 0.77
Log-Normal dist.	m_2	0.42 – 0.94	0.47 – 0.92	0.45 – 0.97	0.18 – 0.74

†In the predictive TSM simulations we entered the actual discharge Q and reach length L.

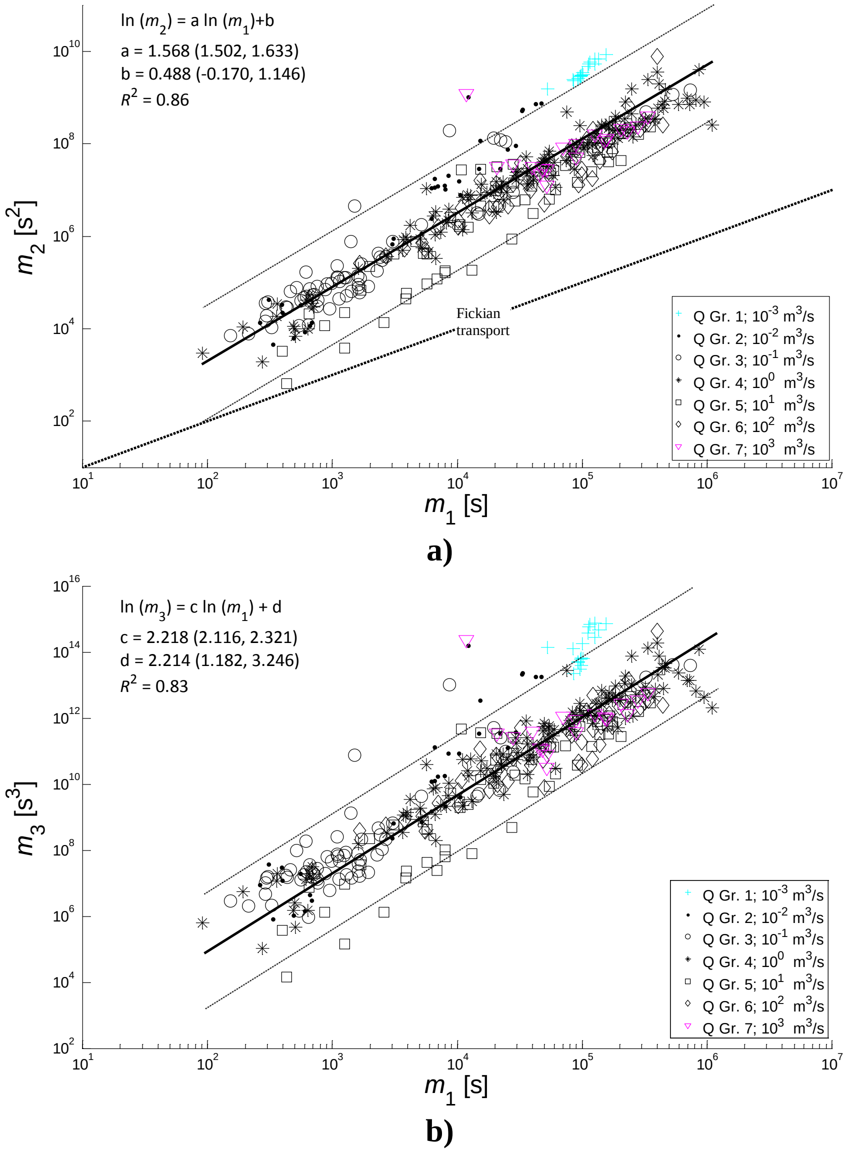

Figure 2.1. Meta-analysis (n=384 BTCs) of conservative solute transport experiments in streams demonstrates the general occurrence of non-Fickian dispersion processes. (a) The growth rate of the variance is non-linear (therefore non-Fickian) with respect to the mean travel time; the thick dashed line represents the slope pattern of Fickian dispersion. (b) Skewness as a function of the mean travel time. Coefficients were fitted with 95% confidence bounds. Thin dashed lines represent 95% prediction bounds.

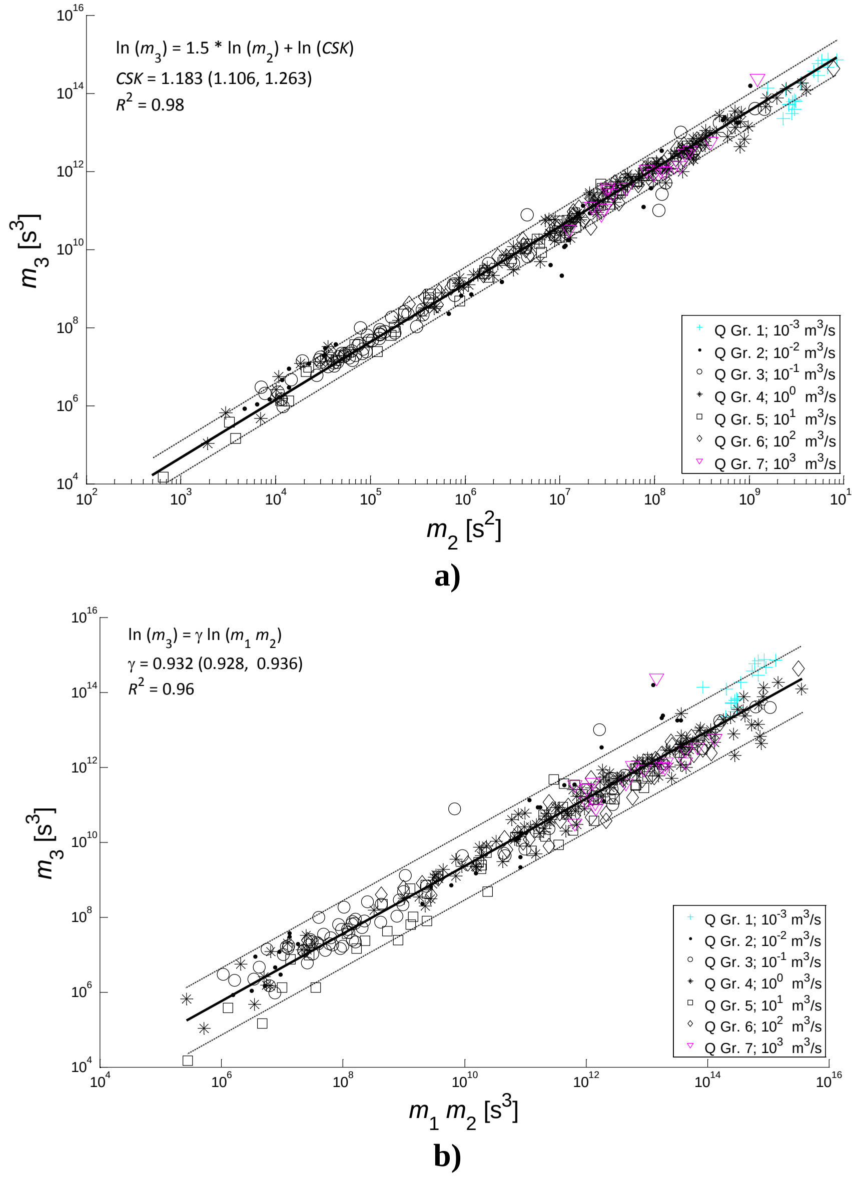

Figure 2.2. a) Meta-analysis (n=384 BTCs) of conservative solute transport experiments from contrasting stream ecosystems suggests that the coefficient of skewness holds statistically constant. Fitted coefficients defined $CSK = 1.18 \pm 0.08$. b) The factor $[m_1\ m_2]$ is a quasi-linear estimator of m_3. However, using m_1 to define the ratio $[m_3 / m_2]$ yields an $R^2 = 0.66$, showing that a satisfactory bottom-up estimation of normalized central moments is restricted to one level, at most. Coefficients were fitted with 95% confidence bounds. Thin dashed lines represent 95% prediction bounds.

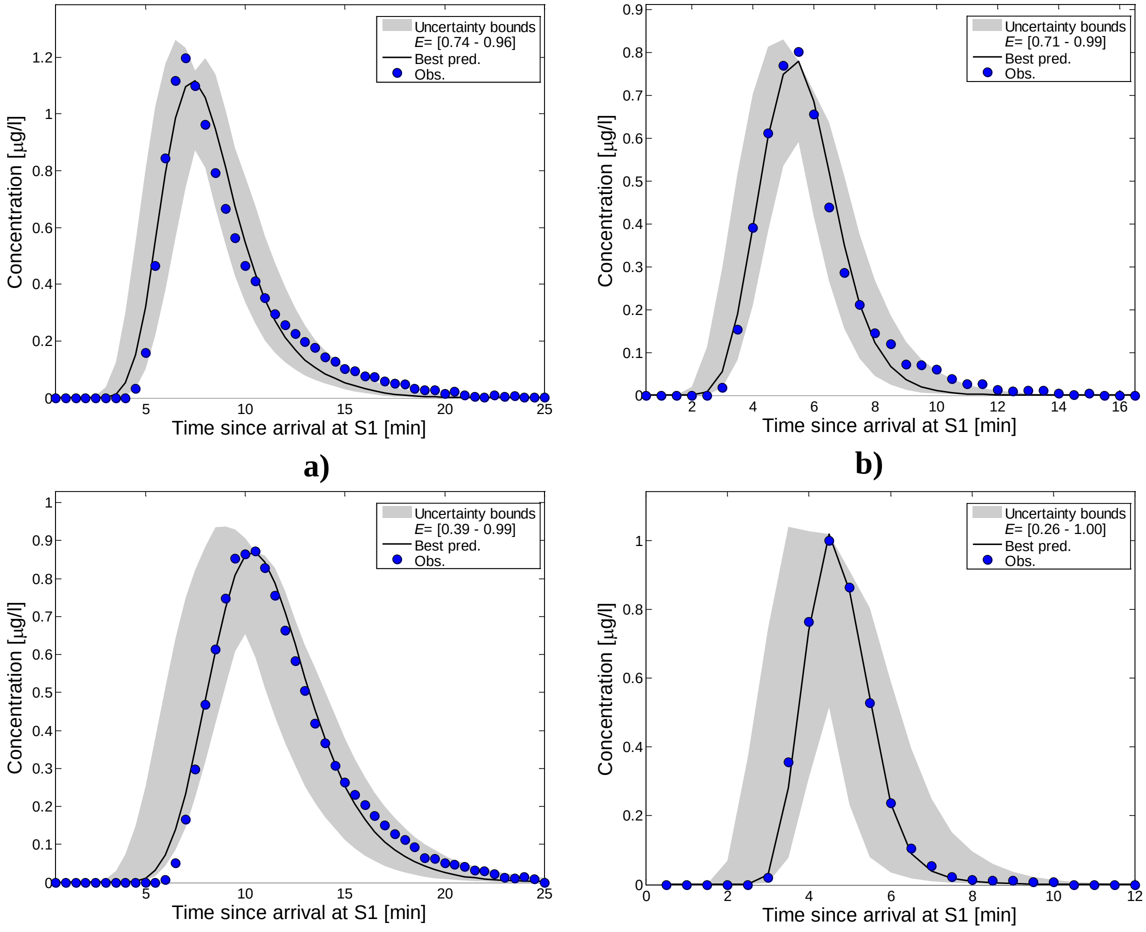

a) **b)** **c)** **d)**

Figure 2.3. Predicted results using empirical relationships derived from normalized central moment meta-analysis (n=384 BTCs) and the moment matching technique for the TSM. The known variables were L, Q and $m_{1\,est.}$, and all others were predicted from 1000 Monte Carlo simulations. The effects of uncertainty in estimating m_1 (i.e., $m_{1\,est.} = \phi m_{1\,obs.}$, with $\phi = [0.8 - 1.2]$), the parameters of the TSM and the fitting coefficients from our meta-analysis are shown as uncertainty bounds. a) River Brock, b) River Conder, c) River Dunsop, d) River Ou Beck. Experimental observations from *Young and Wallis* [1993]. The best parameter sets from the simulations are presented in Table 2.3. Goodness of fit was estimated with the Nash–Sutcliffe model efficiency coefficient (E).

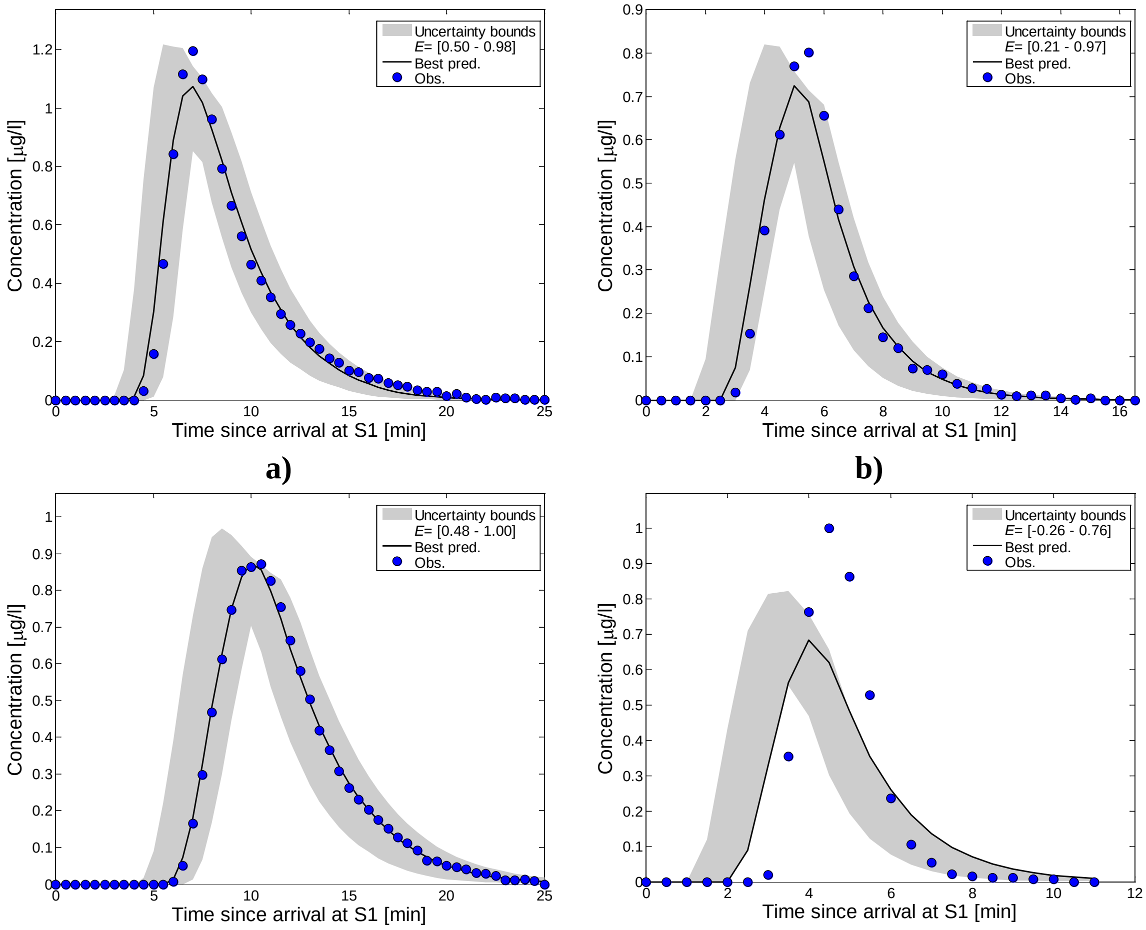

a) **b)** **c)** **d)**

Figure 2.4. Predicted results using empirical relationships derived from normalized central moment meta-analysis (n=384 BTCs) and the moment matching technique for the ADZM. The known variable was m_1 (or $\bar{t}$), and τ_{ADZ} was predicted from 1000 Monte Carlo simulations. The effects of uncertainty in m_1 (i.e., $m_{1\,est.} = \phi m_{1\,obs.}$, with $\phi = [0.8 - 1.2]$) and the fitting coefficients from our meta-analysis are shown as uncertainty bounds. a) River Brock, b) River Conder, c) River Dunsop, d) River Ou Beck. Experimental observations from *Young and Wallis* [1993]. The best parameter sets from the simulations are presented in Table 2.3. Goodness of fit was estimated with the Nash–Sutcliffe model efficiency coefficient (E).

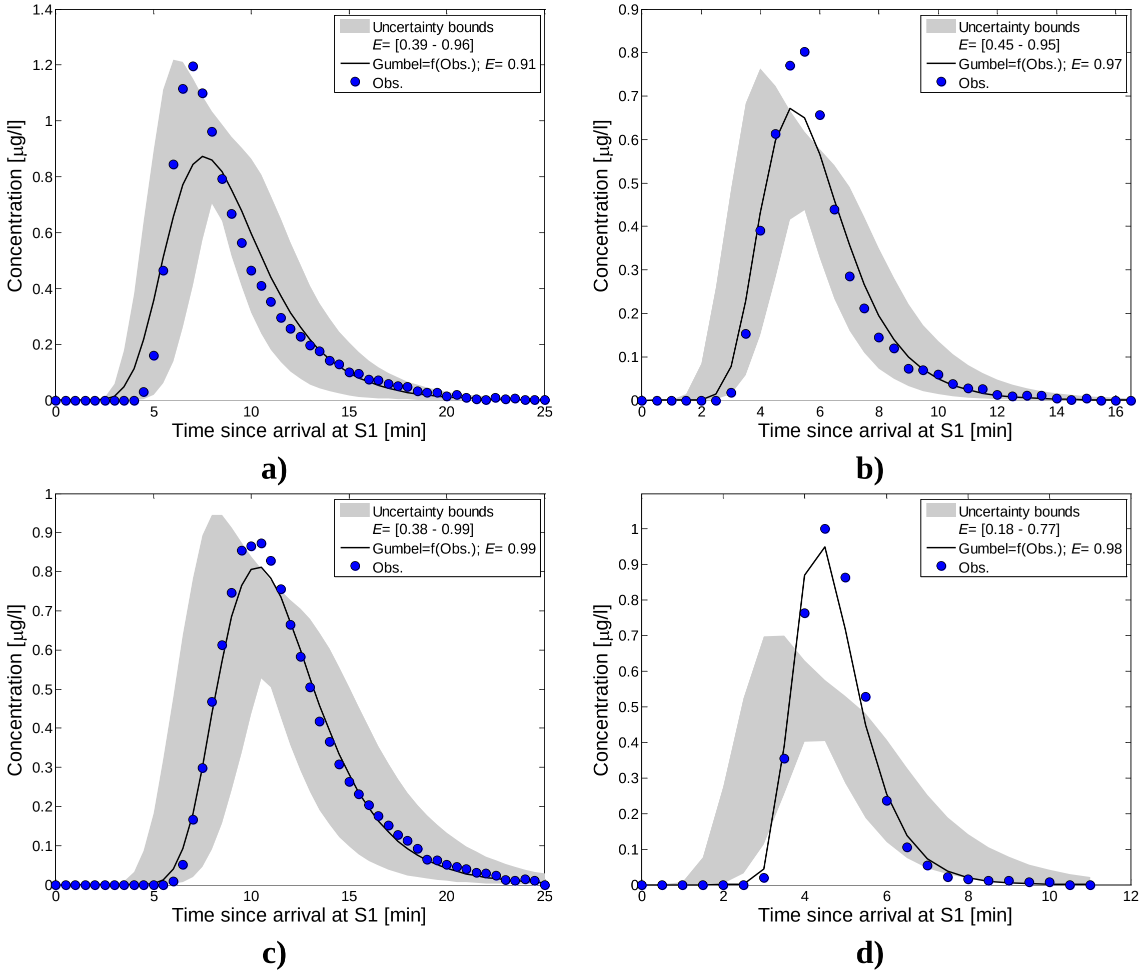

a) b)

c) d)

Figure 2.5. Predicted results using empirical relationships derived from normalized central moment meta-analysis (n=384 BTCs) and the Gumbel distribution, which has a constant $CSK_{Gumbel} = 1.1395$. Uncertainty bounds represent 1000 Monte Carlo simulations where $m_{1\,est.} = \phi m_{1\,obs.}$, with $\phi = [0.8 - 1.2]$, and $m_{2\,est.} = (m_{1\,est.})^{\theta}$, with $\theta = [1.601 - 1.629]$. The "Gumbel=f(Obs.)" simulation uses the actual m_1 and m_2 moments derived from the observed data. a) River Brock, b) River Conder, c) River Dunsop, d) River Ou Beck. Experimental observations from *Young and Wallis* [1993]. Goodness of fit was estimated with the Nash–Sutcliffe model efficiency coefficient (E).

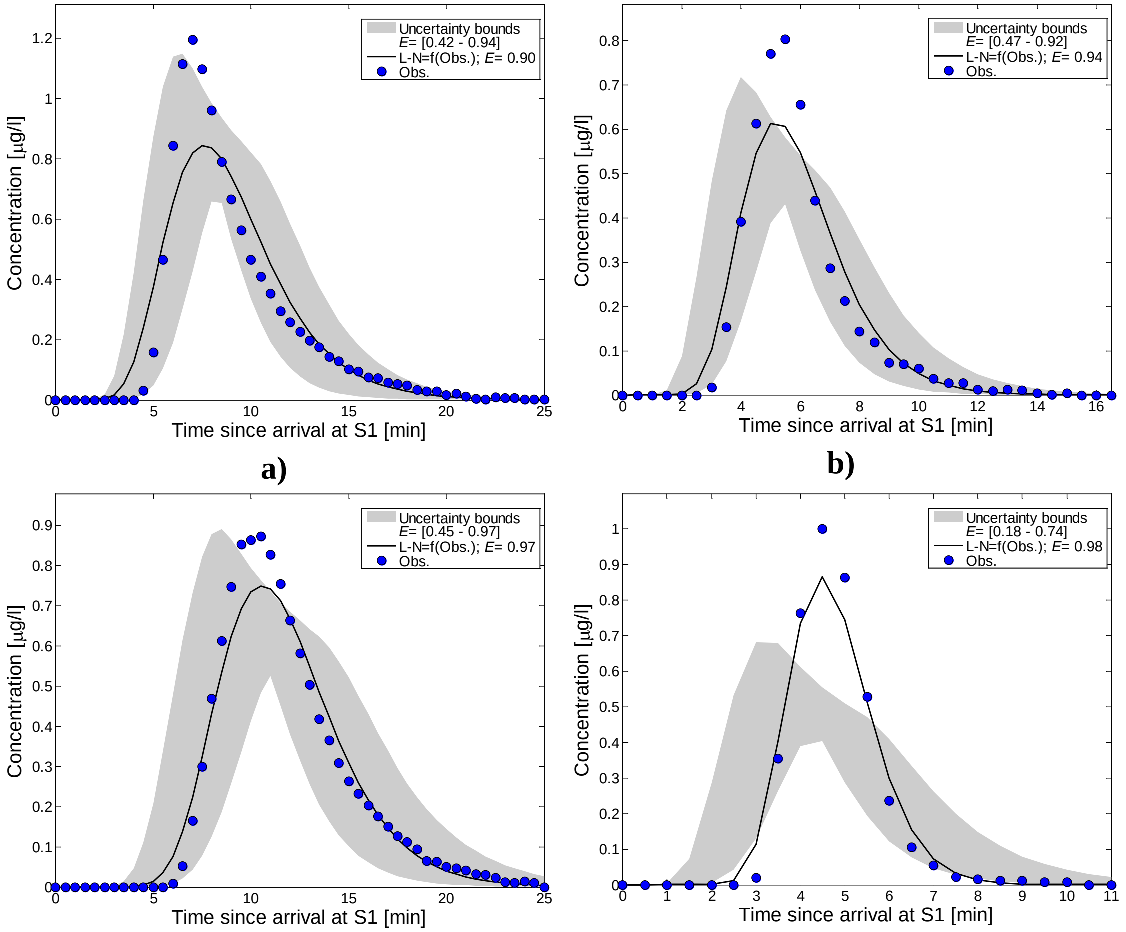

a) b) c) d)

Figure 2.6. Predicted results using empirical relationships derived from normalized central moment meta-analysis (n=384 BTCs) and the log-normal distribution. Uncertainty bounds represent 1000 Monte Carlo simulations where $m_{1\,est.} = \phi m_{1\,obs.}$, with $\phi = [0.8 - 1.2]$, and $m_{2\,est.} = \left(m_{1\,est.}\right)^{\theta}$, with $\theta = [1.601 - 1.629]$. The "L-N=f(Obs.)" simulation uses the actual m_1 and m_2 moments derived from the observed data. a) River Brock, b) River Conder, c) River Dunsop, d) River Ou Beck. Experimental observations from *Young and Wallis* [1993]. Goodness of fit was estimated with the Nash–Sutcliffe model efficiency coefficient (E).

APPENDICES

Appendix A: Multi rate mass transfer (MRMT) model

$$\frac{\partial C}{\partial t}+\beta\int_0^\infty \frac{\partial C_s(\alpha_2)}{\partial t}\,p(\alpha_2)\,d\alpha_2=-\frac{Q}{A}\frac{\partial C}{\partial x}+D\frac{\partial^2 C}{\partial x^2}\,, \tag{A1}$$

$$\frac{\partial C_s(\alpha_2)}{\partial t}=\alpha_2\,\left(C-C_s(\alpha_2)\right),\qquad 0<\alpha_2<\infty\,. \tag{A2}$$

The theoretical temporal moments were computed in a manner similar to *Cunningham and Roberts* [1998]:

$$\begin{aligned} m_1 &= \tau(1+\beta) \\ m_2 &= \frac{2\tau^2(1+\beta)^2}{Pe}+2\tau\beta\hat{\mu} \\ m_3 &= \frac{12\tau^3(1+\beta)^3}{Pe^2}+\frac{12\tau^2\beta(1+\beta)}{Pe^2}\hat{\mu}+6\tau\beta\left(\hat{\mu}^2+\hat{\sigma}^2\right) \\ CSK_{MRMT} &= \frac{3\tau\left(2\frac{(1+\beta)^3\tau^2}{Pe^2}+\beta\left(\frac{2(1+\beta)\hat{\mu}\,\tau}{Pe}+\left(\hat{\mu}^2+\hat{\sigma}^2\right)\right)\right)}{\sqrt{2}\left(\frac{\tau\left((1+\beta)^2\tau+Pe\,\beta\,\hat{\mu}\right)}{Pe}\right)^{3/2}} \end{aligned}, \tag{A3}$$

where $C_s(\alpha_2)$ [ML^{-3}] the concentration of the solute in the storage zone; p is the probability density function of mass transfer exchange rates; $\hat{\mu}$ and $\hat{\sigma}^2$ are the mean and variance of the distribution of transient storage residence times [cf. *Haggerty and Gorelick*, 1995; *Cunningham and Roberts*, 1998]. Other variables are as defined for the TSM. When $\beta=0$, $CSK_{MRMT}=CSK_{ADE}$. If dispersion is negligible ($D=0$):

$$CSK_{MRMT:\,(D=0)}=\frac{3\,\tau\,\beta\left(\hat{\mu}^2+\hat{\sigma}^2\right)}{\sqrt{2}\,(\beta\,\hat{\mu}\,\tau)^{3/2}}\,. \tag{A4}$$

If CSK_{MRTM} is not fixed, the MRMT model will represent BTCs with longitudinally decreasing skewness ($CSK_{MRMT}\sim x^{-1/2}$), becoming asymptotically Gaussian (i.e., $CSK_{MRMT\,(x\to\infty)}=0$).

Appendix B: Decoupled continuous time random walk (dCTRW) model

The Laplace Transform (LT) of $f(x,t)$ for a dCTRW model is given by [*Dentz et al.*, 2004]:

$$\bar{f}(x,s)=\exp\left[-\frac{xu}{2D}\left(\sqrt{1+\frac{4M(s)D}{u^{2}}}-1\right)\right], \qquad \text{(B1)}$$

where s is the LT variable. Other variables have been defined previously in the ADE. The memory function $M(s)$ is defined by:

$$M(s)=\frac{1-\bar{\varphi}(s)}{\tau_1\,\bar{\varphi}(s)}, \qquad \text{(B2)}$$

where $\bar{\varphi}(s)\equiv\sum\bar{\varphi}(x,s)$ is the LT of the time transition probability density function; $\bar{\varphi}(x,s)=p(x)\,\bar{\varphi}(s)$ is the LT of a joint space ($p(x)$) and time transition probability density function; and τ_1 is a median transition time. We estimated the temporal moments using the method by *Aris* [1958].

$$m_1=\left.\frac{x}{u}\frac{M(s)'}{\sqrt{1+\frac{4M(s)D}{u^{2}}}}\right|_{s=0}$$

$$m_2=\left.-\frac{x}{u}\frac{M(s)''}{\sqrt{1+\frac{4M(s)D}{u^{2}}}}+\frac{2xD}{u^{3}}\frac{\left(M(s)'\right)^{2}}{\left(1+\frac{4M(s)D}{u^{2}}\right)^{3/2}}\right|_{s=0} \qquad \text{(B3)}$$

$$m_3=\left.\frac{x}{u}\frac{M(s)'''}{\sqrt{1+\frac{4M(s)D}{u^{2}}}}-\frac{4xD}{u^{3}}\frac{M(s)'\left(M(s)'\right)^{2}}{\left(1+\frac{4M(s)D}{u^{2}}\right)^{3/2}}+\frac{12xD^{2}}{u^{5}}\frac{\left(M(s)'\right)^{3}}{\left(1+\frac{4M(s)D}{u^{2}}\right)^{5/2}}\right|_{s=0}$$

.

The solution for the Fickian case is found when $M(s) = s$, which yields $CSK_{Fickian} = 3\sqrt{2}\big/\sqrt{Pe}$, as it was shown for the ADE (section 2.3.2.1.). A general pattern for the CSK_{dCTRW} can be inferred from this particular condition, and the specifics will depend on the memory function defined for the model. In summary, if CSK_{dCTRW} is not fixed, a dCTRW model will represent BTCs with longitudinally decreasing skewness ($CSK_{dCTRW} \sim x^{-1/2}$), becoming asymptotically Gaussian (i.e., $CSK_{dCTRW\,(x\to\infty)} = 0$).

Appendix C: Lévy-flight dynamics model (LFDM)

We consider here a Lévy-flight type dynamics model, which has a fractal dependence on the sampling position, and takes the form:

$$\begin{aligned} x_{n+1} &= x_n + \xi_n \\ t_{n+1} &= t_n + \tau_0 \end{aligned}, \qquad \text{(C1)}$$

where τ_0 is a constant time increment, and $\xi_n > 0$ are independent identically power-law distributed random variables such that:

$$p(x) \propto x^{-1-\alpha}. \qquad \text{(C2)}$$

For large α (Lévy-flight variable), $p(x)$ could be a Pareto distribution, for example. The spatial Laplace transform of $p(x)$ for $1 < \alpha < 2$ then would be:

$$\overline{p}(\kappa) = 1 - a\kappa + b\kappa^{\alpha}. \qquad \text{(C3)}$$

We are interested in the distribution of arrival times $t(x)$ at a position x, which is given by:

$$t(x) = t_{n_x} \qquad \text{(C4)}$$

where $n_x = \max(n | x_n < x)$ is the number of steps needed to arrive at position x by the Lévy process shown in eqn. (C1). It is equivalent to $x_n < x < x_{n+1}$. Thus, we obtain for the arrival time density:

$$f(x,t) = \left\langle \delta\left(t - t_{n_x}\right)\right\rangle , \tag{C5}$$

where $\delta(t)$ denotes the Dirac delta distribution and the angular brackets denote the noise average over ξ_n. Expression (C5) can be written as:

$$f(x,t) = \sum_{n=0}^{\infty} \delta\left(t - t_n\right)\left\langle \delta_{n,n_x}\right\rangle = \sum_{n=0}^{\infty} \delta\left(t - t_{n_x}\right)\left\langle I\left(0 \le x - x_n \le \xi_n\right)\right\rangle , \tag{C6}$$

where $I(0 \le x < \xi)$ is an indicator function that is 1 if the condition in its argument is true and 0 otherwise. The latter equation can be further developed as:

$$f(x,t) = \int_0^x \sum_{n=0}^{\infty} \delta\left(t - t_{n_x}\right)\left\langle \delta\left(x' - x_n\right)\right\rangle \left\langle I\left(0 \le x - x' \le \xi_n\right)\right\rangle dx' . \tag{C7}$$

Computing the second average we get:

$$f(x,t) = \int_0^x R(x',t)dx' \int_{x-x'}^{\infty} p(\xi)d\xi , \tag{C8}$$

$$R(x',t) = \sum_{n=0}^{\infty} \delta\left(t - t_n\right)\left\langle \delta\left(x' - x_n\right)\right\rangle . \tag{C9}$$

The latter satisfies the Kolmogorov type equation:

$$R(x,t) = \delta(x)\delta(t) + \int_0^{\infty} p(\xi)R\left(x - \xi, t - \tau_0\right) d\xi \quad . \tag{C10}$$

Combining eqn. (C8) and eqn. (C10) in Laplace space we get:

$$\kappa \overline{f}(\kappa,t) = \delta(t) + \overline{M}(\kappa)\left[\overline{f}(\kappa,t-\tau_0) - \overline{f}(\kappa,t)\right], \tag{C11}$$

$$\overline{M}(\kappa) = \frac{\kappa\,\overline{p}(\kappa)}{1-\overline{p}(\kappa)}. \tag{C12}$$

The time increment τ_0 is supposed to be small compared to the observation time, so that we can write (C11) as:

$$\kappa \overline{f}(\kappa,t) = \delta(t) - \overline{M}(\kappa)\tau_0 \frac{\partial \overline{f}(\kappa,t)}{\partial t}. \tag{C13}$$

In real space, it reads as:

$$\frac{\partial f(x,t)}{\partial t} = -\int_0^x M(\xi)\,\tau_0 \frac{\partial f(x-\xi,t)}{\partial t}\,d\xi \quad . \tag{C14}$$

Defining the moments of $f(x,t)$ by:

$$\mu_n(x) = \int_0^\infty t^n f(x,t)dt\,. \tag{C15}$$

We obtain from eqn. (C14) the moment equations

$$\frac{\partial \mu_n(x)}{\partial x} = n\int_0^x M(\xi)\,\tau_0\,\mu_{i-1}\,(x-\xi)\,d\xi\,, \tag{C16}$$

where $\mu_n(x) = 0$ for $n < 0$. This equation can, again, be solved in Laplace space:

$$\kappa\,\overline{\mu}_{\,n}(\kappa) = \delta_{n0}(t) + n\,\overline{M}(\kappa)\,\tau_0\;\overline{\mu}_{\,n-1}(\kappa). \tag{C17}$$

For $n = 1$ we obtain:

$$\overline{\mu}_{\,1}(\kappa) = \overline{M}(\kappa)\;\kappa^{-2}\,, \tag{C18}$$

because $\overline{\mu}_0(\kappa) = \kappa^{-1}$. We are interested in the behavior at large distances, which means at small κ. Inserting eqn. (C12) above gives:

$$\overline{\mu}_1(\kappa) = \tau_0\ \kappa^{-1} \frac{\overline{p}(\kappa)}{1-\overline{p}(\kappa)} . \tag{C19}$$

Inserting now eqn. (C3) and expanding up to leading order gives:

$$\overline{\mu}_1(\kappa) = \tau_0\, \kappa^{-1} \frac{1}{a\kappa - b\kappa^{\alpha}} = \frac{\tau_0}{a^2}\kappa^2 + \ldots \quad . \tag{C20}$$

Thus, the first moment is given by:

$$\mu_1(x) = \frac{x\ \tau_0}{a} \ . \tag{C21}$$

For the second moment we have:

$$\overline{\mu}_2(\kappa) = 2\tau_0^2\, \kappa^{-1} \frac{\overline{p}(\kappa)^2}{\left[1-\overline{p}(\kappa)\right]^2} . \tag{C22}$$

Inserting eqn. (C3) and expanding up to leading orders we have:

$$\overline{\mu}_2(\kappa) = 2\frac{\tau_0^2}{a^2\kappa^3} + 4\frac{\tau_0^2\, b}{a^3}\kappa^{\alpha-4} + \ldots . \tag{C23}$$

Inversion of this expression gives:

$$\mu_2(x) = \frac{\tau_0^2}{a^2}x^2 + 4\frac{\tau_0^2\, b}{a^3\,\Gamma(4-\alpha)}x^{3-\alpha} . \tag{C24}$$

The second normalized central moment is:

$$m_2(x) = 4\frac{\tau_0^2\, b}{a^3\,\Gamma(4-\alpha)}x^{3-\alpha} . \tag{C25}$$

For the third moment we have:

$$\overline{\mu}_3(\kappa) = 6\tau_0^3\,\kappa^{-1}\,\frac{\overline{p}(\kappa)^3}{\left[1-\overline{p}(\kappa)\right]^3}\,. \tag{C26}$$

Inserting eqn. (C3) and expanding up to leading orders we have:

$$\overline{\mu}_3(\kappa) = 6\frac{\tau_0^3}{a^3\kappa^4} + 18\frac{\tau_0^3\,b}{a^4}\,\kappa^{\alpha-5} + \ldots\,. \tag{C27}$$

Inversion of this expression gives:

$$\mu_3(x) = \frac{\tau_0^3}{a^3}\,x^3 + \frac{18\,\tau_0^3 b}{a^4\,\Gamma(5-\alpha)}\,x^{4-\alpha}\,. \tag{C28}$$

The third normalized central moment is:

$$m_3(x) = \frac{3\,\tau_0^3 b}{a^4}\left[\frac{6}{\Gamma(5-\alpha) - \dfrac{4}{\Gamma(4-\alpha)}}\right]x^{4-\alpha}\,. \tag{C29}$$

We can now estimate the scaling of CSK as:

$$CSK_{LFDM} = \frac{m_3(x)}{m_2(x)^{1.5}} \sim \frac{x^{4-\alpha}}{x^{3\cdot(1.5)-\alpha\cdot(1.5)}}\,. \tag{C30}$$

For CSK_{LFDM} to be independent of x (or persistent) we need:

$$\alpha = \frac{4-3\cdot(1.5)}{1-1.5} = 1\,. \tag{C31}$$

References

Argerich, A., R. Haggerty, E. Martí, F. Sabater, and J. Zarnetske (2011), Quantification of metabolically active transient storage (MATS) in two reaches with contrasting transient storage and ecosystem respiration, *J. Geophys. Res.*, *116*, G03034, doi:10.1029/2010JG001379.

Aris, R. (1958), On the dispersion of linear kinetic waves, *Proc. Royal Soc., London Ser. A 245*, 268-277.

Beer, T., Young P. (1983), Longitudinal dispersion in natural streams, *J. Environ. Eng.*, *109*, *(5)*, 1049-1067.

Bencala, K. E. and R. A. Walters (1983), Simulation of solute transport in a mountain pool-and-riffle stream: A transient storage model, *Water Resour. Res.*, *19(3)*, 718–724, doi:10.1029/WR019i003p00718.

Beven, K.J., and A.M. Binley (1992), The future of distributed models: Model calibration and uncertainty prediction, *Hydrol. Processes*, *6*, 279-298.

Beven, K. (1993), Models of channel networks: Theory and predictive uncertainty, in *Channel Network Hydrology*, edited by K. Beven and M.J. Kirby, pp. 129-173, John Wiley & Sons Ltd, Chichester, England.

Boano, F., A. I. Packman, A. Cortis, R. Revelli, and L. Ridolfi (2007), A continuous time random walk approach to the stream transport of solutes, *Water Resour. Res.*, *43*, W10425, doi:10.1029/2007WR006062.

Botter, G., N. B. Basu, S. Zanardo, P. S. C. Rao, and A. Rinaldo (2010), Stochastic modeling of nutrient losses in streams: Interactions of climatic, hydrologic, and biogeochemical controls, *Water Resour. Res.*, *46*, W08509, doi:10.1029/2009WR008758.

Bukaveckas, P.A. (2007), Effects of channel restoration on water velocity, transient storage, and nutrient uptake in a channelized stream, *Environ, Sci. Technol.*, *41*, 1570–1576.

Briggs, M.A., Lautz, L.K., Hare, D.K., González-Pinzón, R., (2012), Relating hyporheic fluxes, residence times and redox-sensitive biogeochemical processes upstream of beaver dams, submitted to *Freshw. Sci.*

Brutsaert, W. (2005), *Hydrology: An Introduction*, Cambridge University Press, United Kingdom.

Calkins, D. and Dunne, T. (1970), A salt tracing method for measuring channel velocities in small mountain streams, *J. Hydrol.*, *11(4)*, 379-392.

Camacho, L.A., and M.J. Lees (1999), Multilinear discrete lag-cascade model for channel routing, *J. Hydrol.*, *226*, 30–47.

Camacho, L.A., González-Pinzón, R. (2008), Calibration and prediction ability analysis of longitudinal solute transport models in mountain streams, *J. Environ Fluid Mech.*, *8(5)*, 597-604.

Cardenas, M.B., J.L. Wilson, and R. Haggerty (2008), Residence time of bedform-driven hyporheic exchange, *Adv. Water Resour.*, *31(10)*, 1382-1386.

Chatwin, P., (1980), Presentation of longitudinal dispersion data, *J. Hydr. Div., 106(1),* 71-83.

Chiu, C-L., and A.A. Said (1995), Maximum and mean velocities and entropy in open-channel flow, *J. Hydraul. Eng., 121(1),* 26-35.

Chiu, C-L., Tung, N-C. (2002), Maximum velocity and regularities in open channel flow, *J. Hydraul. Eng., 128(4),* 390-398.

Chow, V.T. (1954), The log-probablity law and its engineering applications, *Proc. Amer. Soc. Civil Eng., 80(5),* 536-1 – 536-25.

Cunningham, J. A., and P. V. Roberts (1998), Use of temporal moments to investigate the effects of nonuniform grain-size distribution on the transport of sorbing solutes, *Water Resour. Res., 34(6),* 1415–1425, doi:10.1029/98WR00702.

Cvetkovic, V., C. Carstens, J.-O. Selroos, and G. Destouni (2012), Water and solute transport along hydrological pathways, *Water Resour. Res., 48,* W06537, doi:10.1029/2011WR011367.

Czernuszenko, W., and P. M. Rowinski (1997), Properties of the dead-zone model of longitudinal dispersion in rivers, *J. Hydraul. Res., 35(4),* 491-504.

Das, B.S., R.S. Govindaraju, G.J. Kluitenberg, A.J. Valocchi, and J.M. Wraith (2002), Theory and applications of time moment analysis to study the fate of reactive solutes in soil, in *Stochastic Methods in Subsurface Contaminant Hydrology*, edited by R.S. Govindaraju, ASCE Press, USA.

Dentz M., and B. Berkowitz (2003), Transport behavior of a passive solute in continuous time random walks and multirate mass transfer. *Water Resour. Res., 39,* 1111, doi:10.1029/2001WR001163, 5.

Dentz, M., A, Cortis, H. Scher, and B. Berkowitz (2004), Time behavior of solute transport in heterogeneous media: Transition from anomalous to normal transport, *Adv. Water Resour*., 27 (2004), 155–173.

Dentz, M., and D. Tartakovsky, (2006). Delay mechanisms of non-Fickian transport in heterogeneous media. *Geophys. Res. Lett., (33),* L16406.

Elliott, A. H., and N. H. Brooks (1997a), Transfer of nonsorbing solutes to a streambed with bedforms: Theory, *Water Resour. Res., 33,* 123–136.

Elliott, A. H., and N. H. Brooks (1997b), Transfer of nonsorbing solutes to a streambed with bedforms: Laboratory experiments, *Water Resour. Res., 33,* 137–151.

Ensign, S.H., and M.W. Doyle (2005), In-channel transient storage and associated nutrient retention: Evidence from experimental manipulations, *Limnol. Oceanogr., 50(6),* 1740-175.

Fischer, H.B. (1967), The mechanics of dispersion in natural streams, *J. Hydraul. Div. Amer. Soc. Civil Eng. 93(HY6),* 187-216.

Fisher, H.B., E.J. List, R.C. Koh, J. Imberger and N.H. Brooks, (1979), *Mixing in Inland and Coastal* Waters, Academic, New York.

Goltz, M. N. and P. V. Roberts (1987), Using the method of moments to analyze three-dimensional diffusion-limited solute transport from temporal and spatial perspectives, *Water Resour. Res.,* 23(8), 1575–1585, doi:10.1029/WR023i008p01575.

González-Pinzón, R.A. (2008), Determinación del comportamiento de la fracción dispersiva en ríos característicos de montaña, M.Sc. thesis, Departamento de Ingeniertía Civil y Agrícola, Universidad Nacional de Colombia, Bogotá.

Gooseff, M.N., S. M. Wondzell, R. Haggerty, and J. Anderson (2003), Comparing transient storage modeling and residence time distribution (RTD) analysis in geomorphically varied reaches in the Lookout Creek basin, Oregon, USA, *Adv. Water Resour.*, *26*, 925–937.

Gooseff, M. N., J. LaNier, R. Haggerty, and K. Kokkeler (2005), Determining in-channel (dead zone) transient storage by comparing solute transport in a bedrock channel–alluvial channel sequence, Oregon, *Water Resour. Res.*, *41*, W06014, doi:10.1029/2004WR003513.

Govindaraju, R.S., and B.S. Das (2007), Moment Analysis for Subsurface Hydrologic Applications, Springer, Dordrecht, The Netherlands.

Graf, B. (1995), Observed and predicted velocity and longitudinal dispersion at steady and unsteady flow, Colorado River, Glen Canyon Dam to Lake Mead. *J. Am. Water Resour. Assoc.*, *31(2),* 265–281.

Haggerty, R., S. M. Wondzell, and M. A. Johnson (2002), Power-law residence time distribution in the hyporheic zone of a 2nd-order mountain stream, *Geophys. Res. Lett.*, *29(13)*, 1640, doi:10.1029/2002GL014743.

Haggerty, R., and S. M. Gorelick (1995), Multiple-rate mass transfer for modeling diffusion and surface reactions in media with pore-scale heterogeneity, *Water Resour. Res.*, *31(10)*, 2383–2400, doi:10.1029/95WR10583.

Hall, R.O., Jr., E.S. Bernhardt, and G.E. Likens (2002). Relating nutrient uptake with transient storage in forested mountain streams, *Limnol. Oceanogr.*, *47(1),* 255–265.

Hall, R.O., Jr et al. (2009). Nitrate removal in stream ecosystems measured by ^{15}N addition experiments: Total uptake, *Limnol. Oceanogr.*, *54(3),* 653–665.

Harvey, J. W. and K. E. Bencala (1993), The Effect of streambed topography on surface-subsurface water exchange in mountain catchments, *Water Resour. Res.*, *29(1),* 89–98, doi:10.1029/92WR01960.

Harvey, C.F., and S. M. Gorelick (1995), Temporal moment-generating equations: Modeling transport and mass transfer in heterogeneous aquifers, *Water Resour. Res.*, *31(8)*, 1895–1911, doi:10.1029/95WR01231.

Jobson, H.E., (1997), Predicting travel time and dispersion in rivers and streams, *J. Hydraul. Eng.*, *123(11),* 971-978.

Jury, W.A., and K. Roth (1990), *Transfer Functions and Solute Movement through Soil: Theory and Applications*, Birkhäuser, Basel, Switzerland.

Kelleher, C., T. W. Wagener, B. McGlynn, A. S. Ward, M. N. Gooseff, and R. A. Payn (2012),

Stream characteristics govern the importance of transient storage processes, submitted to *Water Resour. Res.*

Lamontagne, S. and P.G. Cook (2007), Estimation of hyporheic water residence time in situ using 222Rn disequilibrium, *Limnol. Oceanogr.: Methods*, *5*, 407–416.

Lautz, L.K., and D.I. Siegel (2007), The effect of transient storage on nitrate uptake lengths in streams: An inter-site comparison, *Hydrol. Processes, 21*, 3533–3548.

Lees, M. J., L. A. Camacho, and S. Chapra (2000), On the relationship of transient storage and aggregated dead zone models of longitudinal solute transport in streams, *Water Resour. Res*., *36(1)*, 213–224, doi:10.1029/1999WR900265.

Lee, K.K. (1995), Stream Velocity and Dispersion Characteristics Determined by Dye-Tracer Studies on Selected Stream Reaches in the Willamette River Basin, Oregon, USGS Water-Resources Investigations Report 95-4078, Portland (OR), USA.

Leube, P.C., W. Nowak, and G. Schneider (2012), Temporal moments revisited: Why there is no better way for physically based model reduction in time?, *Water Resour. Res*., *48*, W011527, doi:10.1029/2012WR011973.

Luo, J., O. A. Cirpka, M. Dentz, and J. Carrera (2008), Temporal moments for transport with mass transfer described by an arbitrary memory function in heterogeneous media, *Water Resour. Res.*, *44*, W01502, doi:10.1029/2007WR006262.

Martí E., N.B. Grimm, and S.G. Fisher (1997), Pre- and post-flood nutrient retention efficiency in a desert stream ecosystem, *J. N. Am. Benthol. Soc*., *16*, 805–819.

Mazijk, A. van (2002), Modelling the effects of groyne fields on the transport of dissolved matter within the Rhine Alarm-Model, *J. Hydrol*., 264, 213-229.

Mazijk, A. van, and E.J.M. Veling (2005), Tracer experiments in the Rhine Basin: evaluation of the skewness of observed concentration distributions, *J. Hydrol*., *307*, 60-78.

McClain, M.E., et al. (2003), Biogeochemical hot spots and hot moments at the interface of terrestrial and aquatic ecosystems, *Ecosystems (N.Y.), 6(4)*, 301–312, doi:10.1007/s10021-003-0161-9.

Mulholland, P.J., E.R. Marzolf, J.R. Webster, D.R. Hart, and S.P. Hendricks (1997), Evidence of hyporheic retention of phosphorus in Walker Branch, *Limnol. Oceanogr*., *42*, 443-451.

Nash, J.E., (1959), Systematic determination of unit hydrograph parameters, *J. Geophys. Res. 64*(1), 111–115, doi:10.1029/JZ064i001p00111.

Nash, J.E., 1960. A unit hydrograph study with particular reference to British catchments, *Proc. Instn. Civ. Engrs*., *17*, 249–282.

Nash, J. E. and J. V. Sutcliffe (1970), River flow forecasting through conceptual models part I — A discussion of principles, *J. Hydrol*., *10 (3)*, 282–290.

Neuman, S. and D.M. Tartakovsky (2009), Perspective on theories of non-Fickian transport in heterogeneous media, *Adv. Water Resour*., *32(5)*, 670–680.

Niyogi D.K., K.S. Simon, and C.R. Townsend (2004), Land use and stream ecosystem functioning: Nutrient uptake in streams that contrast in agricultural development, *Archiv für Hydrobiologie*, *160*, 471–486.

Nordin, C.F., and G.B. Sabol (1974), Empirical data on longitudinal dispersion in rivers, USGS Water-Resources Investigations Report 74-20, USA.

Nordin, C. F., Jr. and B. M. Troutman (1980), Longitudinal dispersion in rivers: The persistence of skewness in observed data, *Water Resour. Res.*, 16(1), 123–128, doi:10.1029/WR016i001p00123.

O’Connor, K.M., (1976), A discrete linear cascade model for hydrology, *J. Hydrol*., *29*, 203–242.

O’Connor, B. L., and J. W. Harvey (2008), Scaling hyporheic exchange and its influence on biogeochemical reactions in aquatic ecosystems, *Water Res. Res.*, *44*(12), W12423.

O’Connor, B.L., M. Hondzo, and J.W. Harvey (2010), Predictive modeling of transient storage and nutrient uptake: Implications for stream restoration, *J. Hydraul. Eng.*, *136(12)*, 1018-1032.

Pachepsky, Ya.A., D. Gimenez, S. Logsdon, R. Allmaras, and E. Kozak (1997), On interpretation and misinterpretation of fractal models, *Soil Sci. Soc. Am. J. 61*,1800–1801.

Pachepsky, Ya.A., D. Benson and W. Rawls (2000), Simulating scale-dependent solute transport in soils with the fractional advective–dispersive equation, *Soil Sci. Soc. Am. J.*, *64*, 1234-1243.

Perumal, M., (1994), Multilinear discrete cascade model for channel routing, *J. Hydrol*., *158*, 135–150.

Pickens, J. F., and G. E. Grisak (1981), Modeling of scale-dependent dispersion in hydrogeologic systems, *Water Resour. Res.*, *17(6)*, 1701–1711, doi:10.1029/WR017i006p01701.

Pilgrim, D.H. (1977), Isochrones of travel time and distribution of flood storage from a tracer study on a small watershed, *Water Resour. Res.*, *13(3)*, 587-595.

Rao, P.S. C., D. E. Rolston, R. E. Jessup, and J. M. Davidson (1980), Solute transport in aggregated porous media: Theoretical and experimental evaluation, *Soil Sci. Soc. Am. J.*, *44(6)*, 1139-1146.

Ratto, M., P.C. Young, R. Romanowicz, F. Pappenberger, A. Saltelli, and A. Pagano (2007), Uncertainty, sensitivity analysis and the role of data based mechanistic modeling in hydrology, *Hydrol. Earth Syst. Sci*., *11(4)*, 1249-1266.

Rogowski, A.S. (1972), Watershed physics: Soil variability criteria, *Water Resour. Res*., *8*, 1015-1023.

Romanowicz, R., M. Osuch, and S. Wallis (2013), Modelling of solute transport in rivers under different flow rates: A case study without transient storage, *Acta Geophysica*, *61(1)*, 98-125.

Runkel, R.L. (1998), One dimensional transport with inflow and storage (OTIS): A solute transport model for streams and rivers, U.S. Geological Survey Water-Resources Investigation Report 98-4018, 73 p.

Runkel, R.L. (2002), A new metric for determining the importance of transient storage, *J. N. Am. Benthol. Soc*., *21*, 529-543.

Runkel, R.L. (2007), Toward a transport-based analysis of nutrient spiraling and uptake in streams, *Limnol. Oceanogr. Methods*, *5*, 50-62.

Runkel, R.L., D.M. McKnight and E.D. Andrews (1998), Analysis of transient storage subject to unsteady flow: Diel flow variation in an Antarctic stream, *J. N. Am. Benthol. Soc*., *17(2)*, 143-154.

Runkel, R. L., and Restrepo, P. J. (1993), Solute transport modeling under unsteady flow regimes: an application of the Modular Modeling System. In: *Water Management in the '90s: A Time for Innovation*, edited by K. Hon, Proc. Wat. Res. Planning & Management Div., ASCE, Seattle, Washington.

Russo, D., and E. Bresler (1981), Soil hydraulic properties as stochastic processes: An analysis of field spatial variability, *Soil Sci. Sac. Am. J.*, *45*, 682-687.

Ryan, R.J., A.I. Packman, and S.S. Kilham (2007), Relating phosphorus uptake to changes in transient storage and streambed sediment characteristics in headwater tributaries of Valley Creek, an urbanizing watershed, *J. Hydrol*., *336*, 444-457.

Sardin, M., D. Schweich, F. J. Leij, and M. Th. van Genuchten (1991), Modeling the nonequilibrium transport of linearly interacting solutes in porous media: A review, *Water Resour. Res*., *27(9)*, 2287–2307, doi:10.1029/91WR01034.

Schmid, B.H. (2002), Persistence of skewness in longitudinal dispersion data: Can the dead zone model explain it after all?, *J. Hydraul. Eng*., *128(9)*, 848-854.

Schmid, B.H. (2003), Temporal moments routing in streams and rivers with transient storage, *Adv. Water Resour*., *26*, 1021–1027.

Scordo, E.B., and R. Dan Moore (2009), Transient storage processes in a steep headwater stream, *Hydrol. Processes*, *23*, 2671-2685.

Shlesingerm M.F., J. Klafter, and Y.M. Wong (1982), Random walks with infinite spatial and temporal moments, *J. Stat. Phys.*, *27*, 499-512.

Silliman, S.E., and E.S. Simpson (1987), Laboratory evidence of the scale effect in dispersion of solutes in porous media, *Water Resour. Res.*, *23(8)*, 1667–1673, doi:10.1029/WR023i008p01667.

Sivapalan, M. (2003), Prediction in ungauged basins: A grand challenge for theoretical hydrology, *Hydrol. Process.*, *17(5)*, 3163-3170.

Sokolov, I.M. (2000), Lévy flights from a continuous-time process, *Phys. Rev. E.*, 63, 011104.

Stendinger, J.R. (1980), Fitting log normal distributions to hydrologic data, *Water Resour. Res.*, *16(3)*, 455–468.

Thomas, S.A., H.M. Valett, J.R. Webster, and P.J. Mulholland (2003), A regression approach to estimating reactive solute uptake in advective and transient storage zones of stream ecosystems, *Adv. Water Resour.*, *26*, 965–976.

Torres-Quintero, E., G. Munárriz, D. Villazón (2006), Determinación de caudal, tiempos de tránsito, velocidad y coeficiente de dispersión en el Río Bogotá, Frío y Magdalena utilizando técnicas nucleares, *Avances Investigación en Ingeniería*, *5*, 21-31.

Valett, H.M., J.A. Morrice, and C.N. Dahm (1996), Parent lithology, surface-groundwater exchange, and nitrate retention in headwater streams, *Limnol. Oceanogr*., *41*, 333–345.

Van De Pol, R. M., P. J. Wierenga, and D. R. Nielsen (1977), Solute movement in a field soil, *Soil Sci. Sac. Am. J.*, *41*, 10-13.

Wagner, B. J. and J. W. Harvey (1997), Experimental design for estimating parameters of rate-limited mass transfer: Analysis of stream tracer studies, *Water Resour. Res.*, *33(7)*, 1731–1741, doi:10.1029/97WR01067.

Wagener, T., L.A. Camacho, and H.S. Wheater (2002), Dynamic identifiability analysis of the transient storage model for solute transport in rivers, *J. Hydroinf.*, *4(3)*, 199-211.

Wagener, T., H.S. Wheater, H.V. Gupta (2004), Rainfall-Runoff modelling In gauged and ungauged catchments, Imperial College Press, London, England.

Webster, J.R. et al. (2003), Factors affecting ammonium uptake in streams - an inter-biome perspective, *Freshwater Biology*, *48*, 1329-1352.

Wallis, S.G., P.C. Young, and K.J. Beven (1989), Experimental investigation of the aggregated dead zone model for longitudinal solute transport in stream channels, *Proc. Instn. Civ. Engrs.*, Part 2, *87*, 1-22.

Wondzell, S. (2006), Effect of morphology and discharge on hyporheic exchange flows in two small streams in the Cascade Mountains of Oregon, USA, *Hydrol. Processes*, *20 (2)*, 267–287.

Wörman, A. (2000), Comparison of models for transient storage of solutes in small streams, *Water Resour. Res.*, *36(2)*, 455–468, doi:10.1029/1999WR900281.

Xia, R. (1997), Relation between mean and maximum velocities in a natural river, *J. Hydraul. Eng.*, *123(8)*, 720-723.

Young, P.C., and S.G. Wallis (1993), Solute transport and dispersion in channels, in *Channel Network Hydrology*, edited by K. Beven and M.J. Kirby, pp. 129-173, John Wiley & Sons Ltd, Chichester, England.

Young, P.C. (1998), Data-based mechanistic modelling of environmental, ecological, economic and engineering systems, *Environ. Modell. Softw.*, *13(2)*, 105-122.

Zhang, Y. and Aral, M.M (2004), Solute transport in open-channel networks in unsteady flow regime, *Environ. Fluid Mech.*, *(4)*, 225-247.

3. AN EFFICIENT METHOD TO ESTIMATE PROCESSING RATES IN STREAMS

Ricardo González-Pinzón and Roy Haggerty

Water Resources Research

Submitted: May 2, 2013

ABSTRACT

We provide an efficient method to estimate processing rates through simple algebraic relationships derived from the transient storage model equations. The method is based on the transport equations, but eliminates the need to calibrate highly uncertain (and intermediate) parameters. We demonstrate that under some common stream transport conditions dispersion does not play an important role in the estimation of processing rates and, therefore, can be neglected. Under such conditions, no computer modeling is needed to estimate processing rates. We also derive algebraic equations to estimate processing rates of target solutes (such as dissolved oxygen) with proxy-tracers (such as resazurin), and show that even if both the target and proxy reactions happen in exactly the same locations at rates that are linearly proportional, the exact relationship between the two volume-averaged rates can be nonlinear and a function of transport. However, the uncertainty in the estimation of the target processing rate is linearly proportional to the proxy-tracer processing rate.

3.1. Introduction

Processing rates (broadly defined as reaction, decay or uptake rates) in streams contain information about physicochemical and biological interactions, and are used in mass balances (e.g., carbon and nitrogen budgets) and environmental impact assessments (e.g., toxicity levels, (bio)accumulation, (bio)remediation). Furthermore, these rates can be used to directly compare spatial processing within and across stream ecosystems. Processing rates are conventionally estimated through the calibration of transport models, and the uncertainty in their estimates is a function of the uncertainty in the rest of the model parameters. Because most physically-based transport models are poorly constrained, the parameters are usually non-unique, interact with each other, and yield equifinal representations of the system, even when the observed data are high quality [*Wagner and Harvey, 1997*; *Wagener et al.*, 2002; *Camacho and González-Pinzón*, 2008; *Kelleher et al.*, 2012; *González-Pinzón et al.*, 2013]. Therefore, current methods to calculate processing rates might yield highly uncertain estimates.

In this technical note we derive (1) an efficient method to estimate processing rates in streams and (2) the relationship between the processing rate of one solute to the processing rate of another solute in streams. Our method simplifies the estimation of such rates to a point where only algebraic equations and experimental data are needed.

3.2. Processing Rates in Streams

The lumped transport equations describing advection, dispersion, transient storage, and first-order irreversible processing in a transient storage compartment are:

$$\frac{\partial C}{\partial t} = -\frac{Q}{A}\frac{\partial C}{\partial x} + D\frac{\partial^2 C}{\partial x^2} - \beta\,\alpha_2 (C - S) - \lambda_{mc} C\,, \tag{1}$$

$$\frac{\partial S}{\partial t} = \alpha_2\,(C - S) - \lambda_{sz}\, S\,, \tag{2}$$

where C and S [M L^{-3}] are the concentrations of the reactive solute in the main channel and transient storage zone; Q [L^{3}T^{-1}] the discharge; D [LT^{-2}] the dispersion coefficient; $\beta = A_s / A$; A [L^2] the cross-sectional area of the main channel; A_s [L^2] the cross-sectional area of the storage zone; α_2 [T^{-1}] the mass-transfer rate between the main channel and transient storage zones (or $\alpha\, A/A_s$ as described by *Runkel* [2007]); x [L] longitudinal distance; t [T] time; λ_{mc} [T^{-1}] the reactive rate in the main channel; and λ_{sz} [T^{-1}] the reactive rate in the lumped transient storage zone.

Departing from the work by *Das et al.* [2002] and *Argerich et al.* [2011], the zeroth temporal moment (m_0) describing the breakthrough curve (BTC) of a reactive solute, subject to the transport equations (1) and (2), is:

$$m_0^{dn} = m_0^{up} \exp\left[\frac{1}{2}\left(Pe - \left[Pe\left(4\tau\,\beta\left(\frac{\alpha_2\ \lambda_{sz}}{\alpha_2 + \lambda_{sz}}\right) + 4\lambda_{mc}\,\tau + Pe\right)\right]^{1/2}\right)\right], \tag{3}$$

where superscript *up* indicates an upstream measurement, superscript *dn* indicates a downstream measurement, $Pe = Lu / D$ [-] is the Peclet number, which describes the relative importance of advection and dispersion in the system; L [L] the length of the reach; u [LT^{-1}] the mean velocity in the reach ($u = Q / A$); and $\tau = L/u$ [T] the mean travel time of a conservative solute in the reach.

Let us define effective processing rates ($\lambda_{eff,\, sz}$, [T^{-1}]) and volume-averaged processing rates ($\lambda_{\theta, sz}$, [T^{-1}]) in the storage zone as:

$$\lambda_{\theta,\, sz} = \beta \left(\frac{\alpha_2 \ \lambda_{sz}}{\alpha_2 + \lambda_{sz}} \right) = \beta \ \lambda_{eff\,,\, sz} \,. \tag{4}$$

Combining (3) and (4) and rearranging, we obtain the total effective processing rate (λ_T, [T^{-1}]) in the stream reach:

$$\lambda_T = \lambda_{\theta,\, sz} + \lambda_{mc} = \frac{\ln[m_o^{up} / m_o^{dn}]}{\tau} \left(1 + \overbrace{\frac{\ln[m_o^{up} / m_o^{dn}]}{Pe}}^{dispersive\ \ term\ \ \Phi} \right). \tag{5}$$

Because $\ln[m_o^{up} / m_o^{dn}]$ is generally less than 5 (e.g., $\ln[m_o^{up} / m_o^{dn}] = 4.6$ for a 99% total processing), and Pe is typically 10 or larger, the magnitude of the dispersive term Φ can be relativley small. For example, $\Phi < 0.1$ for $Pe > 100$, which makes Φ effectively negligible. If the dispersive term Φ and reactions in the main channel are negligible (most reactions happen in the sediment), λ_T simplifies to:

$$\lambda_{T_{(D\to 0;\, \lambda_{mc}\to 0)}} = \lambda_{\theta,\, sz_{(D\to 0)}} = \frac{\ln[m_o^{up} / m_o^{dn}]}{\tau} \ . \tag{6}$$

Equations (5) and (6) show the conditions for which dispersion can be assumed negligible. This assumption was made by *Argerich et al.* [2011] and implicitly by *Tank et al.* [2008]. Note that in (5) and (6), plateau (steady-state) concentrations can be substituted for the zeroth temporal moments (see, for example, equations related to (6) in *Runkel* [2007]).

Normalized central moments of order *n* ($\overline{m_n}$) can be estimated from experimental BTCs as [*Das et al.*, 2002]:

$$\overline{m_n} = \sum_{j=1}^{r} \left(0.5t_k + 0.5t_{k+1}\right)^n \left(0.5C_k + 0.5C_{k+1}\right)\left(t_{k+1} - t_k\right), \tag{7}$$

where $C(t)$ [ML^{-3}] is the measured concentration at time t [T]; j [-] is an index and r [-] the total number of observations. The mean travel time τ between two sampling locations can be estimated with the conservative tracer BTCs as:

$$\tau = \frac{m_{1,cons}^{dn}}{m_{o,cons}^{dn}} - \frac{m_{1,cons}^{up}}{m_{o,cons}^{up}}. \tag{8}$$

3.3. Relationship between Processing Rates of Two Solutes

We derive how a reactive solute (referred to as ‘proxy-tracer’ from here on) can be used to estimate processing rates of another solute of interest (referred to as ‘target’ from here on). We consider proxy-tracers that decay (are transformed) linearly proportional to the target. We assume that reactivity preferentially takes place in transient storage zones, where processing rates are significantly higher due to enhanced redox gradients and/or larger volume of colonized sediments (e.g., the hyporheic zone). Furthermore, we analyze a system where the dispersive term is negligible.

An example of these conditions is the use of resazurin in hydrologic applications. Resazurin is a bioreactive compound that can be used as a proxy-tracer to quantify oxygen (target) consumption in stream ecosystems [*Haggerty et al.*, 2008, 2009; *Argerich et al.*, 2011; *González-Pinzón et al.*, 2012; *Stanaway et al.*, 2012; *Lemke et al.*, 2013]. Resazurin is a proxy-tracer because it has been found that there is a nearly perfect linear relationship between oxygen consumption and resazurin uptake [*González-Pinzón et al.*

2012]. However, this relationship has to be found via calibration, i.e., it is ecosystem-dependent. Other examples are the use of CO_2 production rates to estimate respiration rates (or vice versa), the use of partitioning tracers to assess NAPL distribution rates, and the use of proxy-tracers to assess environmental impacts of hazardous or emerging contaminants [*Sabatini and Austin*, 1991; *Morel and Hering*, 1993; *Rao et al*., 2000; *Kunkel and Radke*, 2011].

We want to know the volume-averaged processing rate of the target, $\lambda_{\theta,\,sz}^{target}$, [T^{-1}]. This rate is related to the volume-averaged processing rate of the proxy-tracer in the storage zone ($\lambda_{\theta,sz}^{proxy}$, [T^{-1}]) (cf. (4)):

$$\lambda_{\theta,\,\mathrm{sz}}^{\mathrm{target}} = \omega\beta\, \lambda_{eff,\,sz}^{proxy} = \omega \lambda_{\theta,\,sz}^{proxy} \ , \tag{9}$$

$$\omega = \frac{K_{target}^{proxy}\left(\lambda_{sz}^{proxy} + \alpha_2\right)}{K_{target}^{proxy}\cdot\lambda_{sz}^{proxy} + \alpha_2}, \tag{10}$$

where ω [-] is a scaling factor between the volume-averaged processing rate of the proxy-tracer and the volume-averaged rate of the target, both in the storage zone; and K_{target}^{proxy} [-] is the molar processing ratio of the target to the proxy-tracer, i.e., K_{target}^{proxy} = [moles of target processed / moles proxy-tracer processed].

Equations (9-10) are interesting. Even if both the target and proxy reactions happen in exactly the same locations at rates that are linearly proportional, the relationship between the two volume-averaged rates can be nonlinear and a function of transport.

K_{target}^{proxy} can be experimentally estimated, whereas λ_{sz}^{proxy} and α_2 need to be estimated through the calibration of the transport model described by (1) and (2). Estimating these parameters might be expensive. Therefore, we investigated convenient simplifications of the scaling factor ω for a range of K_{target}^{proxy}, α_2 and λ_{sz}^{proxy}. To do so, we used the ratio of the characteristic transient storage residence time τ_{sz} ($\tau_{sz} = 1/\alpha_2$) to the characteristic reaction time of the proxy-tracer τ_{sz}^{proxy} ($\tau_{sz}^{proxy} = 1/\lambda_{sz}^{proxy}$), i.e., the Dahmköhler number (Da):

$$Da = \lambda_{sz}^{proxy} \Big/ \alpha_2 \ . \tag{11}$$

Da reflects the relative importance of reactive and hydrological processes (cf. (4)). *González-Pinzón et al.* [2012] showed that when $Da > 10$, α_2 controls the effective processing rate λ_{eff}^{proxy} and the processing rate is transport-limited. Conversely, when $Da < 0.1$, λ_{sz}^{proxy} controls λ_{eff}^{proxy}, and the processing rate is reaction-limited. Reaction-limited conditions mean that the reaction rate is much slower than the exchange of mass between the main channel and transient storage zones. Transport-limited conditions mean the reverse.

We let Da span 9 orders of magnitude (10^{-4} to 10^{4}) to encompass mass-transfer and processing rates observed in field experiments [*Hall et al.*, 2002; *Runkel*, 2007; *Haggerty et al.*, 2008, 2009; *Zarnetske et al.*, 2012; *Briggs et al.*, 2013]. We also bounded $K_{target}^{proxy} = [0.2, 4.0]$ to encompass expected values (cf., *González-Pinzón et al.* [2012] for an example of molar uptake ratios observed for resazurin and dissolved oxygen; note that $K_{DO}^{Raz} = 1/K_{Raz}^{DO}$).

Figure 3.1 shows that when streams are transport-limited, the scaling factor $\omega \to 1$, regardless of the magnitude of K_{target}^{proxy}. Conversely, when the system is reaction-limited, the scaling factor $\omega \to K_{target}^{proxy}$. A detailed analysis shows that when transport-limited conditions are assumed to occur at $Da > 10$, only values of $K_{target}^{proxy} < 0.2$ yield $\omega < 0.8$. On the other end, when reaction-limited conditions are assumed to occur at $Da < 0.1$, only values of $K_{target}^{proxy} > 3.8$ yield $\omega / K_{target}^{proxy} < 0.8$.

The behavior of the scaling factor ω as a function of Da constrains the estimation of $\lambda_{\theta,\, sz}^{target}$ with $\lambda_{\theta, sz}^{proxy}$. Also, (9) and (10) show that when $K_{target}^{proxy} = 1$, $\omega = 1$, and $\lambda_{\theta,\, sz}^{target} = \lambda_{\theta,\, sz}^{proxy}$. Altogether, these conditions bracket the estimation of $\lambda_{\theta,\, sz}^{target}$, allowing an explicit estimate of the uncertainty propagated from the estimation of the transport parameters.

These simplifications can be summarized as:

$$\lambda_{\theta,\ sz}^{\mathrm{target}} = \begin{cases} \lambda_{\theta,sz}^{proxy},\ \text{if}\ \ Da > 10: transport - limited\ system \\ \lambda_{\theta,sz}^{proxy} \cdot \omega,\ \text{if}\ \ 0.1 < Da < 10: dynamic\ \ equilibrium \\ \lambda_{\theta,sz}^{proxy} \cdot K_{\mathrm{target}}^{proxy},\ \text{if}\ \ Da < 0.1: reaction - limited\ system \end{cases} \tag{12}$$

Note that (9), (10) and (12) suggest that K_{target}^{proxy} defines at least one of the two uncertainty bounds when estimating $\lambda_{\theta,\ sz}^{target}$ from $\lambda_{\theta,sz}^{proxy}$. Because ω converges to either 1 (one) or to K_{target}^{proxy}, when estimations of K_{target}^{proxy} yield magnitudes that are both less than 1 (one) and larger than 1 (one) (e.g., $K_{target}^{proxy} = 0.9 \pm 0.3$), such values will bound the estimation of $\lambda_{\theta,\ sz}^{target}$, i.e., $\lambda_{\theta,\ sz}^{\mathrm{proxy}}\ K_{\mathrm{target\ min}}^{proxy} \le \lambda_{\theta,\ sz}^{\mathrm{target}} \le \lambda_{\theta,\ sz}^{\mathrm{proxy}}\ K_{\mathrm{target\ max}}^{proxy}$. Otherwise, $\lambda_{\theta,\ sz}^{\mathrm{proxy}} \le \lambda_{\theta,\ sz}^{\mathrm{target}} \le \lambda_{\theta,\ sz}^{\mathrm{proxy}}\ K_{\mathrm{target\ max}}^{proxy}$ or $\lambda_{\theta,\ sz}^{proxy}\ K_{target\ \mathrm{min}}^{proxy} \le \lambda_{\theta,\ sz}^{target} \le \lambda_{\theta,\ sz}^{proxy}$. Describing the uncertainty in $\lambda_{\theta,\ sz}^{target}$ as a function of K_{target}^{proxy}, and using square brackets to indicate parameter ranges [min, max], the previous analysis can be summarized as:

$$\lambda_{\theta,\ sz}^{\mathrm{target}} = \begin{cases} [\lambda_{\theta,\ sz}^{\mathrm{proxy}}\ K_{\mathrm{target\ min}}^{proxy},\ \ \lambda_{\theta,\ sz}^{\mathrm{proxy}}],\ \text{if}\ \ K_{\mathrm{target}}^{proxy} = [<1,\ <1] \\ [\lambda_{\theta,\ sz}^{\mathrm{proxy}}\ K_{\mathrm{target\ min}}^{proxy},\ \ \lambda_{\theta,\ sz}^{\mathrm{proxy}}\ K_{\mathrm{target\ max}}^{proxy}],\ \text{if}\ \ K_{\mathrm{target}}^{proxy} = [<1,\ >1] \\ [\lambda_{\theta,\ sz}^{\mathrm{proxy}},\ \ \lambda_{\theta,\ sz}^{\mathrm{proxy}}\ K_{\mathrm{target\ max}}^{proxy}],\ \text{if}\ \ K_{\mathrm{target}}^{proxy} = [>1,\ >1] \end{cases} \tag{13}$$

Put in words, (12) and (13) show that the uncertainty in the estimation of $\lambda_{\theta,\ sz}^{target}$ is proportional to the uncertainty in the estimation of K_{target}^{proxy}. Also, the uncertainty in the transport conditions (i.e., model-based estimation of λ_{sz}^{proxy} and α_2) is less significant than (or bracketed by) the uncertainty in K_{target}^{proxy}.

3.4. Conclusions

We present an efficient method to estimate processing rates in streams that incorporates transport theory. The method consists of algebraic equations that can be easily implemented by researchers and practitioners in routine investigations of (bio)reactivity in stream ecosystems. The method requires estimates or measurements of the zeroth temporal moments of the upstream and downstream BTCs of a reactive solute (or plateau concentrations), the mean travel time in the stream reach (which is estimated with first temporal moments of a conservative solute) and an estimate of the Peclet number. However, the Peclet number is not needed (dispersion can be assumed effectively negligible) under some common transport conditions and, therefore, no computer modeling would be needed to estimate processing rates. The method is efficient because it does not require the calibration of other intermediate transport parameters, thus reducing the uncertainty in the estimated processing rates.

We also derived algebraic equations to estimate processing rates from one solute (proxy-tracer, $\lambda_{\theta,\,sz}^{\mathrm{proxy}}$) to another (target, $\lambda_{\theta,\,sz}^{\mathrm{target}}$). We showed that the relationship between the two rates is a function of the molar processing ratio of the target to the proxy-tracer (K_{target}^{proxy}) and the Dahmköhler number (Da). We analyzed the coupling between solute transport and in-stream processing within the three characteristic transport conditions defined by Da and showed that the uncertainty in the estimation of $\lambda_{\theta,\,sz}^{\mathrm{target}}$ is linearly proportional to the uncertainty in the estimation of K_{target}^{proxy}. Furthermore, the uncertainty in the transport parameters is less significant than the uncertainty in K_{target}^{proxy}. Altogether, our results show that only algebraic equations are needed to estimate processing rates in streams.

Acknowledgements

This work was funded by NSF grant EAR 08-38338.

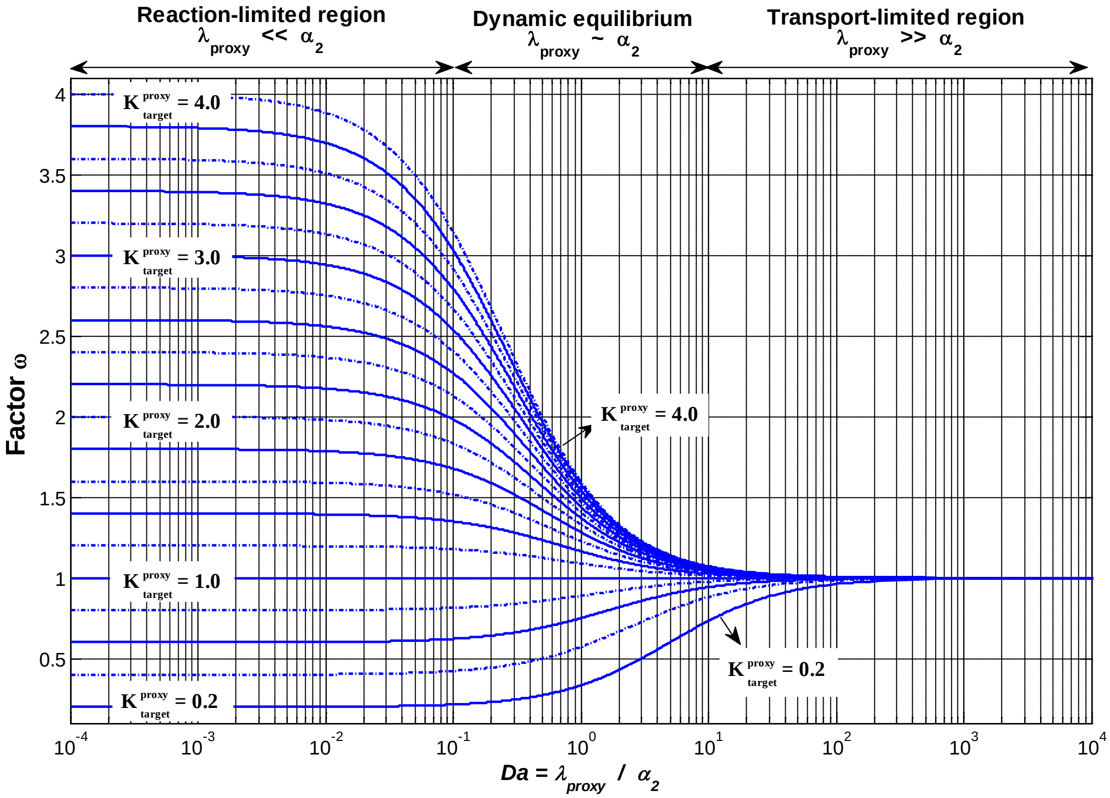

Figure 3.1. The scaling factor ω to estimate processing rates of a target solute ($\lambda_{\theta, sz}^{target}$) from a proxy-tracer ($\lambda_{\theta, sz}^{proxy}$) is a function of the molar uptake ratio K_{target}^{proxy} and the Da. The Da defines three characteristic regions under which solute transport and processing reactions operate. When the system is transport-limited, $\omega \to 1$, and $\lambda_{\theta, sz}^{target} \approx \lambda_{\theta, sz}^{proxy}$. When the system is reaction-limited, $\omega \to K_{target}^{proxy}$, and $\lambda_{\theta, sz}^{target} \approx \lambda_{\theta, sz}^{proxy} K_{target}^{proxy}$. Under 'dynamic-equilibrium' conditions, both hydrology and reactivity define the scaling factor ω, and $\lambda_{\theta, sz}^{target} \approx \lambda_{\theta, sz}^{proxy} \omega$.

References

Argerich, A., R. Haggerty, E. Martí, F. Sabater, and J. Zarnetske (2011), Quantification of metabolically active transient storage (MATS) in two reaches with contrasting transient storage and ecosystem respiration, *J. Geophys. Res.*, *116*(G3), G03034.

Briggs, M. A., L. K. Lautz, D. K. Hare, and R. González-Pinzón (2013), Relating hyporheic fluxes, residence times, and redox-sensitive biogeochemical processes upstream of beaver dams, *Freshw. Sci*., 622–641, doi:10.1899/12-110.1.

Camacho, L.A., González-Pinzón, R. (2008), Calibration and prediction ability analysis of longitudinal solute transport models in mountain streams, *J. Environ Fluid Mech., 8(5)*, 597-604.

Das, B.S., R.S. Govindaraju, G.J. Kluitenberg, A.J. Valocchi, and J.M. Wraith (2002), Theory and applications of time moment analysis to study the fate of reactive solutes in soil, in *Stochastic Methods in Subsurface Contaminant Hydrology*, edited by R.S. Govindaraju, ASCE Press, USA.

González-Pinzón, R., R. Haggerty and M. Dentz (2013), Scaling and predicting solute transport in streams, submitted to *Water Resour. Res*.

González-Pinzón, R., R. Haggerty, and D. D. Myrold (2012), Measuring aerobic respiration in stream ecosystems using the resazurin-resorufin system, *J. Geophys. Res*., 117, G00N06, doi:10.1029/2012JG001965.

Goudar, C. T., J. M. Piret, and K. B. Konstantinov (2011), Estimating cell specific oxygen uptake and carbon dioxide production rates for mammalian cells in perfusion culture, *Biotechnol. Prog*., 27, 1347-1357.

Haggerty, R., A. Argerich, and E. Marti (2008), Development of a "'smart'" tracer for the assessment of microbiological activity and sediment-water interaction in natural waters: The resazurin-resorufin system, *Water Resour. Res., 44, W00D01*, doi:10.1029/2007WR006670.

Haggerty, R., E. Marti, A. Argerich, D., von Schiller, and N. Grimm (2009), Resazurin as a "'smart'" tracer for quantifying metabolically active transient storage in stream ecosystems, *J. Geophys. Res*, 114, G03014, doi:doi:10.1029/2008JG000942.

Hall, R. O., E. S. Bernhardt, and G. E. Likens (2002), Relating nutrient uptake with transient storage in forested mountain streams, Limnol. Oceanogr, Vol. 47, 255–265.

Kelleher, C., T. W. Wagener, B. McGlynn, A. S. Ward, M. N. Gooseff, and R. A. Payn (2012), Stream characteristics govern the importance of transient storage processes, submitted to *Water Resour. Res*.

Kunkel, U., and M. Radke (2011), Reactive Tracer Test To Evaluate the Fate of Pharmaceuticals in Rivers, *Environ. Sci. Technol.*, *45*(15), 6296–6302, doi:10.1021/es104320n.

Lemke, D., P.-A. Schnegg, M. Schwientek, K. Osenbrück, and O. A. Cirpka (2013), On-line fluorometry of multiple reactive and conservative tracers in streams, *Environ. Earth Sci.*, doi:10.1007/s12665-013-2305-3.

Morel, F.M.M., and J.G. Hering (1993), *Principles and Applications of Aquatic Chemistry*, Wiley, New York.

Rao, P. S. C., M. D. Annable, and H. Kim (2000), NAPL source zone characterization and remediation technology performance assessment: recent developments and applications of tracer techniques, *J. Contam. Hydrol.*, *45*(1–2), 63–78, doi:10.1016/S0169-7722(00)00119-4.

Runkel, R. L. (2007), Toward a transport-based analysis of nutrient spiraling and uptake in streams, *Limnol. Oceanogr. Methods*, *5*, 50-62.

Sabatini, D. A., and T. A. Austin (1991), Characteristics of Rhodamine WT and Fluorescein as Adsorbing Ground-Water Tracers, *Ground Water*, *29*(3), 341–349, doi:10.1111/j.1745-6584.1991.tb00524.x.

Stanaway, D., R. Haggerty, S. Benner, A. Flores, and K. Feris (2012), Persistent metal contamination limits lotic ecosystem heterotrophic metabolism after more than 100 years of exposure: A novel application of the resazurin resorufin smart tracer, *Environ. Sci. Technol.*, 46(18), 9862–9871, doi:10.1021/es3015666.

Tank, J. L., E. J. Rosi-Marshall, M. A. Baker, and J. Robert O. Hall (2008), Are rivers just big streams? A pulse method to quantify nitrogen demand in a large river, *Ecology*, 89(10), 2935–2945.

Wagner, B. J. and J. W. Harvey (1997), Experimental design for estimating parameters of rate-limited mass transfer: Analysis of stream tracer studies, *Water Resour. Res.*, *33(7)*, 1731–1741, doi:10.1029/97WR01067.

Wagener, T., L.A. Camacho, and H.S. Wheater (2002), Dynamic identifiability analysis of the transient storage model for solute transport in rivers, *J. Hydroinf.*, *4(3)*, 199-211.

Zarnetske, J. P., R. Haggerty, S. M. Wondzell, V. A. Bokil, and R. González-Pinzón (2012), Coupled transport and reaction kinetics control the nitrate source-sink function of hyporheic zones, *Water Resour. Res.*, *48*, W11508, doi:10.1029/2012WR011894.

4. MEASURING AEROBIC RESPIRATION IN STREAM ECOSYSTEMS USING THE RESAZURIN-RESORUFIN SYSTEM

Ricardo González-Pinzón, Roy Haggerty and David D. Myrold

Journal of Geophysical Research - Biogeosciences

117, G3

DOI: 10.1029/2012JG001965

ABSTRACT

The use of smart tracers to study hydrologic systems is becoming more widespread. Smart tracers are compounds that irreversibly react in the presence of a process or condition under investigation. Resazurin (Raz) is a smart tracer that undergoes an irreversible reduction to resorufin (Rru) in the presence of cellular metabolic activity. We quantified the relationship between the transformation of Raz and aerobic bacterial respiration in pure culture experiments using two obligate aerobes and two facultative anaerobes, and in colonized surface and shallow (<10 cm) hyporheic sediments using reach-scale experiments. We found that the transformation of Raz to Rru was nearly perfectly (min $r^2 = 0.986$), positively correlated with aerobic microbial respiration in all experiments. These results suggest that Raz can be used as a surrogate to measure respiration *in situ* and *in vivo* at different spatial scales, thus providing an alternative to investigate mechanistic controls of solute transport and stream metabolism on nutrient processing. Lastly, a comparison of respiration and mass-transfer rates in streams suggests that field-scale respiration is controlled by the slower of respiration and mass transfer, highlighting the need to understand both biogeochemistry and physics in stream ecosystems.

4.1. Introduction

After three decades of active research coupling hydrology and stream ecology, the connection among stream solute transport, metabolism and nutrient dynamics is still unresolved. These knowledge gaps obscure the functioning of stream ecosystems and how those ecosystems interact with other landscape processes. To date, stream metabolism has been measured with techniques that have large uncertainties and are not spatially representative. Reach-scale approaches based on oxygen mass balance require a reaeration coefficient to estimate atmosphere-stream mass transfer, and correction for groundwater oxygen flux. These quantities can be highly uncertain. Because reaeration is a major component of oxygen mass balance, uncertain reaeration coefficients negatively affect the quantification of community respiration, particularly in headwater streams

[*Marzolf et al.,* 1994, 1998; *Aristegi et al.*, 2009]. Also, substantial groundwater inflows with relatively low concentrations of dissolved oxygen (*DO*) strongly bias estimates of community respiration [*McCutchan et al.*, 1998, 2002; *Hall and Tank*, 2005*; McCutchan and Lewis,* 2006]. Measuring accurate groundwater *DO* flux is technically and logistically challenging and this flux term is often neglected. Furthermore, correcting respiration rates by temperature might be misleading because metabolically active compartments typically experience significantly different diel changes [*e.g., Constantz,* 2008] than those where temperature is routinely measured during metabolism studies, i.e., above the streambed. On the other hand, direct measurement with respiration chambers is problematic because the sample volume is much smaller than the reach of interest, and because reproducing *in situ* hydrodynamic and heat transfer conditions is virtually impossible [*Bott et al.,* 1997; *Naegeli and Uehlinger,* 1997; *Aristegi et al.*, 2010]. Clearly, these limitations mask the true role of metabolism in nutrient processing and call for more robust techniques to improve our fundamental understanding of in-stream processes and how streams interact with other ecosystems.

With outstanding redox and fluorescent properties, the resazurin-resorufin system was introduced as a “smart tracer” in hydrology [*Haggerty et al.*, 2008, 2009]. Resazurin (Raz) is a redox-sensitive phenoxazine frequently used to estimate biological activity. In appropriate reducing conditions, Raz (blue in color) irreversibly loses an oxygen ion to become resorufin (Rru) (Figure 4.1). Rru (pink in color) also can undergo a further reduction to colorless dihydroresorufin, but this reaction is reversible by atmospheric oxygen and is mainly favored upon total consumption of Raz [*O’Brien et al.,* 2000; *Guerin et al.,* 2001]. Raz reacts in the presence of dehydrogenases, which are enzymes involved in many of the vital metabolic processes (catabolic and anabolic) of living organisms [*Liu,* 1986*; Strotman et al.,* 1993; *Zalata et al.*, 1998; *O’Brien et al.,* 2000]. *O´Brien et al.* [2000] found that Raz is reduced to Rru in a medium by cellular activity, but that a highly reduced medium without viable cells did not support the reduction.

In the last 25 years, some of the applications of Raz as a bioreactive tracer have included the detection of chemical toxicity [*Liu*, 1986], sludge activity in wastewater treatment [*Strotmann et al.,* 1993; *McNicholl et al.,* 2007], cell viability in mammals [*O'Brien et al.,* 2000], abundance of contaminant-degrading microorganisms [*Guerin et al.,* 2001], differentiation of aerobic and anaerobic bacteria [*Karakashev et al.,* 2003], detection of activity of disinfectants against biofilms [*Mariscal et al.,* 2009], seed viability assays [*Min and Kang,* 2011] and, most recently, cell counting in breast cancer treatment experiments [*Ziegler et al.,* 2011]. Particularly important for applications in hydrology and biogeochemistry, these studies reported that Raz can be reduced by strict aerobes, facultative anaerobes, aerotolerant and microaerophile organisms, but not by strict anaerobes.

Raz is a “smart” tracer because it provides information about the environment through which it travels that is specific to the process of interest [*Haggerty et al.,* 2008]. Raz is a promising tool to investigate physically different environments with respect to transient storage and stream metabolism (Figure 4.2). Using column experiments and batch reactors, the transformation rate of Raz was found to be ~1400-fold faster in hyporheic sediments than in the water column [*Haggerty et al.,* 2008], which agrees with the larger biomass abundance observed in sediments or surfaces compared to microbes suspended in the water column [*Findlay,* 2010]. A metabolically active transient storage (MATS) model [*Haggerty et al.,* 2009; *Argerich et al.,* 2011] based on the Raz-Rru system was developed to organize transient storage from a metabolically-based perspective, rather than from a physically-based perspective, as it was conceptualized before [*Bencala and Walters,* 1983; *Harvey et al.,* 1996; *Gooseff et al.,* 2005]. In a reach-scale study comparing distinctive types of transient storage, Raz was sensitive to differences in channel configuration and morphology [*Argerich et al.,* 2011].

Although Raz has been widely used to assess metabolic activity, to our knowledge no study has addressed how the transformation of Raz is related to cellular respiration. In this paper, we want to answer two questions. First, is the Raz-Rru transformation related quantitatively to aerobic respiration? Second, what does reach-scale Raz-Rru transformation tell us about reach-scale respiration?

4.2. Materials and Methods

4.2.1 Pure culture experiments:

4.2.1.1 Bacteria species:

Four species of bacteria were used. Two species are obligate aerobes: *Arthrobacter chlorophenolicus* A6, ATCC (700700) (*A. chlorophenolicus*), and *Sinorhizobium meliloti* 1021, ATCC (51124) (*S. meliloti*); the others are facultative anaerobes: *Bacillus subtilis* 168, ATCC (23857) (*B. subtilis*), and *Pseudomonas putida* KT2440, ATCC (47054) (*P. putida*). *A. chlorophenolicus* is a Gram-positive soil-dwelling bacterium with the ability to degrade chlorophenol [*Sahoo et al*., 2011a, 2011b]. *S. meliloti* is a Gram-negative soil bacterium capable of fixing nitrogen in root nodules [*Marketon et al.,* 2002]. *B. subtilis* is a Gram-positive soil and water-dwelling bacterium, commercially important for its highly concentrated production of the enzymes amylases and proteases [*Itaya and Tanala,* 1991]. *P. putida* is a Gram-negative, soil-dwelling bacterium, with the ability to degrade organic solvents [*Hill and Robinson,* 1975; *Jiménez et al.,* 2002].

Two to four days prior to each experiment, Luria Broth (LB) bacterial culture medium was prepared and sterilized. The medium was inoculated and incubated in the dark for two days at 24°C room-temperature for *A. chlorophenolicus, S. meliloti* and *B. subtilis,* and 37°C for *P. putida*. From here on, we will refer to the use of each species of bacteria as one experiment.

4.2.1.2 Bioreactors setup:

The day of each experiment, absorbance of the culture medium was measured on a Beckman Coulter (DU® 530) spectrophotometer at a wavelength of 660 nm (hereafter Abs_{660}). Abs_{660} showed no interferences with Raz or Rru signals, allowing measurement of growth for all four species. An initial optical density Abs_{660} = 0.050 was used as a target to determine the volume of inoculated medium to be added. Sterile media and a known concentration of Raz were also added to sterilized 500-mL Erlenmeyer flasks. All flasks were stocked with an initial liquid phase (i.e., LB medium, bacterial inoculum in LB medium, and DI-based Raz solution) of about half their total capacity. Flasks were wrapped in aluminum foil to prevent any photo-decay of Raz and Rru, as well as to provide a dark environment for the bacteria. Once the LB medium and Raz solution were added and mixed, flasks were sealed with septum stoppers. Within 20 min of the Raz addition, inoculated LB was injected through the septa to complete the total liquid. To maintain atmospheric pressure during the inoculated LB injection, an exit needle was inserted temporarily across the septum and was removed immediately afterwards. The flasks were then set on a rotary shaker table (Orbit Shaker, Lab-line) and agitated at 100 rpm. We refer to each flask filled with LB medium, Raz and bacterial inoculum as a bioreactor. Each experiment with a given species of bacteria had four replicates with identical volumes of LB medium and bacterial inoculum, but with different Raz concentrations (Table 4.1).

4.2.1.3 Experimental sampling and readings:

The experiments were run at room temperature (21°C to 23°C) for about six hours. The sampling in each of the four bioreactors consisted of taking eight to ten rounds of 1 mL gas samples to estimate CO_2 concentrations, and 8 mL of liquid samples. The liquid samples were taken for making measurements in three aliquots. The aliquots were 1 mL for cell growth measurement, 2 mL for Raz, Rru, and dissolved oxygen (*DO*) concentrations, and 5 mL for temperature and *pH*.

Gas samples were taken from the headspace of the bioreactor with a Hamilton Gastight® 500-µL syringe and stored in 2-mL septum vials (National Scientific), previously purged with 99.9% Argon. CO_2 samples were read within 24 h on a Hach-Carle (Series 100 AGC) gas chromatograph. Liquid samples were taken with BD™ Luer-Lock disposable syringes. Abs_{660} was read within 2 min of sampling from VWR® two-sided polystyrene cuvettes containing 1 mL of the unfiltered sample. The rest of the liquid samples were filtered with 0.2-µm polycarbonate Whatman® filter membranes to remove cells. *DO* was measured with a YSI ProODO probe and *pH* and temperature with a VWR® sympHony® *pH* Meter. The Raz and Rru samples were standardized to *pH* 8.5 by pouring 2 mL of the filtered sample into VWR® four-sided cuvettes and buffered (1:10

buffer-to-sample ratio) with ~1 M sodium phosphate [*Haggerty et al.*, 2008]. After each sample was buffered and vortexed (Fisher Scientific Vortex Genie 2), the fluorescence signals were measured with a Cary Eclipse Fluorescence Spectrophotometer (Agilent Technologies) within 10 min of sampling. The excitation/emission wavelengths for Raz and Rru were set to 602/632 nm and 571/584 nm, respectively. Initial conditions for all monitored parameters were measured before bacteria were added and before sealing the flasks with rubber stoppers.

4.2.1.4 Estimation of CO_2 production and DO consumption

We measured *DO* consumption from the amount of CO_2 generated. Before describing this method, we explain why we chose it. We first attempted to measure *DO* continuously inside the bioreactors using dip-type oxygen microelectrodes (MI-730 Microelectrodes Inc.); however, measurements with all bacteria species generated irregular readings that were affected by the agitation of the bioreactors and by biofouling of the probe membranes. We next tried to measure *DO* from unfiltered and filtered liquid samples extracted from the bio-reactors, but these methods suffered from inconsistencies due to continued cellular respiration (unfiltered samples) and reoxygenation (filtered samples). To overcome the difficulties of directly measuring *DO* consumption, we used the carbonate system as a proxy [e.g., *Morel and Hering*, 1993; *Goudar et al.*, 2011]. The assumption in this approach is that 1 mol CO_2 generated in the system resulted from cellular respiration of 1 mol O_2, i.e., we assumed a respiratory quotient of 1.0. Otherwise, equilibrium between the gas and liquid phases was guaranteed by the reaction rates and the mixing effects of the shaker table.

The carbonate system, i.e., gaseous carbon dioxide $CO_{2(g)}$, carbonic acid H_2CO_3, bicarbonate HCO_3^- and carbonate CO_3^{2-}, was balanced using the following reactions:

$$CO_{2(g)} \leftrightarrow CO_{2(aq)}, \tag{1}$$

$$CO_{2(aq)} + H_2O \leftrightarrow H_2CO_3. \tag{2}$$

For aqueous solutions, it is common to express (1) and (2) as:

$$CO_{2(g)} + H_2O \leftrightarrow H_2CO_{33}^{*};\ K_g = 10^{-1.47}\ , \tag{3}$$

where $H_2CO_{33}^{*} = CO_{2(aq)} + H_2CO_3$ and K_g is an equilibrium constant for standard conditions. The dissociation of carbonic acid and bicarbonate are shown in (4) and (5), where K_1 and K_2 are also equilibrium constants for standard conditions.

$$H_2CO_{33}^{*} \leftrightarrow HCO_{3\,3}^{-} + H^{+}; K_1 = 10^{-6.35}\ , \tag{4}$$

$$HCO_{3\,3}^{-} \leftrightarrow CO_{3}^{2-}{}_{3} + H^{+}; K_2 = 10^{-10.33}\ . \tag{5}$$

The total concentration of CO_2 in the system is:

$$CO_2 = H_2CO^{*}_{3\,3} + HCO^{-}_{3\,3} + CO_3^{2-}\ \ . \tag{6}$$

In these experiments we measured $CO_{2(g)}$ directly from the gas samples and estimated CO_2 using the previous equations and the *pH* of the liquid samples. To estimate the change of *DO* due to respiration, we assumed that *DO* consumption was inversely proportional to CO_2 production:

$$\frac{-dO_2}{dt} = \frac{dCO_2}{dt}\ . \tag{7}$$

The time-varying concentration of *DO* was estimated from (7), using the measured initial concentration of *DO*. For all experiments, the medium was saturated with *DO* before the addition of bacteria and *DO* concentration was a function of the temperature of the medium. To validate the use of the carbonate system to measure *DO* change, the final concentration of *DO* in each of the four bioreactors was measured directly in the liquid-phase with the YSI ProODO, no later than 1 min from the time that the bio-reactors were opened.

4.2.1.5 Estimation of Raz transformation (ΔRaz, ΔRru) and respiration (ΔDO)

We calculated the transformation of Raz as *ΔRaz* and *ΔRru*, and respiration activity (*ΔDO*) as normalized transformations with respect to their initial concentration. These values allowed us to compare the transformation of Raz by different microorganisms, independently of their metabolic patterns and the initial concentration of Raz.

$$\Delta Raz_t = \frac{Raz_0 - Raz_t}{Raz_0}, \quad (8) \qquad [0 \text{ at } t=0 \text{ and 1 when all Raz is transformed to Rru}]$$

$$\Delta Rru_t = \frac{Rru_t}{Raz_0}, \quad (9) \qquad [0 \text{ at } t=0 \text{ and 1 when all Raz is transformed to Rru}]$$

$$\Delta DO_t = \frac{DO_0 - DO_t}{DO_0}, \quad (10) \qquad [0 \text{ at } t=0 \text{ and 1 when all } DO \text{ is consumed}]$$

where subscript *t* represents a time-dependent variable and subscript *0* represents the initial value of each state-variable.

4.2.2 Reach-scale experiments:

To study the rates of Raz transformation mediated by diverse microorganism communities in stream ecosystems, we used benthic and shallow hyporheic sediments (<10 cm depth) collected in two watersheds located in the H.J. Andrews Experimental Forest. Watershed 1 (WS1) and Watershed 3 (WS3) are second-order tributaries of Lookout Creek, located in the western Cascade Mountains (Oregon, USA). A detailed description of the study sites has been presented by *Kasahara and Wondzell* [2003] and *Argerich et al.* [2011]. The two watersheds are less than 2 km apart and the stream reaches investigated were 81 m and 160 m long. Sediments smaller than pebbles were collected by hand from each watershed and placed in three rectangular fiberglass mesh bags of 25 cm x 45 cm x 7 cm. These sediments were incubated *in situ* for 10 d (WS1) and 7 d (WS3) (Figure 4.3). At each watershed, respiration chamber experiments were run for about 8 h, i.e., incubated sediments were placed in recirculating chambers closed to the atmosphere where Raz was injected and sampled through time. Oxygen consumption was measured instantaneously inside the chambers with YSI ProODO and HACH HQ40D probes, whereas Raz samples were collected, filtered, refrigerated at 4°C and then read within 72 h of sampling. Filtering and reading procedures were performed as described for pure culture experiments. *ΔRru* and *ΔDO* were estimated as previously described.

Although the experiments with respiration chambers are not accurate to estimate *in situ* respiration rates, these experiments provided an ideal set-up to eliminate reaeration effects from the oxygen mass balance. This allowed us to directly correlate the transformation of Raz and oxygen consumption by field microbial communities.

4.3. Results and Discussion

4.3.1 CO_2 production and cell growth in pure culture experiments

We estimated cellular CO_2 production ratios through time in the bioreactors, i.e., R_t $[mol\ L^{-1}\ abs^{-1}]$, to detect changes in metabolic activity due to the addition of the organic compound Raz. We used absorbance as a proxy to estimate the relative number of cells in each bioreactor [*Nerbrink et al.,* 1999; *Dalgaard and Koutsoumanis,* 2001].

$$R_t = CO_2(t) / Abs_{660}(t)\ . \tag{11}$$

These ratios were calculated for every sample and then normalized (R_N) with respect to those from the control bioreactor (R_{tc}) for each experiment.

$$R_N = R_t / R_{tc}\ . \tag{12}$$

Although this indirect estimator was not standardized for every species, i.e., we did not correlate Abs_{660} with absolute cell concentrations, a comparison of the normalized cellular CO_2 production rates (R_N) is adequate to evaluate changes in metabolic activity by adding Raz to the different species. We did not find significant changes, or patterns, in (R_N) as a function of the initial concentration of Raz at the 95% confidence interval (Figure 4.4), i.e., *p*-values from ANOVA F-tests > 0.05 in all cases (STATGRAPHICS®

Centurion XVI). This suggests that all bioreactors had similar metabolic activity; i.e., Raz neither stimulated nor inhibited respiratory activity.

Correlations between CO_2 concentration and cell growth are presented in Figure 4.5. The linear trends observed are due to the exponential CO_2 production (or oxygen consumption) and exponential cell growth observed during the experiments. This behavior is due to the short times elapsed between the incubation of the microorganisms and the performance of the experiments (2 d), and confirms that the microorganisms were in the exponential phase of growth [*Zwietering et al.,* 1990]. The differences in the slopes most likely reflect the efficiency with which the different bacterial species utilized the substrate found in the medium used and would likely vary if the medium constituents were changed.

4.3.2 Raz transformation and DO consumption

To relate quantitatively the transformation of Raz to cellular respiration, we plotted the results of ΔRru vs. ΔDO obtained in the pure culture experiments (Figure 4.6). Each plot shows results from all bioreactors used for a given species, i.e., three different initial concentrations of Raz for each. Table 4.2 shows the statistical significances of the regressions presented in Figure 4.6.

Figure 4.6 shows strong quantitative relationships between the transformation of Raz and cellular respiration for each of the species studied. However, the relationships were organism-dependent. These differences in the ability of bacteria to transform one mole of Raz, per mole of oxygen consumed, could be due to variations in the electron transport chains of the different bacterial species or, more likely, differences in Raz and *DO* uptake diffusivities for each bacterium. These results suggest that a quantitative relationship between Raz and *DO* must be found via calibration, i.e., a standard curve will have to be developed for Raz to be used as a bioassay for aerobic respiration. However, a Raz-based bioassay is not restricted to the use of pure cultures, because the transformation of Raz for multiple species can be characterized by a linear combination of the type of signals shown in Figure 4.6. We tested this hypothesis with field experiments.

Figure 4.7 and Table 4.2 present the results obtained from field chamber incubation experiments in WS1 and WS3 at the H.J. Andrews Experimental Forest, where Raz was transformed by a mixture of microbial communities present in the natural biofilms developed on the sediments. The field results are qualitatively similar to the lab results and are quantitatively bracketed by the lab results. Further, the field results are similar to each other. Although little can be concluded based on only two sets of field data, it does suggest strong similarities between the microbial communities present in the two streams, or at least that the rates of transformation of Raz were very similar. However, no information about microbial communities present at the sites was available from this or previous studies to resolve this duality. Regardless of the microbial communities present, we found a strong quantitative relationship between the transformation of Raz and microbial respiration.

4.3.3 Implications of hydrologic processes on field-scale use of Raz for measuring respiration

We now turn our attention to the how stream hydrology modifies respiration at the field scale and on the implications for use of Raz to measure respiration. In contrast to pure culture and chamber experiments where respiration is controlled by biologically mediated reactions, in stream ecosystems respiration is also controlled by hydrological processes [for related conclusions for both nutrients and respiration see *Harvey and Wagner*, 2000; *Gooseff et al.*, 2005; *Runkel*, 2007; *Argerich et al.*, 2011]. Assuming first-order reaction rates, quantitative approaches to estimate volume-weighted effective respiration rates yield expressions of the form [*Runkel*, 2007; *Botter et al.*, 2010; *Argerich et al.*, 2011]:

$$\lambda_{\theta}^{DO} = \beta\ f\ \frac{\lambda_b^{DO}\alpha_2}{\lambda_b^{DO} + \alpha_2} = \beta\ f\ \lambda_{eff}^{DO}\ , \tag{13}$$

where λ_{θ}^{DO} [T^{-1}] is the volume-weighted effective respiration rate in metabolically active zones or hotspots; β [-] is the volumetric ratio of transient storage and in-channel transport zones (or A_s/A as described by *Runkel* [2007] and *Botter et al.* [2010]); f [-] is the fraction of the transient storage zone that is metabolically active (or "hot"; e.g., [*McClain et al.*, 2003]); λ_{b}^{DO} [T^{-1}] is the biological respiration rate in metabolically active zones; α_2 [T^{-1}] is the mass-transfer rate between in-channel transport and transient storage zones (or $\alpha\, A/A_s$ as described by *Runkel* [2007] and *Botter et al.* [2010]); and λ_{eff}^{DO} [T^{-1}] is the effective respiration rate. Equation (13) could be applied to any dissolved bio-reactive compound that is taken-up through metabolic activity, but we restrict our discussion to *DO*.

Based on (13), we can infer an effective respiration rate (λ_{eff}^{DO}) in streams from the Raz-Rru system. To do so, we introduce a constant of proportionality to relate the biotic transformation rate of Raz (λ_{b}^{Raz}) with oxygen consumption (λ_{b}^{DO}). This constant, K_{DO}^{Raz}, is the inverse of the slope of the correlation between *ΔRaz* (or *ΔRru*) and *ΔDO* (cf. Figs. 6 and 7 and Table 4.2), i.e., $K_{DO}^{Raz} = \left(K_{Raz}^{DO}\right)^{-1}$:

$$\lambda_{\theta}^{DO} = \beta\ f\ \lambda_{eff}^{DO} = \beta\ f\ \frac{\left(K_{DO}^{Raz}\,\lambda_{b}^{Raz}\right)\alpha_2}{\left(K_{DO}^{Raz}\,\lambda_{b}^{Raz}\right)+\alpha_2}. \tag{14}$$

According to (14), the effective respiration rate (λ_{eff}^{DO}) will be reaction-limited when reaction rates (λ_{b}^{DO}) are small compared to mass-transfer rates (α_2), i.e., for relatively large values of α_2, (14) becomes $\lambda_{eff}^{DO} \to \lambda_{b}^{DO}$ (or $\lambda_{eff}^{DO} \to K_{DO}^{Raz}\,\lambda_{b}^{Raz}$). Conversely, the system will shift to a transport-limited condition when reaction rates are relatively large, i.e., $\lambda_{eff}^{DO} \to \alpha_2$ [*Argerich et al*, 2011]. Using ϕ as the relative fraction of effective uptake controlled by either λ_{b}^{DO} or α_2, Table 4.3 presents a quantitative analysis of biological and transport rate-control for effective respiration rates; note that $\lambda_b^{DO} / \alpha_2$ is used as a descriptor of rate-control in this analysis.

Table 4.3 shows that when biological and mass-transfer rates differ by one order of magnitude, the smallest rate controls the effective rate, i.e., for ϕ>0.9, $\lambda_{eff}^{DO} \approx \min(\lambda_b^{DO}, \alpha_2)$. The maximum efficiency of effective respiration for a particular reach (or stream) is achieved when biological and mass-transfer rates are balanced (i.e., $\lambda_b^{DO} / \alpha_2 = 1$). This suggests that instances of rate-control (ϕ>0.9) may be most prevalent after significant disturbances [e.g., *Sabater and Tockner*, 2010]. At other times, the metabolic activity of microbial communities (represented by λ_b^{DO}) is likely synchronized with the supply of nutrients and dissolved oxygen (regulated by α_2) to achieve a dynamic equilibrium [*Peterson et al.,* 2001; *Orr et al.,* 2009].

The use of smart tracers such as Raz and, in the near future, others such as synthetic DNA tracers [e.g., *Foppen et al.*, 2011], will help us to illuminate how effective respiration rates (or effective uptake rates in the case of nutrients) are affected at different temporal and spatial scales by stream management programs. Such effective uptake rates are direct indicators of stream functioning.

Estimating effective respiration rates with a tracer technique offers important advantages, compared to traditional methods. Raz allows us to separate and quantify with improved certainty the relative effects of biology and hydrologic exchange in stream respiration at different spatial and temporal scales. Tracer injections of Raz and a conservative tracer avoid the difficulties of measuring lateral inflows of dissolved oxygen by tributaries and groundwater seepage, which is particularly required to calculate oxygen mass balances in gaining streams [*McCutchan et al.,* 2002; *Hall and Tank,* 2005; *Reichert et al.,* 2009]. Since the transformation of Raz is directly proportional to oxygen consumption, regardless of the rate of metabolic activity, no assumption has to be made about the importance of diurnal temperature fluctuations controlling respiration rates, i.e., respiration can be actually measured at day and night times, which might be particularly important in streams with significant temperature differences from day to night.

4.4. Conclusions

We have introduced an alternative approach to estimate aerobic respiration in stream ecosystems using the smart tracer resazurin. This approach seeks to overcome important limitations of current methods in stream ecology, particularly, the sampling disturbance of *in situ* biological and hydrodynamic conditions, and the overlooking of well-understood biophysical controls. The use of Raz as a bio-reactive tracer to estimate metabolic activity enables us to integrate our knowledge of solute transport and stream metabolism, thus advancing our understanding of stream ecosystem functioning. Although this new approach needs further validation, it appears to have several advantages: 1) Raz is not naturally present in streams, the atmosphere or groundwater; 2) Raz is a compound that allows *in vivo* and *in situ* assays without altering microbial communities and hydrodynamic conditions; 3) Raz can be used at very low concentrations (~200 ppb at plateau concentrations), thus being a cost-effective technique, and 4) Raz follows the same flow paths as conservative tracers, allowing the partitioning between metabolically active and inactive transient storage.

Further research is needed to understand the nature of the different rates of Raz and oxygen uptake observed at the cellular scale, as well as the significance of such differences under natural conditions, i.e., in biofilms. Experimental research in different stream compartments and biomes is warranted to advance the use of Raz as a tracer to quantify stream respiration. Interestingly (and perhaps ironically), if Raz can be used to measure respiration in stream ecosystems, it could be used as a technique to estimate reaeration rates in reaches with negligible inputs of groundwater, i.e., a combination of upstream-downstream oxygen signals and Raz-based respiration measurements could be used to isolate the reaeration flux term in oxygen mass balances.

Acknowledgments

This work was funded by NSF grant EAR 08-38338. Funding for work in WS1 and WS3 was provided by the HJ Andrews Experimental Forest research program, funded by the National Science Foundation's Long-Term Ecological Research Program (DEB 08-23380), US Forest Service Pacific Northwest Research Station, and Oregon State University. We thank Sarah Acker and Jon Sanfilippo for lab and field assistance. We also thank Brian Wood and Stanley Gregory for allowing us to use lab equipment. Finally, we thank the anonymous reviewers who provided insightful comments on the manuscript. Bacterial strains were the gift of Janet Jansson (Lawrence Berkeley Natl. Lab., *A. chlorophenolicus* A6), Peter Zuber (Oregon Graduate Inst., *B. subtilis* 168), and Sharon Long (Stanford Univ., *S. meliloti* 1021).

Table 4.1. Experimental configuration to determine the relationship between Raz and oxygen uptake in pure culture experiments.

Experiment No.	Species of bacteria	Raz initial concentrations (μg L^{-1})	Average *DO* initial and final concentrations (mg L^{-1})
1	*B. subtilis*	0 (control), 50, 100, 150	8.2 – 1.5
2	*A. chlorophenolicus*	0 (control), 55, 110, 160	8.3 – 1.7
3	*P. putida*	0 (control), 100, 200, 300	8.5 – 4.8
4	*S. meliloti*	0 (control), 125, 235, 345	8.6 – 6.2

Table 4.2. Statistical results from *ΔRru* vs. *ΔDO* linear regressions in pure culture and field experiments. All regressions have a *p*-value < 0.001.

Species or site	Correlation coefficient	K_{Raz}^{DO} = slope of trend line	Standard error
B. subtilis	0.994	1.162	0.020
A. chlorophenolicus	0.986	1.004	0.038
P. putida	0.989	0.435	0.015
S. meliloti	0.988	2.348	0.076
WS1	0.997	1.717	0.038
WS3	0.990	1.428	0.058
WS1&WS3	0.989	1.552	0.046

Table 4.3. Quantitative analysis of rate-control on effective respiration rates in stream ecosystems[**].

Biological rate-control[♣♣] $\lambda_{eff}^{DO} \rightarrow \lambda_b^{DO}$	Transport rate-control $\lambda_{eff}^{DO} \rightarrow \alpha_2$	ϕ = fraction of respiration controlled by smaller rate $\phi = \lambda_{eff}^{DO} / \min(\lambda_b^{DO}, \alpha_2)$
$\lambda_b^{DO}/\alpha_2 = 1/49$	$\lambda_b^{DO}/\alpha_2 = 49$	0.98
$\lambda_b^{DO}/\alpha_2 = 1/9$	$\lambda_b^{DO}/\alpha_2 = 9$	0.90
$\lambda_b^{DO}/\alpha_2 = 1/4$	$\lambda_b^{DO}/\alpha_2 = 4$	0.80
$\lambda_b^{DO}/\alpha_2 = 1$	$\lambda_b^{DO}/\alpha_2 = 1$	0.50

[**] This analysis can be extended to other bio-reactive compounds by substituting *DO*

[♣♣] $\lambda_{eff}^{DO} = K_{DO}^{Raz} \lambda_b^{Raz}$

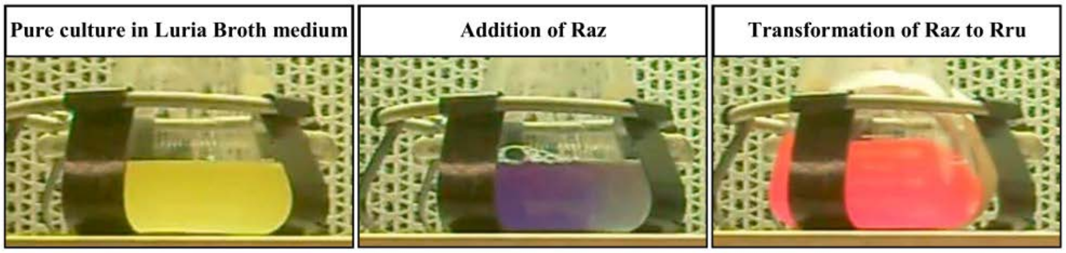

Figure 4.1. Resazurin (Raz) is irreversibly transformed to resorufin (Rru) by aerobic metabolism. The figure shows Raz being transformed by *Sinorhizobium meliloti* 1021.

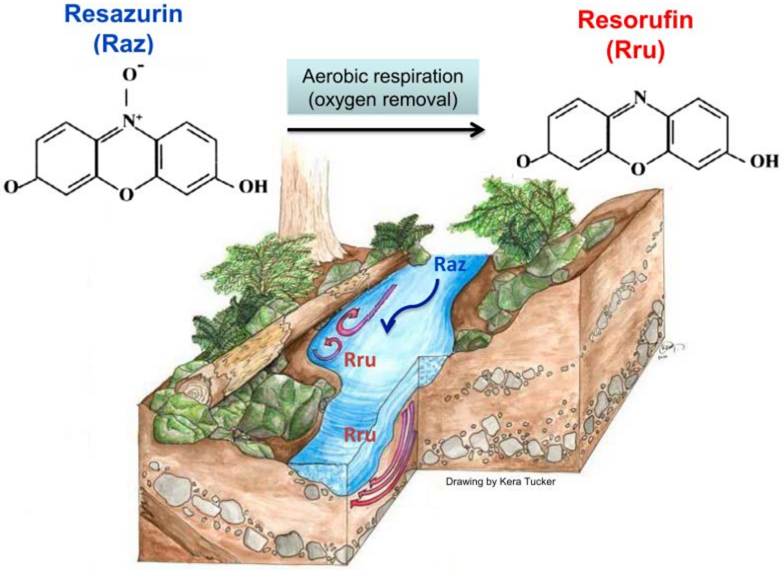

Drawing by Kera Tucker

Figure 4.2. The resazurin-resorufin (Raz-Rru) system can be used to estimate aerobic respiration in stream ecosystems. Raz is transformed to Rru in surface and hyporheic metabolically active zones.

Figure 4.3. Respiration chamber experiments conducted at the H.J. Andrews Experimental Forest to test the correlation between ΔRru and ΔDO. Left) fiberglass incubation meshes. Right) recirculating chamber with incubated sediments.

a) Aerobe. *A. chlorophenolicus* A6

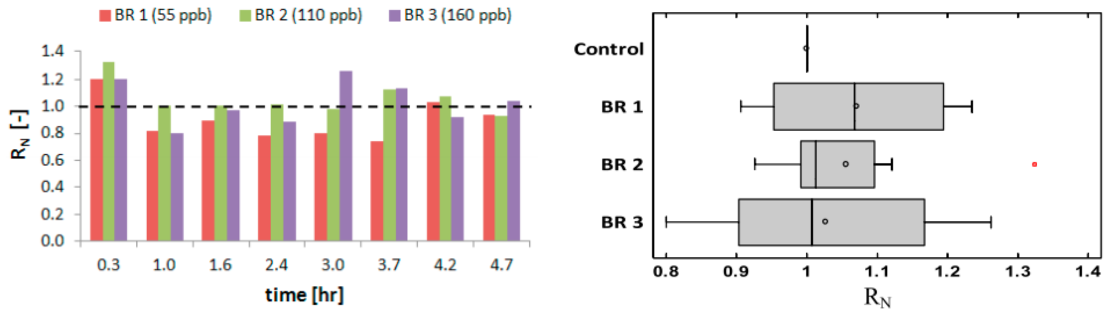

b) Facultative anaerobe. *P. putida KT2440*

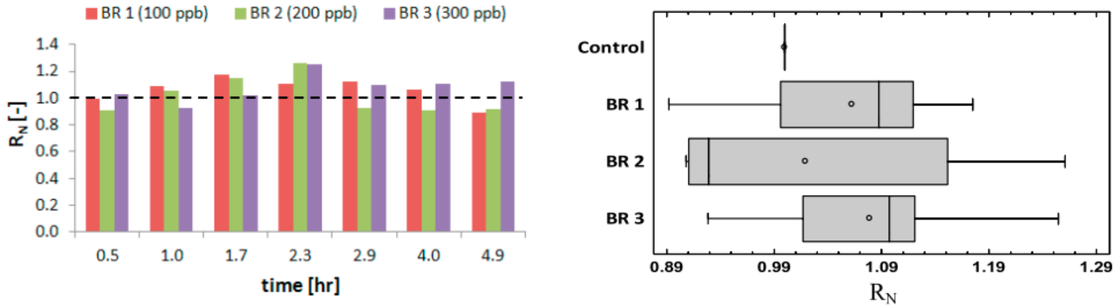

Figure 4.4. At the 95% confidence level, respiration is not a function of Raz at concentrations < 300 μg L^{-1}. The figure shows normalized cellular CO_2 production rates (R_N) relative to the control, for two species of bacteria and three different concentrations of Raz (cf. Table 4.1). a) *A. chlorophenolicus* A6. b) *P. putida KT2440*. Left) temporal variations with respect to the control bioreactor (dashed-line). Right) box-and-whisker plots of the same data.

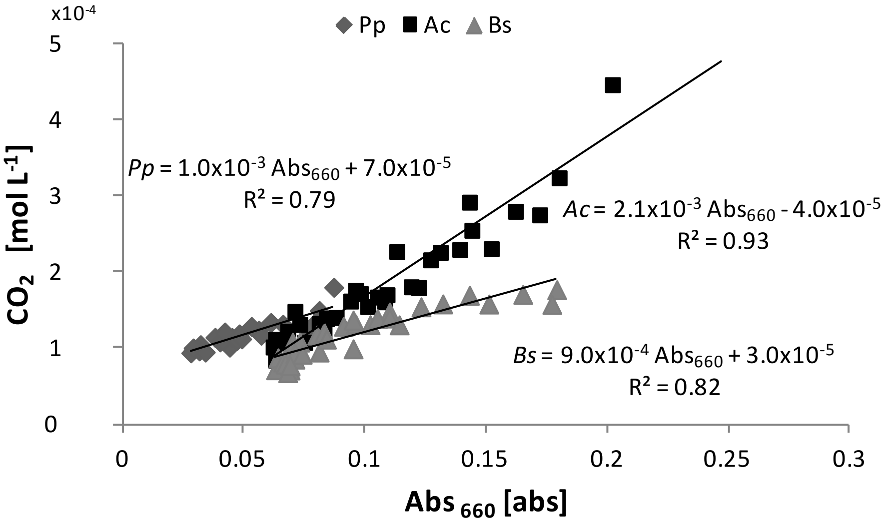

Figure 4.5. Correlation between *CO_2* production and cell growth for *P. putida* (*Pp*), *A. chlorophenolicus* (*Ac*) and *B. subtilis* (*Bs*). Data from the four bioreactors are included for each species.

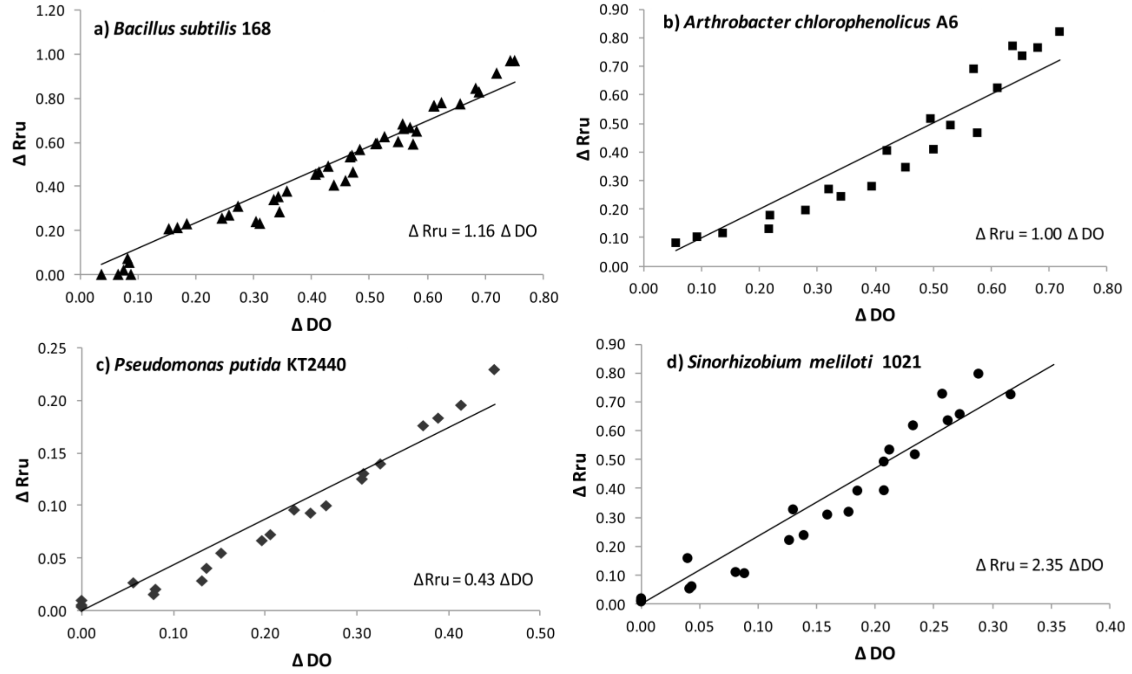

Figure 4.6. Raz transformation is linearly proportional to aerobic respiration in pure cultures. The figures show correlations between Raz transformation (as *ΔRru*) and cellular respiration (*ΔDO*) in pure culture experiments. Linear trend-lines, valid over the entire range of *DO,* are presented to facilitate the discussion. Power-law trend-lines with exponents between 1 and 1.3 also fit the data, and such behavior was previously discussed by *Haggerty et al.* [2009, cf. eqn. 5-7].

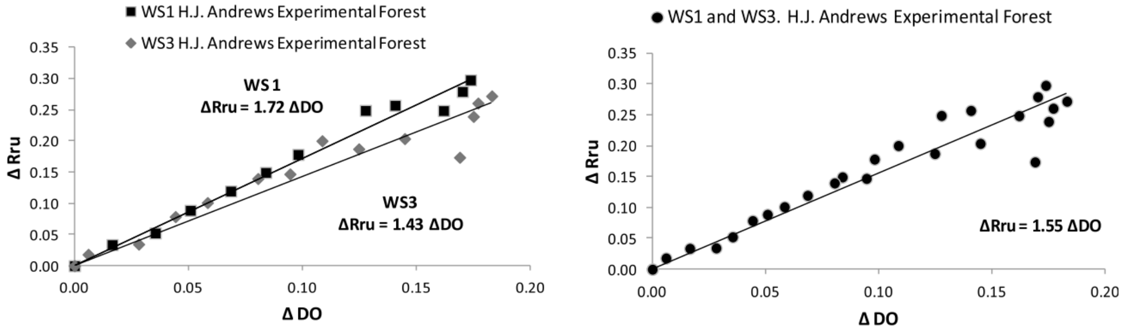

Figure 4.7. Raz transformation is linearly proportional to aerobic respiration in stream sediments. The figure shows a reach-scale experimental correlation between Raz transformation (as *ΔRru*) and cellular respiration (*ΔDO*). Left) regressions for experiments in two streams. Right) regression including both streams.

References

Argerich, A., R. Haggerty, E. Martí, F. Sabater, and J. Zarnetske (2011), Quantification of metabolically active transient storage (MATS) in two reaches with contrasting transient storage and ecosystem respiration, *J. Geophys. Res*., 116, G03034, doi:10.1029/2010JG001379.

Aristegi, L., O. Izagirre, and A. Elosegi (2009), Comparison of several methods to calculate reaeration in streams, and their effects on estimation of metabolism, *Hydrobiologia*, 635, 113–124.

Aristegi, L., O. Izagirre, and A. Elosegi (2010), Metabolism of Basque streams measured with incubation chambers, *Limnetica*, 29, 301-310.

Bencala, K. E., and R. A. Walters (1983), Simulation of solute transport in a mountain pool-and-riffle stream: a transient storage model, *Water Resour*. *Res*., 19, 718-724.

Bott, T. L., J. T. Brock, A. Baattrup-Pedersen, P. A. Chambers, W. K. Dodds, K. T. Himbeault, J. R. Lawrence, D. Planas, E. Snyder, and G. M Wolfaardt (1997), An evaluation of techniques for measuring periphyton metabolism in chambers, *Can. J. Fish. Aquat. Sci.*, 54, 715-725.

Botter, G., N. B. Basu, S. Zanardo, P. S. C. Rao, and A. Rinaldo (2010), Stochastic modeling of nutrient losses in streams: Interactions of climatic, hydrologic, and biogeochemical controls, *Water Resour. Res.*, 46, W08509, doi:10.1029/2009WR008758.

Constantz, J. (2008), Heat as a tracer to determine streambed water exchanges, *Water Resour. Res.*, 44, W00D10, doi:10.1029/2008WR006996.

Dalgaard P., K. Koutsoumanis (2001), Comparison of maximum specific growth rates and lag times estimated from absorbance and viable count data by different mathematical models, *J. Microbiol. Methods*, 43, 183–196.

Findlay, S. (2010), Stream microbial ecology, *J. N. Am. Benthol. Soc*., 29, 170–181.

Foppen, J. W., C. Orup, R. Adell, V. Poulalion, and S. Uhlenbrook (2011), Using multiple artificial DNA tracers in hydrology, *Hydrol. Process.*, 25, 3101-3106.

Gooseff, M. N., J. LaNier, R. Haggerty, and K. Kokkeler (2005), Determining in-channel (dead zone) transient storage by comparing solute transport in a bedrock channel-alluvial channel sequence, Oregon, *Water Resour. Res*., 41, W06014, doi:10.1029/2004WR003513.

Goudar, C. T., J. M. Piret, and K. B. Konstantinov (2011), Estimating cell specific oxygen uptake and carbon dioxide production rates for mammalian cells in perfusion culture, *Biotechnol. Prog*., 27, 1347-1357.

Guerin, T., M. Mondido, B. McClenn, and B. Peasley (2001), Application of resazurin for estimating abundance of contaminant-degrading micro-organisms, *Lett. Appl. Microbiol.*, 32, 340-345.

Haggerty, R., A. Argerich, and E. Martí (2008), Development of a ‘‘smart’’ tracer for the assessment of microbiological activity and sediment-water interaction in natural waters: The resazurin-resorufin system, *Water Resour. Res*., 44, W00D01, doi:10.1029/2007WR006670.

Haggerty, R., E. Martí, A. Argerich, D. von Schiller, and N. Grimm (2009), Resazurin as a ‘‘smart’’ tracer for quantifying metabolically active transient storage in stream ecosystems, *J. Geophys. Res.*, 114, G03014, doi:10.1029/2008JG000942.

Hall, R. O., and J. L Tank (2005), Correcting whole-stream estimates of metabolism for groundwater input, *Limnol. and Oceanogr. Methods*, 3, 222-229.

Harvey, J. W., B. J. Wagner, and K. Bencala (1996), Evaluating the reliability of the stream tracer approach to characterize stream-subsurface water interactions, *Water Resour. Res*., 32, 2441-2451.

Harvey, J.W., and B.J. Wagner (2000), Quantifying hydrologic interactions between streams and their subsurface hyporheic zones, in: *Streams and Ground Waters*, edited by Jones, J.B., and P.J. Mulholland, Academic Press: London, pp. 3-44.

Hill, G. A., and C. W. Robinson (1975), Substrate inhibition kinetics - phenol degradation by Pseudomonas-putida, *Biotechnol. Bioeng*., 17, 1599-1615.

Itaya, M., and T. Tanaka (1991), Complete physical map of the Bacillus subtilis 168 chromosome constructed by a gene-directed mutagenesis method, *J. Mol. Biol*., 220, 631-648.

Jiménez, J. I., B. Miñambres, J. L. García, and E. Díaz (2002), Genomic analysis of the aromatic catabolic pathways from Pseudomonas putida KT2440, *Environ. Microbiol*., 4, 824-841.

Karakashev, D., D. Galabova, and I. Simeonov (2003), A simple and rapid test for differentiation of aerobic from anaerobic bacteria, *World J. Microbiol. Biotechnol.*, 19, 233-238.

Kasahara, T., and S. M. Wondzell (2003), Geomorphic controls on hyporheic exchange flow in mountain streams, *Water Resour. Res*., 39, 1005, doi:10.1029/2002WR001386.

Liu, D (1986), Resazurin reduction method for toxicity assessment of water soluble and insoluble chemicals, *Toxic. Assess*, 1, 253-258.

Mariscal, A., R. Lopez-Gigosos, M. Carnero-Varo, and J. Fernandez-Crehuet (2009), Fluorescent assay based on resazurin for detection of activity of disinfectants against bacterial biofilms, *Appl. Microbiol. Biotechnol*., 82, 773-783.

Marketon, M. M., M. R. Gronquist, A. Eberhard, and J. E. González (2002), Characterization of the sinorhizobium meliloti sinR/sinI locus and the production of novel N-Acyl homoserine lactones, *J. Bacteriol*., 184, 5686–5695.

Marzolf, E. R., P. J. Mulholland, and A. D. Steinman (1994), Improvements to the diurnal upstream-downstream dissolved oxygen change technique for determining whole-stream metabolism, *Can. J. Fish Aquat. Sci*., 51, 1591-1599.

Marzolf, E. R., P. J. Mulholland and A. D. Steinman (1998), Reply: Improvements to the diurnal upstream-downstream dissolved oxygen change technique for determining whole-stream metabolism in small streams, *Can. J. Fish Aquat. Sci.,* 55, 1786-1787.

McClain, M. E., et al. (2003), Biogeochemical hot spots and hot moments at the interface of terrestrial and aquatic ecosystems, *Ecosystems, 6*(4), 301-312.

McCutchan, J., W. Lewis, and J. Saunders (1998), Uncertainty in the estimation of stream metabolism from open-channel oxygen concentrations, *J.N. Am. Benthol. Soc*, 17, 155-164.

McCutchan, J. H., and W. M. Lewis (2006), Groundwater flux and open-channel estimation of stream metabolism: response to Hall and Tank, *Limnol. Oceanogr Methods*, 4, 213-215.

McCutchan, J., J. F. Saunders III, W. M. Lewis Jr., and M. G. Hayden (2002), Effects of groundwater flux on open-channel estimates of stream metabolism, *Limnol. Oceanogr.*, 47, 321-324.

McNicholl, B. P., J. W. McGrath, and J. P. Quinn (2007), Development and application of a resazurin-based biomass activity test for activated sludge plant management, *Water Res.*, 41, 127–133.

Min, T. G., and W. S. Kang (2011), Simple, quick and nondestructive method for Brassicaceae seed viability measurement with single seed base using resazurin, *Hortic., Environ. Biotechnol.*, 52, 240-245.

Morel, F.M.M., and J.G. Hering (1993), *Principles and Applications of Aquatic Chemistry*, Wiley, New York.

Naegeli, M. W., and U. Uehlinger (1997), Contribution of the hyporheic zone to ecosystem metabolism in a prealpine gravel-bed-river, *J.N. Am. Benthol. Soc*, 16, 794-804.

Nerbrink, E., E. Borch, H. Blom, and T. Nesbakken (1999), A model based on absorbance data on the growth rate of Listeria monocytogenes and including the effects of pH, NaCl, Nathe lactate and Na-acetate, *Int. J. Food Microbiol.*, 47, 99–109.

O'Brien, J., I. Wilson, T. Orton, and F. Pognan (2000), Investigation of the Alamar Blue (resazurin) fluorescent dye for the assessment of mammalian cell cytotoxicity, *Eur. J. Biochem*., 267, 5421-5426.

Orr, C. H., J. J. Clark, P. R. Wilcock, J. C. Finlay, and M. W. Doyle (2009), Comparison of morphological and biological control of exchange with transient storage zones in a field-scale flume, *J. Geophys. Res.*, 114, G02019, doi:10.1029/2008JG000825.

Peterson, B. J., W. M. Wollheim, P. J. Mulholland, J. R. Webster, J. L. Meyer, J. L. Tank, E. Martí, W. B. Bowden, H. M. Valett, A. E. Hershey, W. H. McDowell, W. K. Dodds, S. K. Hamilton, S. Gregory, and D. D. Morrall (2001), Control of nitrogen export from watersheds by headwater streams, *Science*, 292, 86-9.

Reichert, P., U. Uehlinger, and V. Acuña (2009), Estimating stream metabolism from oxygen concentrations: Effect of spatial heterogeneity, *J. Geophys. Res.*, 114, G03016, doi:10.1029/2008JG000917.

Runkel, R. L (2007) Toward a transport-based analysis of nutrient spiraling and uptake in streams, *Limnol. Oceanogr: Methods*, 5, 50-62.

Sabater, S., and K. Tockner (2010) Effects of hydrologic alterations on ecological quality of river ecosystems, in: *The Handbook of Environmental Chemistry: Water Scarcity in the Mediterranean,* edited by Barceló Damia and A. G. Kostianoy, Springer Berlin: Heidelberg, pp. 15-39.

Sahoo, N. K., K. Pakshirajan, P. K. Ghosh, and A. Ghosh (2011), Biodegradation of 4-chlorophenol by Arthrobacter chlorophenolicus A6: effect of culture conditions and degradation kinetics, *Biodegradation*, 22, 275-286.

Sahoo, N. K., K. Pakshirajan, and P. K. Ghosh (2011), Biodegradation of p-nitrophenol using Arthrobacter chlorophenolicus A6 in a novel upflow packed bed reactor, *J. Hazard. Mater.,* 190, 729-737.

Strotmann, U. J., B. Butz, and W. R. Bias (1993) A dehydrogenase assay with resazurin-practical performance as a monitoring-system and pH-dependent toxicity of phenolic-compounds, *Ecotoxic Environ. Safe*., 25, 79-89.

Zalata, A. A., N. Lammertijn, A. Christophe, and F. H. Comhaire (1998), The correlates and alleged biochemical background of the resazurin reduction test in semen, *Int J. Androl*, 21, 289-294.

Ziegler, V. G., J. Knaup, D. Stahl, B. Krammer, and K. Plaetzer (2011), Fluorescence detection and depletion of T47D breast cancer cells from human mononuclear cell-enriched blood preparations by photodynamic treatment: basic in vitro experiments towards the removal of circulating tumor cells, *Lasers Surg. Med.,* 42, 548-556.

Zwietering, M. H., I. Jongenburger, F. M. Rombouts, and K. van 't Riet (1990), Modeling of the Bacterial Growth Curve, *Appl. Environ. Microbiol*., 56, 1875–1881.

5. QUANTIFYING SPATIAL DIFFERENCES IN METABOLISM IN HEADWATER STREAMS

Ricardo González-Pinzón, Roy Haggerty and Alba Argerich

For submission to Freshwater Biology

ABSTRACT

Stream functioning is characterized by the simultaneous interaction among solute transport, nutrient processing, and metabolism. Metabolism is measured with methods that have limited spatial representativeness and are highly uncertain. These problems restrict the development of methods for upscaling biological processes that mediate nutrient processing. We use the resazurin-resorufin (Raz-Rru) tracer system to estimate metabolism at different spatial scales (habitat, subreach and reach) in two headwater streams of the H. J. Andrews Experimental Forest (Oregon, USA), and present a mathematical framework for its application. We investigate the relationship between metabolism and hydrodynamics, i.e., geomorphic units (e.g., pool-riffle, pool-cascade), bed materials (i.e., alluvium vs. bedrock channels) and type of transient storage (i.e., pure hyporheic exchange, pure surface transient storage and a combination of both). The metabolic hot spots detected by the Raz-Rru system were related to hydrodynamic conditions known to increase biological processing (e.g., hyporheic flow and flow through large woody debris). Because such hydrodynamic conditions and their effects on stream processing are difficult to quantify in headwater streams without the use of tracer techniques, the Raz-Rru system proved to be a good integrator of solute transport and stream metabolism processes.

5.1. Introduction

Headwater streams drain 60 – 80% of the terrestrial landscape [*Benda et al.*, 2005], play an important role in global carbon and nutrient cycles [*Triska et al.*, 1989; *Dent et al.*, 2001; *Battin et al.*, 2009; *Zarnetske et al.*, 2012] and provide ecosystem services such as water supply, flood control and recreation [*Lowe and Likens*, 2005]. Headwater streams continuously exchange nutrients, substrates, heat and oxygen with aquifers and with the atmosphere, primarily due to large topographic gradients and coarse sediments [*Elliott and Brooks*, 1997; *Morrice et al.*, 1997; *Peterson et al.*, 2001; *Alexander et al.*, 2007; *MacDonald and Coe*, 2007; *Meyer et al.*, 2007]. These interactions enhance the development of a wide range of microbial communities that, according to recent estimates, maintain the largest biofilm density associated with streambed surfaces and the highest rate of metabolic processing of all lotic systems in the whole river continuum [*Battin et al.*, 2003, 2008; *Bottacin-Busolin et al.*, 2009].

The same biogeochemical properties that make headwater streams highly valuable challenge us when quantifying mass and heat budgets. Headwater streams are characterized by heterogeneous geomorphic and biochemical properties. Because the classic hydrodynamics theory (developed for alluvial channels) is not directly applicable in headwater streams, in the last three decades many researchers have worked on new methods and techniques to model the flow of water through these systems [*Bathurst*, 1985; *Thome and Zevenbergen*, 1985; *Jarrett*, 1990; *Stone and Hotchkiss*, 2007; *Baki et al.*, 2012]. Advances also have taken place in stream solute transport theory [*Beer and Young*, 1983; *Bencala and Walters*, 1983; *Haggerty et al.*, 2002; *Boano et al.*, 2007]. Even after the advent of remote sensing and progress in computing, most of the challenges of studying headwater streams are linked to the difficulty of measuring their geomorphic properties, which are characterized by large-scale heterogeneities (e.g., boulders and large woody debris), high canopy densities which limit the use of remote sensing, irregular bank delineations, and even complete subsurface (hyporheic) flows nearby topographic breakpoints [*Montgomery and Buffington*, 1997; *Adams and Spotila*, 2005; *Wörman et al.*, 2007; *Jiménez and Wohl*, 2013].

Stream functioning is characterized by the simultaneous interaction among solute transport, metabolism and nutrient processing [*Cummins*, 1974; *Young and Huryn*, 1999; *Peterson et al.*, 2001; *Allan and Castillo*, 2007; *Aristegi et al.*, 2009]. Stream metabolism accounts for the fluxes of oxygen and carbon through primary production and community respiration. Therefore, estimates of metabolism are necessary to quantify stream carbon budgets. Additionally, they provide useful information about the ‘health’ of the ecosystem [*Young et al.*, 2008] and routine measures of respiration and primary production are being incorporated in monitoring programs to assess the success of restoration projects and the effects of perturbations [*Bunn et al.*, 2010].

Stream metabolism is estimated with oxygen mass balances, which depend on metabolic processes, stream-atmosphere mass transfer (reaeration), and stream-groundwater interactions [*McCutchan et al.*, 2002; *Bott*, 2007; *Reichert et al.*, 2009]. Quantifying stream oxygen fluxes is difficult because of the elevated background oxygen concentrations in the stream and in the atmosphere, and also because of the multiple existing pathways for production and consumption [*Reichert et al.*, 2009; *Riley and Dodds*, 2013]. Moreover, logistical challenges restrict the use of stable isotopes (e.g., ^{18}O) for routine estimations of stream metabolism, either for technical or scientific applications [*Tobias et al.*, 2007].

All other hydrodynamic and thermodynamic conditions being equal, respiration drives surface-atmosphere mass transfer (both day and night), which tends to equilibrate the imbalance produced by respiration. Therefore, respiration should be the targeted process for estimating metabolism, instead of the estimation of reaeration rates (*status quo*), which are known to be highly uncertain.

The use of theoretical approaches to estimate reaeration rates have generally resulted in highly uncertain predictions of stream-atmosphere mass transfer [*Kilpatrick et al.*, 1989; *Genereux and Hemond*, 1992; *Melching and Flores*, 1999; *Jha et al.*, 2004; *Aristegi et al.*, 2009]. Also, measuring reaeration can be technically challenging and, therefore, numerous empirical methods based on geomorphic parameters have been proposed [*Grace and Imberger*, 2006; *Raymond et al.*, 2012; *Demars and Manson*, 2013]. In an extensive review, *Aristegi et al.* [2009] studied 21 streams with a wide range of hydrodynamic conditions in northern Spain and measured metabolism using several methods to estimate reaeration rates, i.e., night-time regression, lag between noon and peak oxygen concentration and 10 empirical equations based on stream geomorphic conditions. These analyses showed that uncertain estimates of reaeration rates could result in uncertainties in the estimation of gross primary production (GPP), community respiration (R) and net metabolism (NM) with magnitudes even larger than the estimated values (e.g., $GPP = 16.6 \pm 19.6$; $R = 18.6 \pm 18$; $\mathrm{NM} = -2.0 \pm 9.4$ [g O_2 m^2 d^{-1}]; see Table 6 in *Aristegi et al.* [2009]). Altogether, these observations suggest that carbon budgets and assessments of human impacts on stream metabolism and nutrient processing are impaired by reliable estimations of reaeration rates.

To address some of these challenges, we have introduced the resazurin-resorufin (Raz-Rru) system as an alternative technique for measuring metabolism in headwater streams [*Haggerty et al.*, 2008, 2009; *Argerich et al.*, 2011; *González-Pinzón et al.*, 2012; *Stanaway et al.*, 2012; *Haggerty*, 2013; *Lemke et al.*, 2013]. Some of the advantages of this smart tracer system are: 1) the irreversible reaction of Raz to Rru is known to be mediated by cellular respiration [*González-Pinzón et al.*, 2012] and, therefore, this tracer technique can be used to measure respiration directly (in contrast to conventional techniques that rely on the net change in oxygen to estimate respiration); 2) Raz, being a tracer, can be used to investigate metabolism *in situ* and *in vivo* at different spatial scales; 3) processing Raz/Rru samples can be as easy as deploying a fluorometer in the field or in the lab to record highly accurate changes in tracer concentrations [*Lemke et al.*, 2013]; and 4) the Raz-Rru system can be easily coupled with other biogeochemical processes of interest, for example, nutrient processing, environmental effects of emerging contaminants and biochemical oxygen demand from waste water discharges.

In this paper we describe how the Raz-Rru system can be used to quantify metabolism and to detect hot spots in stream ecosystems. We then apply this approach in two headwater streams of the H.J. Andrews Experimental Forest (OR, USA).

5.2. Estimating Rates and Fluxes of Metabolism from the Transformation of Raz

In this section we describe how the transformation of Raz can be used to estimate rates and fluxes of respiration, reaeration and primary production. First, we estimate respiration rates and fluxes using Raz as a proxy-tracer for dissolved oxygen (DO). Then, we estimate the other two components of metabolism using night-time and day-time DO mass balances.

5.2.1. Estimating rates of respiration

González-Pinzón and Haggerty [2013] developed an efficient method to use Raz transformation rates in streams to measure aerobic respiration rates, λ_{resp}. Assuming that respiration in the water column and dispersion are negligible [cf. *Wörman et al.*, 2002; *Runkel*, 2007; *Argerich et al.*, 2011], λ_{resp} [T^{-1}] can be estimated as:

$$\lambda_{\theta,\,sz}^{\mathrm{Raz}} = \frac{\ln[m_{o,Raz}^{up} \big/ m_{o,Raz}^{dn}]}{\tau} \;, \tag{1}$$

$$\lambda_{resp} = \begin{cases} [\lambda_{\theta,\,sz}^{\mathrm{Raz}}\, K_{\mathrm{DO\ min}}^{Raz},\;\; \lambda_{\theta,\,sz}^{\mathrm{Raz}}],\ \text{if}\ \ K_{\mathrm{DO}}^{Raz} = [<1,\ <1] \\ [\lambda_{\theta,\,sz}^{\mathrm{Raz}} K_{\mathrm{DO\ min}}^{Raz},\;\; \lambda_{\theta,\,sz}^{\mathrm{Raz}}\ K_{\mathrm{DO\ max}}^{Raz}],\ \text{if}\ \ K_{\mathrm{DO}}^{Raz} = [<1,\ >1] \\ [\lambda_{\theta,\,sz}^{\mathrm{Raz}}\,,\;\; \lambda_{\theta,\,sz}^{\mathrm{Raz}}\ K_{\mathrm{DO\ max}}^{Raz}],\ \text{if}\ \ K_{\mathrm{DO}}^{Raz} = [>1,\ >1] \end{cases}, \tag{2}$$

where $\lambda_{\theta,\,sz}^{\mathrm{Raz}}$ [T^{-1}] is the volume-averaged transformation rate of Raz in the storage zone , square brackets indicate parameter ranges [min, max], $m_{o,Raz}^{up}$ and $m_{o,Raz}^{dn}$ are the zeroth temporal moments of the upstream and downstream breakthrough curves (BTCs) of Raz [M T L^{-3}], τ is the mean travel time in the stream reach [T], and K_{DO}^{Raz} is the the molar processing ratio of DO to Raz [moles DO processed / moles Raz processed].

Normalized central moments of order *n* ($\overline{m_n}$) can be estimated from experimental BTCs as [*Das et al.*, 2002]:

$$\overline{m_n} = \sum_{j=1}^{r} \left(0.5t_k + 0.5t_{k+1}\right)^n \left(0.5C_k + 0.5C_{k+1}\right)\left(t_{k+1} - t_k\right), \tag{3}$$

where $C(t)$ [ML^{-3}] is the measured concentration at time t [T]; *j* [-] is an index and *r* [-] the total number of observations. The mean travel time τ between two sampling locations can be estimated with the conservative tracer BTCs as:

$$\tau = \frac{m_{1,cons}^{dn}}{m_{o,cons}^{dn}} - \frac{m_{1,cons}^{up}}{m_{o,cons}^{up}}. \tag{4}$$

5.2.2. Estimating rates of reaeration and primary production

Once the respiration rate $\lambda_{resp.}$ is estimated, reaeration and GPP can also be estimated from nighttime and daytime oxygen mass balances. Nighttime oxygen fluxes are only a function of respiration, reaeration and groundwater inputs because GPP is zero. Conventionally, we obtain independent estimates of the last two fluxes to solve for respiration, but it has been shown that these fluxes are highly uncertain and lead to poorly constrained estimations of stream metabolism [*Marzolf et al.*, 1994; *Hall and Tank*, 2005; *McCutchan and Lewis*, 2006; *Aristegi et al.*, 2009; *Riley and Dodds*, 2013]. In this regard, three advantages of using the Raz-Rru system to estimate stream metabolism are: 1) respiration can be directly measured at day or night, 2) independent estimations of the reaeration coefficient are not required, and 3) uncertainties in the estimation of metabolism can be explicitly accounted for.

The oxygen mass balance for a parcel of water flowing between two stations can be described as [*McCutchan et al.*, 2002; *McCutchan and Lewis*, 2006]:

$$\frac{dm}{dt} = C_g \cdot Q_g + (GPP - R)\overline{A} + \lambda_{reae.}\left(S \cdot v(t) - m(t)\right), \tag{5}$$

$$\frac{dv}{dt} = Q_g, \tag{6}$$

where m [M] is the DO parcel mass; C_g [ML^{-3}] the DO concentration in the incoming groundwater; Q_g [L^{3}T^{-1}] the groundwater discharge, respectively; GPP and R [ML^{-2}T^{-1}] the GPP and community respiration fluxes; $\overline{A}$ [L^2] the planar area of the channel covered by the parcel of water ($\overline{A} \approx L \cdot width$); $\lambda_{reae.}$ [T^{-1}] the reaeration rate; S [ML^{-3}] the DO saturation concentration; $v(t)$ [L^3] the volume of the parcel at time t [T]. This mass balance assumes that 1) the parcel is well-mixed, 2) the temperature, barometric pressure, and groundwater inputs are spatially homogeneous, and 3) the channel is approximately rectangular.

We can rearrange eqn. (5) to explicitly estimate rates of metabolism:

$$\frac{dm}{dt} = C_g \cdot Q_g + (\lambda_{PP} - \lambda_{resp.})\, m(t) + \lambda_{reae.} \left(S \cdot v(t) - m(t) \right),$$

(7)

where λ_{PP} and $\lambda_{resp.}$ [T^{-1}] are the respiration and primary production rates, respectively.

The analytical solution for the downstream reach concentration $O_2(t)$ (solving (6) and (7)), with initial upstream concentration $O_{2,\,up}$ is:

$$O_2(t) = \frac{\exp[-\Lambda \cdot t] \cdot V_{ini}}{\theta^2 \, (V_{ini} + Q_g \cdot t)} \cdot \begin{bmatrix} \Lambda \left(\dfrac{C_g \cdot Q_g}{V_{ini}} \left(\exp[\Lambda \cdot t] - 1 \right) + O_{2,up} \cdot \Lambda \right) + \\ \dfrac{\lambda_{resp.} \cdot S}{V_{ini}} \left(Q_g - \theta \cdot V_{ini} + \exp[\Lambda \cdot t] \cdot \left(\Lambda \cdot V_{ini} + Q_g \left(\Lambda \cdot t - 1 \right) \right) \right) \end{bmatrix}, \tag{8}$$

$$\Lambda = \lambda_{reae.} + \lambda_{resp.} - \lambda_{PP}, \tag{9}$$

$$V_{ini} = \overline{A} \cdot z_0, \tag{10}$$

where z_0 is the initial average depth of the parcel. When groundwater inputs are negligible ($Q_g \to 0$), (8) simplifies to:

$$O_2(t) = O_{2,\,up} \cdot \exp[-\Lambda \cdot t] + \frac{\lambda_{reae.} \cdot S}{\Lambda} \left(1 - \exp[-\Lambda \cdot t] \right). \tag{11}$$

If DO is recorded with probes, $O_2(t)$, $O_{2,\,up}$ and S are known quantities. $\lambda_{resp.}$ can be independently estimated from the Raz-Rru system with (2). Therefore, (8) or (11) can be used to estimate $\lambda_{reae.}$ when night-time DO signals are used (i.e., when $\lambda_{PP} = 0$).

If the $\lambda_{reae.}$ estimated from the night-time mass balance can be assumed representative of the day-time reaeration patterns, λ_{PP} would be the only unknown when day-time DO signals are subsequently used. Otherwise, the net effects of reaeration and primary production would have to be integrated into a single rate $\lambda_{input} = \lambda_{reae.} + \lambda_{PP}$. Also, if two separate Raz injections are conducted, i.e., at night-time and at day-time conditions, independent respiration rates can be estimated ($\lambda_{resp.}^{day}, \lambda_{resp.}^{night}$). If only one injection is conducted, respiration at day and night-times would have to be assumed equivalent (*status quo*).

5.2.3. Estimating fluxes of metabolism

Once $\lambda_{resp.}$ and λ_{PP} have been estimated, the associated fluxes can be computed equating the analytical solutions of (5) and (7):

$$GPP - R = \frac{\exp[-\Lambda \cdot t] \cdot z_0}{\left(\exp[-\lambda_{reaer.} \cdot t] - 1\right)\Lambda^2} \cdot \left[\begin{array}{l} \exp[\Lambda \cdot t]\Lambda^2 \left(-\lambda_{reaer.} \cdot O_{2,up} + \frac{Q_g}{V_{ini}}\left(C_g - S\right) + \lambda_{reaer.} \cdot S \right) + \\ \exp[\Lambda \cdot t]\lambda_{reaer.} \left(\Lambda \left(\Lambda \cdot O_{2,up} - \frac{Q_g \cdot C_g}{V_{ini}} \right) + \frac{\lambda_{reaer.} \cdot S}{V_{ini}} \left(Q_g - \Lambda \cdot V_{ini} \right) \right) + \\ \exp[\left(\lambda_{reaer.} + \Lambda\right)t] \frac{\left(\lambda_{reaer.} - \Lambda\right)}{V_{ini}} \left(\begin{array}{l} \Lambda \cdot Q_g \left(C_g - S\right) + \\ \lambda_{reaer.} \cdot S\left(Q_g \cdot \left(\Lambda \cdot t - 1\right) + \Lambda \cdot V_{ini}\right) \end{array} \right) \end{array} \right]. \tag{12}$$

When groundwater inputs are negligible ($Q_g \to 0$), (12) simplifies to:

$$GPP - R = \frac{\exp[-\Lambda \cdot t] \cdot z_0 \cdot \lambda_{reaer.}}{\left(\exp[\lambda_{reaer.} \cdot t] - 1\right)\Lambda} \cdot \left[\begin{array}{l} \exp[\left(\lambda_{reaer.} + \Lambda\right)t] \cdot S\left(\lambda_{reaer.} - \Lambda\right) - \exp[\Lambda \cdot t] \cdot \Lambda\left(O_{2,up} - S\right) + \\ \exp[\lambda_{reaer.} \cdot t]\left(O_{2,up} \cdot \Lambda - \lambda_{reaer.} \cdot S\right) \end{array} \right] . \qquad (13)$$

The respiration flux R can be estimated at night-time conditions ($GPP = 0$) with eqns. (12) – (13), replacing Λ ($\Lambda = \lambda_{reae.} + \lambda_{resp.} - \lambda_{PP}$) by $\phi = \lambda_{reaer.} + \lambda_{resp.}$.

5.2.4. Estimating oxygen longitudinal profiles

Once $\lambda_{resp.}$, $\lambda_{reae.}$ and λ_{PP} are estimated, (8) or (11) can be used to generate longitudinal profiles of DO concentrations following the same parcel of water, i.e., moving downstream with the mean travel time along the DO stations. Longitudinal DO profiles are calculated using DO concentrations for nighttime conditions with reaeration subtracted. Mathematically, $\lambda_{reae.} = 0$, and then $O_2(t)$ is estimated for each subreach between consecutive DO stations. Starting at the most upstream station, $O_{2,\,up}$ is a known (measured) oxygen concentration. From the second station on, the initial concentration $O_{2,\,up}$ is the $O_2(t)$ previously found, e.g., to estimate the DO concentration at S3 ($O_{2(@S3)}$), $O_{2,\,up} = O_{2(@S2)}$, and so forth thereafter. We refer to these concentrations as “DO after respiration”. The effects of reaeration can be estimated in the actual DO concentrations observed at night-time conditions, by subtracting “DO after respiration” from the “DO actual reading” values. We refer to these concentrations as “DO reaeration”.

Following the same procedure described above for night-time conditions, we can also outline DO profiles for day-time conditions. Again, $\lambda_{reae.} = 0$ and also $\lambda_{PP} = 0$ to solve for $O_2(t)$ for each subreach within consecutive DO stations (starting at S1). These concentrations are referred to as “DO after respiration”. Afterwards, we can estimate the combined effects of reaeration and primary production with the actual DO concentrations by subtracting “DO after respiration” from the “DO actual reading” values. These concentrations reflect the net input of oxygen to the stream and can be referred to as "DO GPP and reaeration".

5.3. Methodology

5.3.1. Research sites

Field experiments were conducted in watershed 1 (WS01) and watershed 3 (WS03) in the H.J. Andrews Experimental Forest (OR, USA), located in the western Cascade Mountains (44° 20'N, 122° 20'W). WS01 and WS03 are second-order tributaries of Lookout Creek, draining areas of 95.9 and 101.1 ha. The average discharges during the experiments were 1.2 Ls^{-1} and 3.9 Ls^{-1}, respectively.

Kasahara and Wondzell [2003], *Gooseff et al.*, [2003] and *Wondzell* [2006] presented a detailed description of the geomorphology of these two watersheds and the most relevant characteristics are revisited here. 1) Stream channel and valley-floor morphology are mainly shaped by infrequent debris flows and, therefore, gross geomorphology does not change significantly from year to year; 2) there are large-scale heterogeneities in the surface and subsurface (i.e., buried and exposed bedrock, boulders and large woody debris) that trap sediments and obstruct the stream channel by forming steps; 3) the valley floor of WS01 is relatively unconstrained and is ~ 3.5‑fold wider than the active channel in the study reach; 4) the valley floor of WS03 is more constrained by bedrock, being ~ 2.3‑ fold wider than the active channel; 5) the slope of the two watersheds is ~0.13m/m with steps accounting for more than 50% of the elevation change along the longitudinal profile of the stream; and 6) there are secondary channels of short distance in both streams. WS01 and WS03 are less than 2 km apart and the reaches investigated were 81 m and 160 m long, respectively.

Previous research work has been done in these streams to investigate the influence of topography in hydrologic exchange patterns. Using data from stream, well and piezometer heads, *Kasahara and Wondzell* [2003] found that: 1) pool-step sequences were the primary drivers of hyporheic exchange, creating lateral flowpaths with relatively short residence times that were captured by down-valley flows, 2) secondary channels were not important drivers of hyporheic exchange because of their proximity to the main channel, 3) although our study reaches were not exactly the same as those analyzed by these authors (i.e., our reaches were located within their reaches and we had similar discharges), we highlight their estimation that ~76% (WS01) and ~100% (WS03) of the stream discharge would flow through the hyporheic zone in a 100 m reach.

Wondzell [2006] found that in WS01 and WS03 at high and low baseflow discharge (< 12 Ls^{-1}): 1) "spatial patterns, exchange fluxes, and residence-time distributions of hyporheic exchange flows are little affected by stream discharge, at least over the range of baseflow discharges and in the types of mountain stream channel examined", 2) at both flow conditions, the size of the hyporheic zone and the residence times were larger where large woody debris were present and formed steps, than in smaller size and even more frequent step-pool sequences, and 3) the in-channel component of transient storage in these headwater streams is small compared to hyporheic exchange processes.

In this study we defined sampling points to characterize distinctive types of geomorphic units, bed materials and type of transient storage (Table 5.1). We also measured flow depths and longitudinal distances following the methods presented by [*Bott*, 2007].

5.3.2. Stream tracer injections and solute transport modeling

We continuously co-injected Raz and NaCl as a conservative tracer for 39 h (WS01) and 48 h (WS03). We attempted to increase Raz concentration in the stream from 0 to 300 ppb and to increase background specific conductance by ~ 250 µS/cm. We collected background samples to characterize ambient conditions at all sampling sites before the injection started. We sampled the breakthrough curves of Raz/Rru and NaCl in six surface water stations (SA to SF) (Table 5.1). This sampling strategy allowed us to quantify stream metabolism at the subreach and whole-reach scales (cf. (2)). Specific conductance was used as a proxy for Cl concentration and was measured every minute with either YSI-6000 MS V2 multiparametric sondes (Yellow-Springs, OH, USA) or Campbell Scientific EC probes (Logan, Utah, USA) in the surface sampling sites. The fluorescence (proxy for concentration) signals of the Raz-Rru samples were measured with a Cary Eclipse Fluorescence Spectrophotometer (Agilent Technologies). All sondes were calibrated prior to the injection and were cross-checked for 3 hours before the injection began and at the end of the experiment. Tracer injections were conducted 9-15 August 2011 in WS01 and 16 – 21 August 2011 in WS03. Stream surface water temperature ranged within [12.5°C, 14°C] in WS01, and [11.8°C, 16.2°C] in WS03.

5.3.3. Calibration of the molar processing ratio K_{DO}^{Raz} at the field sites

We conducted chamber experiments to calibrate the molar processing ratio K_{DO}^{Raz} (mol O_2 / mol Raz) at each watershed, as described in *González-Pinzón et al.* [2012]. We took sediment samples (smaller than pebbles) by hand every ~10 m along the reach and incubated them in recirculating chambers (*n* = 2 for each watershed) closed to the atmosphere. Raz was injected instantaneously to generate a concentration of about 300 μg/L upon complete mixing. Oxygen consumption was measured inside the chambers with YSI ProODO (Yellow-Springs, OH, USA) and HACH HQ40D probes (Loveland, CO, USA). Water samples were collected, filtered, refrigerated at 4°C, and then read within 72 h of sampling.

5.3.4. Two-station diel technique to estimate stream metabolism

We deployed YSI-6000 MS V2 multiparametric sondes in each stream to measure oxygen concentration [mg/L], oxygen saturation [%], temperature [°C] and specific conductance [μS/cm] every minute. The sondes were located immediately upstream the injection point and in the BTC locations. The sondes were deployed in the stream 22 hours before the injection was started and were removed 76 hours after the injection was stopped.

The mean travel times within consecutive DO stations complied with recommendations for optimum experimental designs for the two-station diel technique [cf. Table 4 in *Grace and Imberger*, 2006] and, therefore, stream metabolism was estimated at the subreach scale. We estimated reaeration rates using the propane gas evasion and night-time regression methods [*Young and Huryn*, 1996; *Fellows et al.*, 2001; *Grace and Imberger*, 2006; *Bott*, 2007]. Propane gas concentrations were measured in four randomly chosen stations to compare estimations of metabolism (Table 5.1). The use of other techniques to estimate reaeration coefficients was restricted because the hydrodynamic conditions of our streams were significantly different than those where most empirical approaches have been developed [*Melching and Flores*, 1999; *Aristegi et al.*, 2009; *Raymond et al.*, 2012]. Stream respiration and GPP were estimated following the methods described by *Bott* [2007] for each of the two techniques used to estimate reaeration rates.

5.4. Results

5.4.1. Stream solute transport

Table 5.2 summarizes the results from the tracer experiments. The conservative mass recovery (CMR) values along the stream reaches suggest that there were not important changes in discharge. At the end of the stream reach in WS03 (see station SF) we did not recover the tail of the BTC completely and, consequently, CMR = 0.86.

5.4.2. Stream metabolism from the transformation of Raz

5.4.2.1. Rates of metabolism and gas exchange

We estimated $\lambda_{\theta,\ Raz}$ using the mean travel times (τ) for the conservative tracer and the zeroth Raz moments (cf. (1) and Table 5.2). We used the values of K_{DO}^{Raz} reported in *González-Pinzón et al*. [2012] (Table 5.2, note that $K_{DO}^{Raz} = 1/K_{Raz}^{DO}$) to estimate $\lambda_{resp.}$ and its associated confidence bounds (cf. (2)).

Because the conservative tracer revealed negligible groundwater inputs, we solved eqn. (11) (no groundwater inputs) to estimate $\lambda_{reae.}$ from a night-time oxygen mass balance ($\lambda_{PP} = 0$) (Figure 5.1), and then estimated λ_{PP} from a day-time oxygen mass balance (Figure 5.2). We assumed negligible changes from day to night for $\lambda_{resp.}$ and $\lambda_{reae.}$ to estimate λ_{PP}.

5.4.2.2. Oxygen longitudinal profiles

Once $\lambda_{resp.}$, $\lambda_{reae.}$ and λ_{PP} were estimated, we used actual DO values measured with the sondes and eqn. (11) to generate longitudinal profiles of DO concentrations (Figures 5.3 and 5.4). First, we estimated DO concentrations for night-time conditions as if they were only affected by respiration. These concentrations are referred to as "DO after respiration" (Figure 5.3). Second, we estimated the effects of reaeration in the actual DO concentrations observed at night-time conditions, by subtracting "DO after respiration" from the "DO actual reading" values. These concentrations are referred to as "DO reaeration" (Figure 5.3).

We also outlined DO profiles for day-time conditions (Figure 5.4). Besides from estimating values of "DO after respiration", we estimated the combined effects of reaeration and primary production as "DO GPP and reae.".

5.5. Discussion

5.5.1. Spatial variability of respiration rates

The coefficient of variation of $\lambda_{resp.}$ (CV-$\lambda_{resp.}$) is an indicator of spatial variability. In WS01, CV-$\lambda_{resp.}$ is 33%, whereas in WS03, CV-$\lambda_{resp.}$ is 61%. This suggests that the WS03 reach has more heterogeneous metabolic flowpaths, which is consistent with the more heterogeneous hydrodynamic conditions observed in our field sampling and previously reported in more detail by *Kasahara and Wondzell* [2003], and more recently by *Ward et al* [2012].

In WS03, the largest $\lambda_{resp.}$ occurred in subreaches SC-SD and SE-SF, which had conditions favoring microbial metabolism (Figure 5.1b). SC-SD contained many step-pool and pool-riffle bedforms, with stream water flowing through large woody debris, which increase retention times, microbial colonization and hyporheic exchange [*Sedell et al.*, 1988; *Nakamura and Swanson*, 1993; *Bilby and Bisson*, 1998; *Kasahara and Wondzell*, 2003]. SE-SF contained completely subsurface (hyporheic) flow, with stream water re-emerging only at the end of the reach.

5.5.2. Reaeration and primary production rates

In WS01 the largest $\lambda_{reae.}$ was obtained for subreach SE-SF (Figure 5.1a), which was characterized by a sequence of pools and riffles formed over a bedrock outcrop (Figure 5.5c). In WS03 the largest reaeration rate was obtained for subreach SC-SD (Figure 5.1b), and it was an equilibrium response (atmosphere to stream mass transfer) to the intense metabolic activity observed in this subreach (Figure 5.5).

Figure 5.2 shows that the lowest primary production rates in WS01 occurred in the subreaches where water flowed over bedrock pools and riffles (i.e., SD-SE and SE-SF) (Figure 5.5c). Also, in WS03 the lowest rate occurred in the subreach with complete subsurface flow (Figure 5.5b).

Altogether, the metabolic and gas exchange rates estimated from the Raz-Rru system are consistent between watersheds. Importantly, the use of Raz as a smart tracer for quantifying metabolic processes in headwater streams integrated into a single measurement the wide range of spatial biogeochemical heterogeneities observed in these complex streams. Otherwise, too many other highly uncertain estimations (e.g., geomorphology, chlorophyll-a, reaeration rates) would still be needed to characterize the functioning of this type of streams.

5.5.3. Oxygen profiles

The DO longitudinal profiles (Figures 5.3 and 5.4) highlight hot spots of metabolic activity, which are indicated by the steep slopes of the “DO after respiration” lines. Although information about the existence of hot spots can also be found from the rates of metabolism previously presented in Figures 5.1 and 5.2, DO profiles show the mass exchange taking place between the atmosphere and the stream, as a response to the imbalance created by community respiration. In streams with significant groundwater inputs the “DO reaeration” profile at night-time conditions would be representative of reaeration after respiration and low DO concentration groundwater inputs. At day-time conditions, the “DO GPP and reae.” would also incorporate the groundwater input effects.

5.5.4. Comparing stream metabolism estimates

We compared reaeration rates (Figure 5.6) and net stream metabolism (Figure 5.7) estimated with the Raz-Rru system and traditional approaches in subreaches with available information. These figures show that the Raz-Rru system yielded larger reaeration rates than the other methods, at the 95% confidence level (Fisher’s least significant difference statistical analyses). The same was true for the estimation of net metabolism. This is a consequence of larger community respiration rates, which resulted in more negative estimations of net metabolism (i.e., more heterotrophic ecosystems).

The main difference between the estimation of metabolism with the traditional oxygen mass balance approach (either one or two-station diel techniques) and with the Raz-Rru system is that the former relies on the estimation of reaeration rates to estimate primary production and community respiration, and the latter directly estimates aerobic respiration and, then, reaeration and primary production. Although there is not a straightforward method to assess which approach is more accurate, the well-documented shortcomings of estimating reaeration rates [e.g., *Genereux and Hemond*, 1992; *Jha et al.*, 2004; *Aristegi et al.*, 2009; *Raymond et al.*, 2012; *Riley and Dodds*, 2013] suggest that it is possible the Raz-Rru method may be more accurate. The Raz-Rru system might be an improved technique in applications seeking to understand stream dynamics at different spatial scales, with the simplicity and thoroughness offered by smart tracers. Moreover, the Raz-Rru system can be directly coupled with other in-stream processes such as nutrient processing [e.g., *Zarnetske et al.*, 2012].

Although the Raz-Rru system theoretically and logistically offers advantages for estimating stream metabolism, further research needs to be done to quantitatively compare the Raz-Rru system and other methods currently used. We envision that a combination of flume studies and the use of controlled bioreactors would be ideal to further assess the advantages and limitations of the Raz-Rru system.

5.6. Conclusions

Headwater streams form networks that integrate key biogeochemical processes. These streams are important players in nutrient processing, retention and breakdown of carbon, flood control, sediment control, irrigation and drinking water supply [*MacDonald and Coe*, 2007; *Meyer et al.*, 2007]. However, quantifying mass and heat budgets in headwater streams is challenging (yet necessary) because of the broad range of heterogeneities encountered [*Montgomery and Buffington*, 1997; *Battin et al.*, 2009; *Buffington and Tonina*, 2009; *Jackson et al.*, 2012; *Ward et al.*, 2012]. For instance, representing the complex arrangement of geomorphic features that mediate biochemical processes in headwater streams is a time consuming and (very often) cost-prohibitive field task, and the use of remote sensing is limited by the high density forest canopy and the presence of exposed boulders and large woody debris [*James et al.*, 2007; *Wechsler*, 2007; *Cavalli et al.*, 2008; *Vianello et al.*, 2009]. Therefore, the use of tracers has become widespread to overcome these issues [*Leibundgut et al.*, 2009]. Tracers allow hydrologists and stream ecologists to integrate biogeochemical processes within a convenient theoretical and logistical framework.

We proposed the use of the Raz-Rru system as an alternative technique to quantify metabolism in headwater streams and presented a simple modeling framework to estimate rates and fluxes of community respiration, primary production, and reaeration. Results from our field experiments in two headwater streams in OR (USA) demonstrated that the Raz-Rru system was capable of detecting spatial variations of in-stream metabolic activity. We found self-consistent relationships between Raz reactivity and (otherwise) difficult-to-quantify geomorphic and hydrodynamic conditions defining metabolic hot spots.

Acknowledgements

This work was funded by NSF grant EAR 08-38338 and the HJ Andrews Experimental Forest research program, funded by the National Science Foundation's Long-Term Ecological Research Program (DEB 08-23380), US Forest Service Pacific Northwest Research Station, and Oregon State University. We thank Nick Kules and Jon Sanfilippo for lab and field assistance. We also thank Brian Wood and Stanley Gregory for allowing us to use lab equipment.

Table 5.1. Geomorphic characteristics of the subreaches studied in WS01 and WS03, H.J. Andrews Experimental Forest (OR, USA).

Subreach	Geomorphic units*	Length (m)	Avg. Depth (cm)	Subreach	Geomorphic units*	Length (m)	Avg. Depth (cm)
Inj-SA	SP, R, L	22	9.0	Inj-SA	PR, R	38	8.1
SA†-SB❦	PR	15	18.0	SA❦-SB	R	18	9.9
SB-SC†	SP, PR, L	6	5.0	SB-SC	SP, PR, L	36	4.3
SC-SD❦	R	21	3.5	SC❦-SD	SP, PR, L	21	6.6
SD-SE❦†	SP, BP	8	3.0	SD-SE❦	R	16	8.7
SE-SF❦†	BP	9	10.0	SE-SF❦	SsF, PR	31	3.3

[*] SP: Step-pool; PR: pool-riffle; BP: bedrock pools and riffles; R: runs; SsF: subsurface flow; L: large woody debris. The symbols ❦ and † represent the stations where propane gas was measured in WS01 and WS03, respectively.

Table 5.2. Conservative and reactive solute transport characteristics.

WS01					WS03				
$Q_{avg.} \approx 1.4\ \mathrm{L\,s^{-1}}$; $K_{DO}^{Raz} = 0.58 \pm 0.03$					$Q_{avg.} \approx 3.8\ \mathrm{L\,s^{-1}}$; $K_{DO}^{Raz} = 0.70 \pm 0.04$				
Station	**τ (h)**	**u (m h^{-1})**	**CMR†**	**RMRc*‡**	**Station**	**τ (h)**	**u (m h^{-1})**	**CMR†**	**RMRc*‡**
Inj-SA	4.4	5.0	1.00	1.00	Inj-SA	2.6	14.6	1.00	1.00
SA-SB	2.0	7.5	1.08	0.58	SA-SB	0.6	30.0	1.02	0.99
SB-SC	0.8	7.5	1.04	0.47	SB-SC	4.4	8.2	1.05	0.62
SC-SD	1.3	16.2	1.04	0.39	SC-SD	1.2	17.5	1.00	0.45
SD-SE	3.4	2.4	1.03	0.26	SD-SE	2.1	7.6	1.00	0.41
SE-SF	0.8	11.3	1.04	0.22	SE-SF	8.2	3.8	0.86	0.11

[†] Conservative mass recovered at the end of the subreach. Values estimated from the zeroth temporal moments.

[‡] Raz mass recovered at the end of the subreach, corrected from conservative mass recovered.

a) WS01

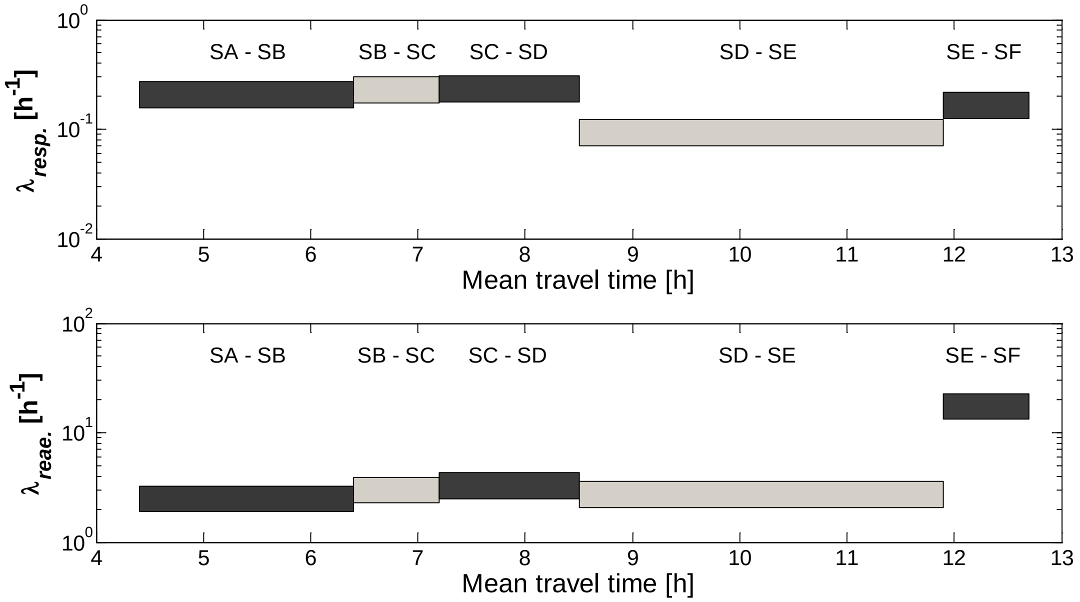

b) WS03

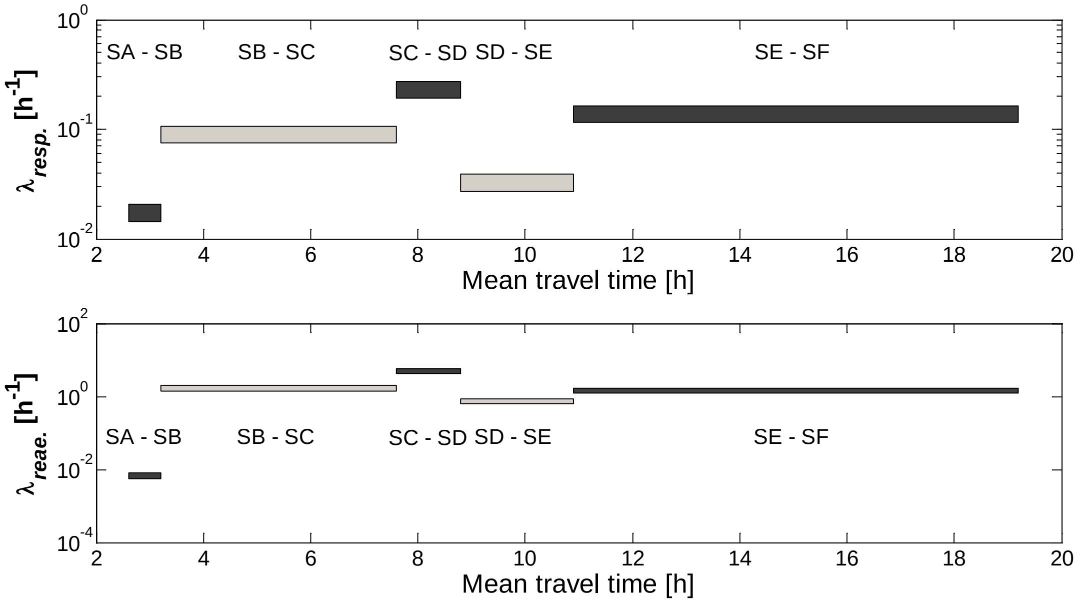

Figure 5.1. Respiration ($\lambda_{resp.}$) and reaeration ($\lambda_{reae.}$) rates estimated from the Raz-Rru system for different subreaches in a) WS01 and b) WS03. Rates were computed using night-time oxygen histories. Lower and upper bounds describe the uncertainty in the estimates (cf. (2)).

a) WS01

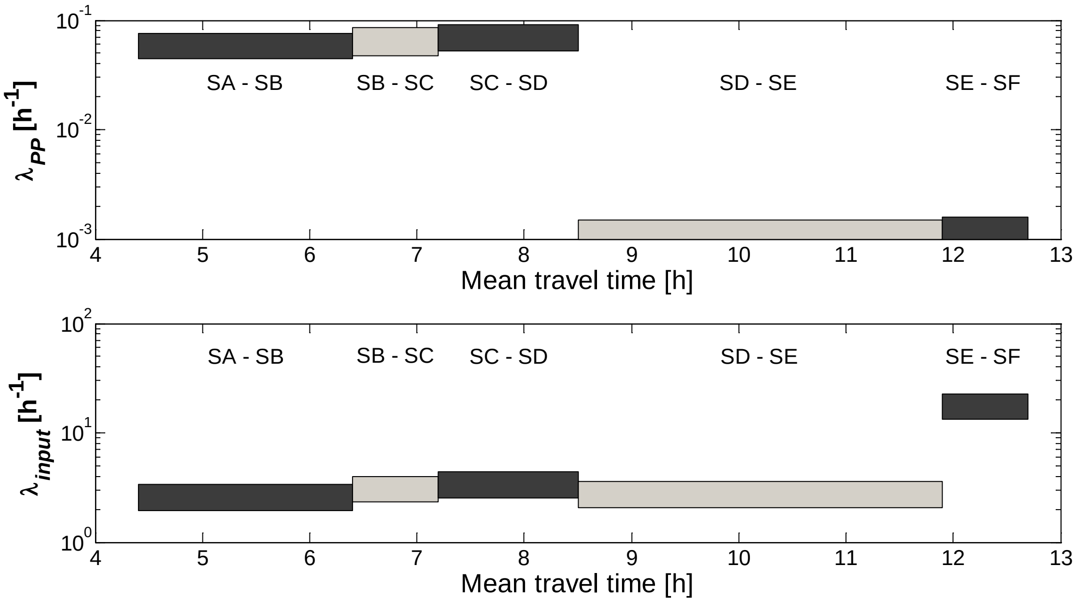

b) WS03

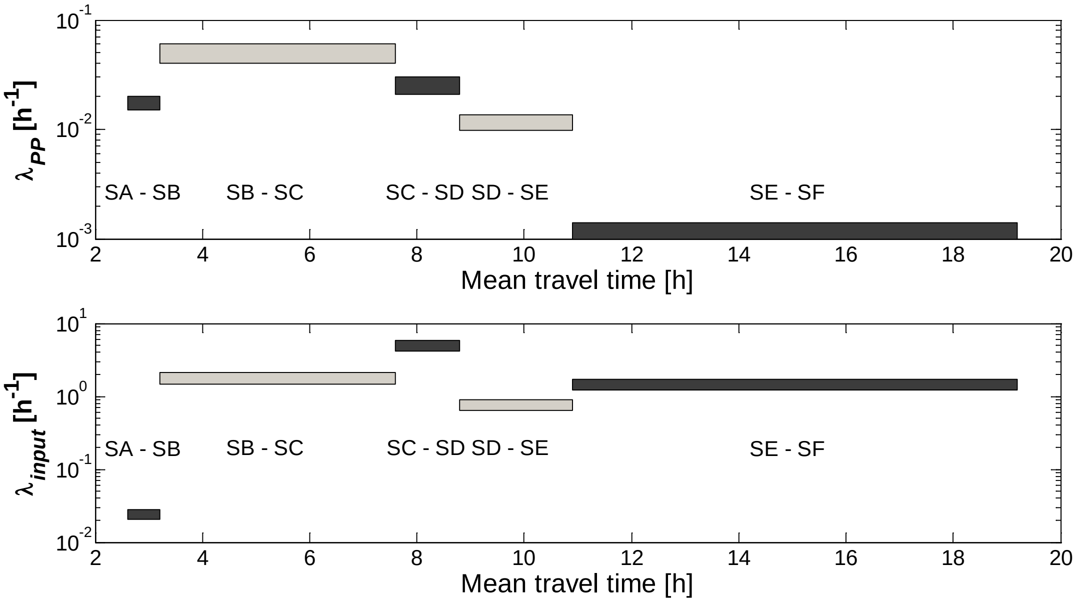

Figure 5.2. Gross primary production ($\lambda_{PP.}$) and net input oxygen ($\lambda_{input.} = \lambda_{PP} + \lambda_{reae.}$) rates estimated from the Raz-Rru system for different subreaches in a) WS01 and b) WS03. Rates were computed using day-time and night-time oxygen histories. Lower and upper bounds describe the uncertainty in the estimates (cf. (2)).

a) WS01

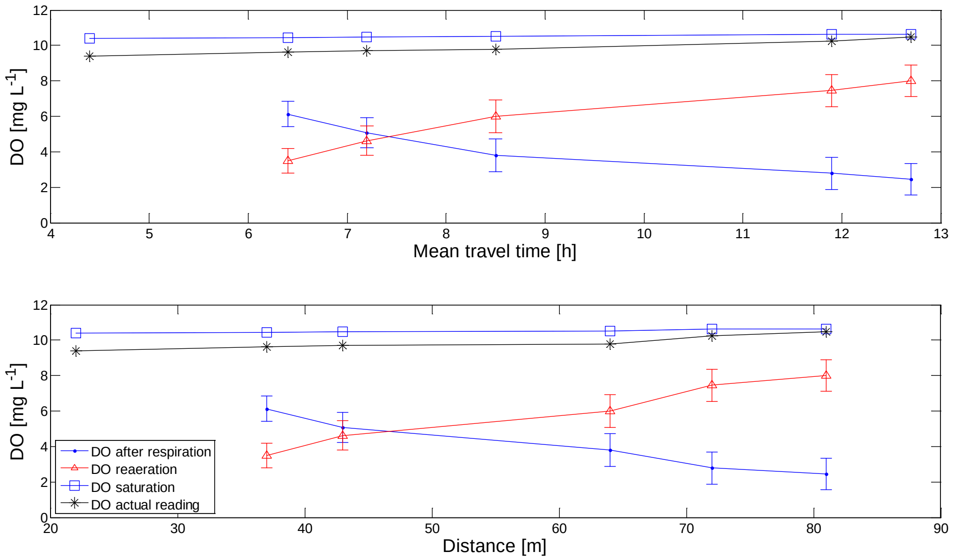

b) WS03

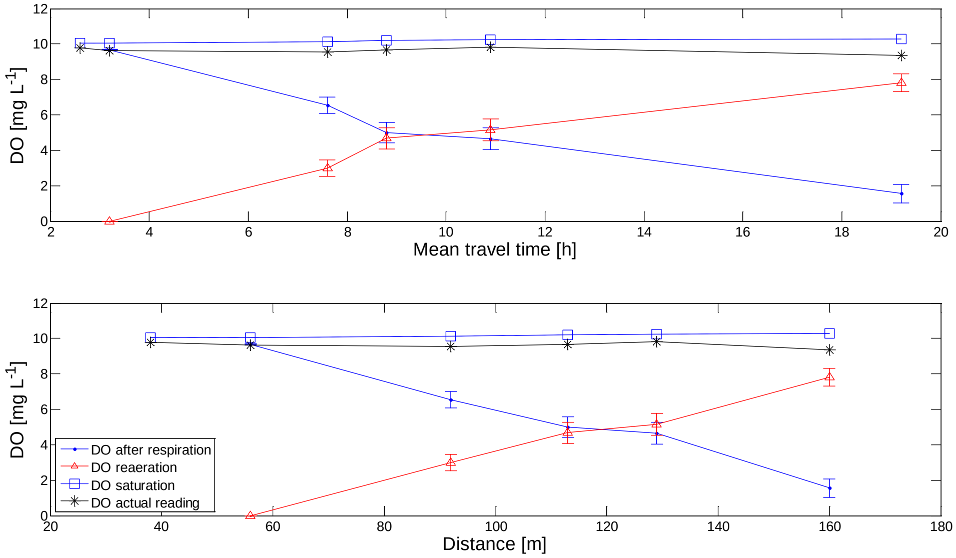

Figure 5.3. Longitudinal profile for DO concentrations in a) WS01, b) WS03; night-time conditions. Markers indicate the location of stations SA – SF. Concentrations have been estimated solving eqn. (11). Lower and upper bounds describe the uncertainty in the estimates (cf. (2)).

a) WS01

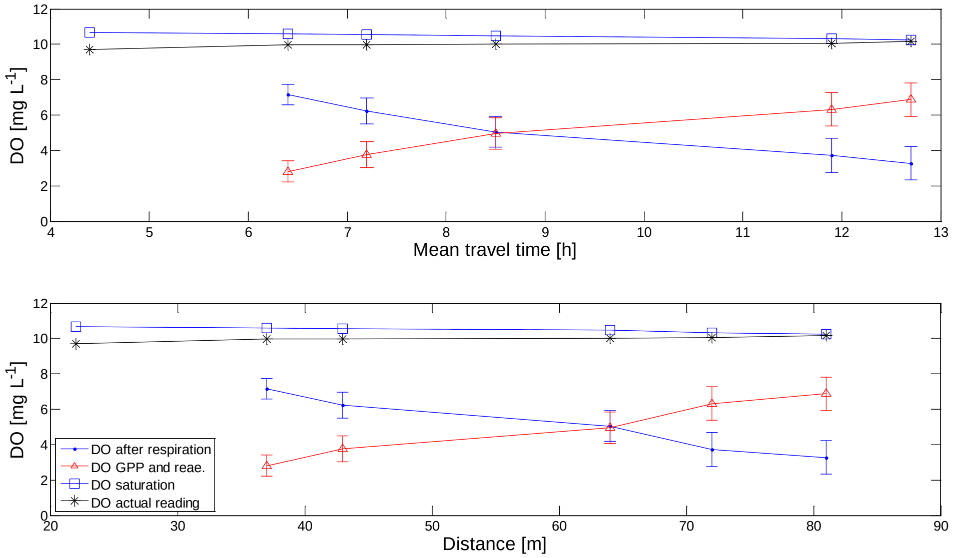

b) WS03

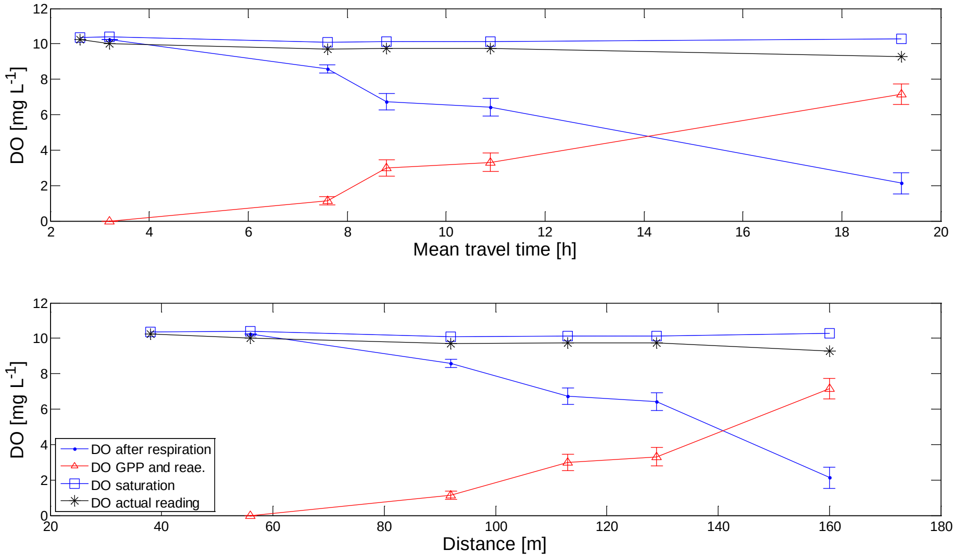

Figure 5.4. Longitudinal profiles for DO concentrations in a) WS01, b) WS03; day-time conditions. Markers indicate the location of stations SA – SF. Concentrations have been estimated solving eqn. (11). Lower and upper bounds describe the uncertainty in the estimates (cf. (2)).

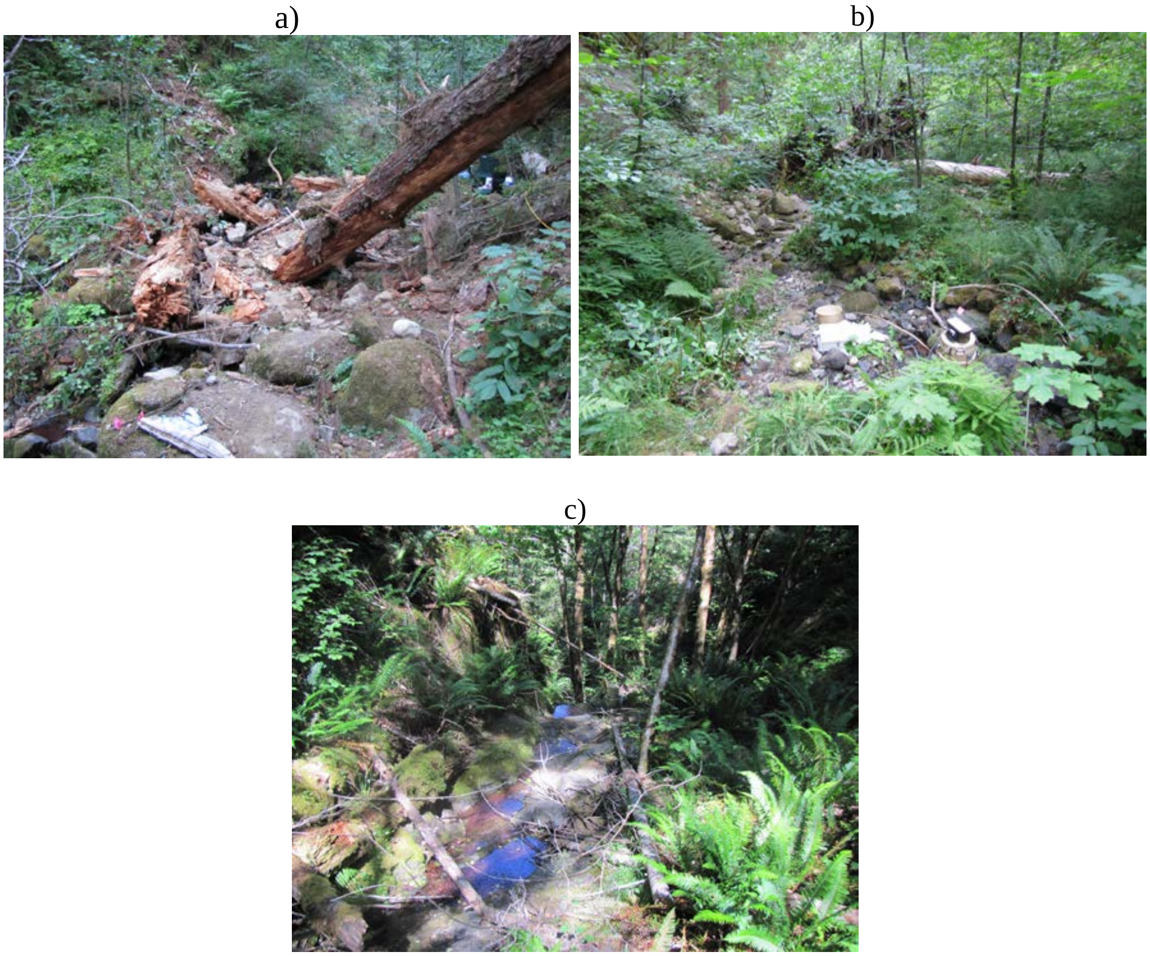

Figure 5.5. The largest respiration and reaeration rates estimated with the Raz-Rru system were obtained for subreaches with observable optimum conditions for such processes. Largest respiration rates: a) WS03 subreach SC-SD was characterized by step-pool and pool-riffle bedforms, with stream water flowing through large woody debris which are known to increase retention times, microbial colonization and hyporheic exchange. b) WS03 subreach SE-SF was characterized by complete subsurface (hyporheic) flow with stream water reemerging only at the end of the reach. Largest reaeration rates: c) WS01 subreach SD-SE and SE-SF were characterized by sequences of pools and riffles formed over a bedrock outcrop.

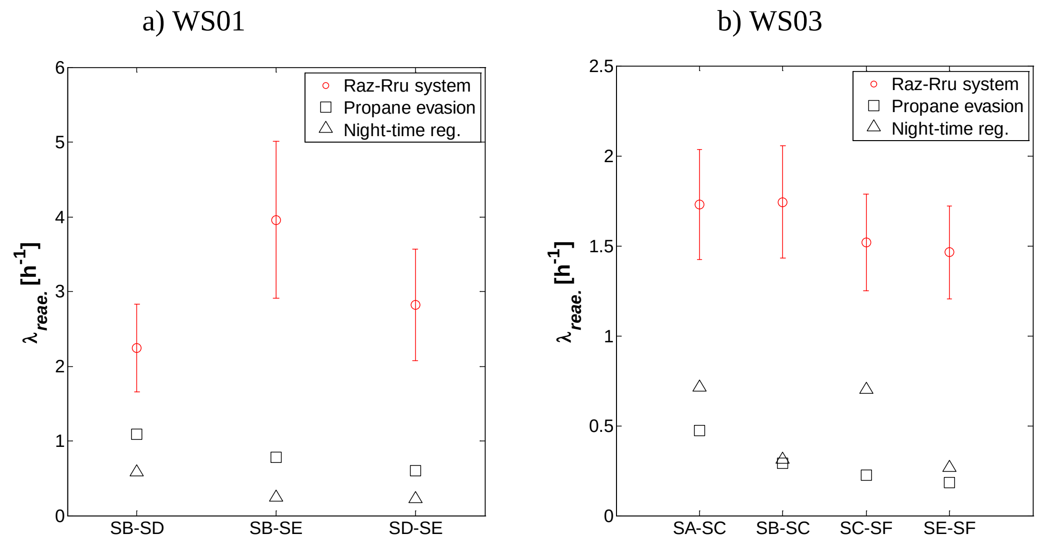

a) WS01

b) WS03

Figure 5.6. Comparison of reaeration rates estimated with the Raz-Rru system and the propane evasion and night-time regression techniques for sites with comparable information. Lower and upper bounds describe the uncertainty in the estimates (cf. (2)).

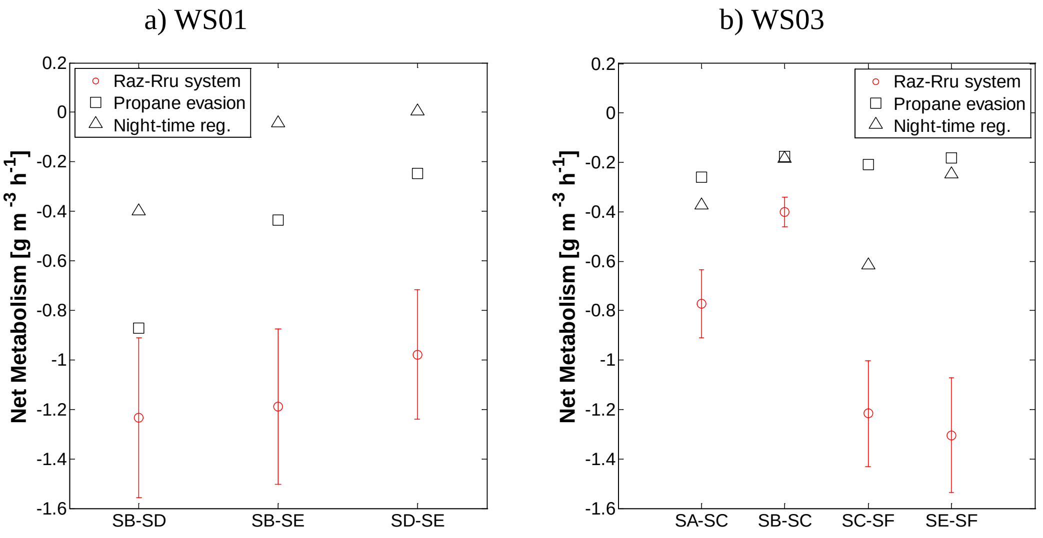

a) WS01

b) WS03

Figure 5.7. Comparison of net metabolism fluxes (per unit depth) estimated with the Raz-Rru system, and the propane evasion and night-time regression techniques for sites with comparable information. Lower and upper bounds describe the uncertainty in the estimates (cf. (2)).

References

Adams, R. K., and J. A. Spotila (2005), The form and function of headwater streams based on field and modeling investigations in the southern Appalachian Mountains, *Earth Surf. Proc. Land.*, 30(12), 1521–1546, doi:10.1002/esp.1211.

Alexander, R. B., E. W. Boyer, R. A. Smith, G. E. Schwarz, and R. B. Moore (2007), The Role of Headwater Streams in Downstream Water Quality, *J. Am. Water Resour. As.*, 43(1), 41–59, doi:10.1111/j.1752-1688.2007.00005.x.

Allan, J. D., and M. Castillo (2007), Stream Ecology: *Structure and function of running waters*, Springer Netherlands.

Argerich, A., R. Haggerty, E. Martí, F. Sabater, and J. Zarnetske (2011), Quantification of metabolically active transient storage (MATS) in two reaches with contrasting transient storage and ecosystem respiration, *J. Geophys. Res.*, 116(G3), G03034.

Aristegi, L., O. Izagirre, and A. Elosegi (2009), Comparison of several methods to calculate reaeration in streams, and their effects on estimation of metabolism, *Hydrobiologia*, 635(1), 113–124.

Baki, A. B. M., D. Z. Zhu, and G. Courtice (2012), Hydraulic geometry and resistance to flow in headwater streams in the Northwest Territories, *Can. J. Civil Eng.*, 39(12), 1252–1263, doi:10.1139/l2012-113.

Bathurst, J. C. (1985), Flow resistance estimation in mountain rivers, *J. Hydraul. Eng.-ASCE*, 111(4), 625–643, doi:10.1061/(ASCE)0733-9429(1985)111:4(625).

Battin, T. J., L. A. Kaplan, J. Denis Newbold, and C. M. E. Hansen (2003), Contributions of microbial biofilms to ecosystem processes in stream mesocosms, *Nature*, 426(6965), 439–442, doi:10.1038/nature02152.

Battin, T. J., L. A. Kaplan, S. Findlay, C. S. Hopkinson, E. Marti, A. I. Packman, J. D. Newbold, and F. Sabater (2008), Biophysical controls on organic carbon fluxes in fluvial networks, *Nature Geosci.*, 1(2), 95–100.

Battin, T. J., S. Luyssaert, L. A. Kaplan, A. K. Aufdenkampe, A. Richter, and L. J. Tranvik (2009), The boundless carbon cycle, *Nature Geosci.*, 2(9), 598–600.

Beer, T., and P. C. Young (1983), Longitudinal dispersion in natural streams, *J. Environ. Eng.-ASCE*, 109 (5), 1049–1067.

Bencala, K. E., and R. A. Walters (1983), Simulation of Solute Transport in a Mountain Pool-and-Riffle Stream: A Transient Storage Model, *Water Resour. Res.*, Vol. 19(3), 718–724.

Benda, L., M. A. Hassan, M. Church, and C. L. May (2005), Geomorphology of steepland headwaters: the transition from hillslopes to channels, *J. Am. Water Resour. As.*, 41(4), 835–851.

Bilby, R. E., and P. A. Bisson (1998), *Function and distribution of large woody debris*, Springer.

Boano, F., A. I. Packman, A. Cortis, R. Revelli, and L. Ridolfi (2007), A continuous time random walk approach to the stream transport of solutes, *Water Resour. Res.*, 43(10), W10425.

Bott, T. L. (2007), Primary productivity and community respiration, in *Methods in stream ecology*, pp. 663–390, Academic Press.

Bottacin-Busolin, A., G. Singer, Mattiazaramella, T. J. Battin, and A. Marion (2009), Effects of Streambed Morphology and Biofilm Growth on the Transient Storage of Solutes, *Environ. Sci. Technol*., 43, 7337–7342.

Buffington, J. M., and D. Tonina (2009), Hyporheic Exchange in Mountain Rivers II: Effects of Channel Morphology on Mechanics, Scales, and Rates of Exchange, *Geography Compass*, 3(3), 1038–1062.

Bunn, S. E., E. G. Abal, M. J. Smith, S. C. Choy, C. S. Fellows, B. D. Harch, M. J. Kennard, and F. Sheldon (2010), Integration of science and monitoring of river ecosystem health to guide investments in catchment protection and rehabilitation, *Freshwater Biol.*, 55, 223–240, doi:10.1111/j.1365-2427.2009.02375.x.

Cavalli, M., P. Tarolli, L. Marchi, and G. Dalla Fontana (2008), The effectiveness of airborne LiDAR data in the recognition of channel-bed morphology, *CATENA*, 73(3), 249–260, doi:10.1016/j.catena.2007.11.001.

Cummins, K. W. (1974), Structure and Function of Stream Ecosystems, *BioScience*, 24(11), 631–641, doi:10.2307/1296676.

Demars, B. O. L., and J. R. Manson (2013), Temperature dependence of stream aeration coefficients and the effect of water turbulence: A critical review, *Water Res.*, 47(1), 1–15, doi:10.1016/j.watres.2012.09.054.

Dent, C. L., N. B. Grimm, and S. G. Fisher (2001), Multiscale Effects of Surface-Subsurface Exchange on Stream Water Nutrient Concentrations, *J. N. Am. Benthol. Soc.*, 20, 162–181.

Elliott, A. H., and N. H. Brooks (1997), Transfer of nonsorbing solutes to a streambed with bed forms: Theory, *Water Resour. Res.*, 33(1), 123–136.

Fellows, C. S., H. M. Valett, and C. N. Dahm (2001), Whole-Stream Metabolism in Two Montane Streams: Contribution of the Hyporheic Zone, *Limn. Oceanogr*., 46(3), 523–531.

Genereux, D. P., and H. F. Hemond (1992), Determination of gas exchange rate constants for a small stream on Walker Branch Watershed, Tennessee, *Water Resour. Res*, 28(9), 2365–2374, doi:10.1029/92WR01083.

González-Pinzón, R., R. Haggerty, and D. D. Myrold (2012), Measuring aerobic respiration in stream ecosystems using the resazurin-resorufin system, *J. Geophys. Res*, 117(G3), doi:10.1029/2012JG001965.

Gooseff, M. N., S. M. Wondzell, R. Haggerty, and J. Anderson (2003), Comparing transient storage modeling and residence time distribution (RTD) analysis in geomorphically varied reaches in the Lookout Creek basin, Oregon, USA, *Adv. Water Resour*., Vol. 26, 925–937.

Grace, M. R., and S. J. Imberger (2006), *Stream Metabolism: Performing & Interpreting Measurements*, Water Studies Centre Monash University, Murray Darling Basin Commission and New South Wales Department of Environment and Climate Change.

Haggerty, R. (2013), Analytical solution and simplified analysis of coupled parent-daughter steady-state transport with multirate mass transfer, *Water Resour. Res*, doi:10.1002/wrcr.20057.

Haggerty, R., S. M. Wondzell, and M. A. Johnson (2002), Power-law residence time distribution in the hyporheic zone of a 2nd-order mountain stream, *Geophys. Res. Lett*., Vol. 29(13), 1640, doi:10.1029/2002GL014743.

Haggerty, R., A. Argerich, and E. Marti (2008), Development of a "'smart'" tracer for the assessment of microbiological activity and sediment-water interaction in natural waters: The resazurin-resorufin system, *Water Resour. Res*, 44.

Haggerty, R., E. Marti, A. Argerich, D. . von Schiller, and N. Grimm (2009), Resazurin as a "'smart'" tracer for quantifying metabolically active transient storage in stream ecosystems, *J. Geophys. Res*., 114, doi:doi:10.1029/2008JG000942.

Hall, R. O., and J. L. Tank (2005), Correcting whole-stream estimates of metabolism for groundwater input, *Limnol. Oceanogr.: Meth.*, 3, 222–229.

Jackson, T. R., R. Haggerty, S. V. Apte, A. Coleman, and K. J. Drost (2012), Defining and measuring the mean residence time of lateral surface transient storage zones in small streams, *Water Resour. Res.*, 48(10), doi:10.1029/2012WR012096.

James, L. A., D. G. Watson, and W. F. Hansen (2007), Using LiDAR data to map gullies and headwater streams under forest canopy: South Carolina, USA, *CATENA*, 71(1), 132–144, doi:10.1016/j.catena.2006.10.010.

Jarrett, R. D. (1990), Hydrologic and hydraulic research in mountain rivers, *J. Am. Water Resour. As.*, 26(3), 419–429, doi:10.1111/j.1752-1688.1990.tb01381.x.

Jha, R., C. S. P. Ojha, and K. K. S. Bhatia (2004), A supplementary approach for estimating reaeration rate coefficients, *Hydrol. Proc.*, 18(1), 65–79, doi:10.1002/hyp.1312.

Jiménez, M. A., and E. Wohl (2013), Solute transport modeling using morphological parameters of step-pool reaches, *Water Resour. Res*, doi:10.1002/wrcr.20102.

Kasahara, T., and S. M. Wondzell (2003), Geomorphic controls on hyporheic exchange flow in mountain streams, *Water Resour. Res*., 39(1), 1005.

Kilpatrick, F. A., R. E. Rathbun, N. Yotsukura, G. W. Parker, and L. L. DeLong (1989), Determination of stream reaeration coefficients by use of tracers, US Government Printing Office.

Leibundgut, C., P. Maloszewski, and C. Külls (2009), *Tracers in hydrology*, John Wiley & Sons, Ltd.

Lemke, D., P.-A. Schnegg, M. Schwientek, K. Osenbrück, and O. A. Cirpka (2013), On-line fluorometry of multiple reactive and conservative tracers in streams, *Environmental Earth Sci.*, doi:10.1007/s12665-013-2305-3.

Lowe, W. H., and G. E. Likens (2005), Moving headwater streams to the head of the class, *BioScience*, 55(3), 196–197.

MacDonald, L. H., and D. Coe (2007), Influence of headwater streams on downstream reaches in forested areas, *Forest Sci.*, 53(2), 148–168.

Marzolf, E. R., P. J. Mulholland, and A. D. Steinman (1994), Improvements to the diurnal upstream-downstream dissolved oxygen change technique for determining whole-stream metabolism, *Can. J. Fish Aquat. Sci*., 51, 1591–1599.

McCutchan, J. H., and W. M. Lewis (2006), Groundwater flux and open-channel estimation of stream metabolism: response to Hall and Tank, *Limnol. Oceanogr.: Meth.*, 4, 213–215.

McCutchan, J. H., J. F. Saunders, W. M. Lewis, and M. G. Hayden (2002), Effects of groundwater flux on open-channel estimates of stream metabolism, *Limnol. Oceanogr.*, 47(1), 321–324.

Melching, C. S., and H. E. Flores (1999), Reaeration Equations Derived from U.S. Geological Survey Database, *J. Environ. Eng.-ASCE*, 125, 407–414.

Meyer, J. L., D. L. Strayer, J. B. Wallace, S. L. Eggert, G. S. Helfman, and N. E. Leonard (2007), The Contribution of Headwater Streams to Biodiversity in River Networks, *J. Am. Water Resour. As.*, 43(1), 86–103, doi:10.1111/j.1752-1688.2007.00008.x.

Montgomery, D. R., and J. M. Buffington (1997), Channel-reach morphology in mountain drainage basins, *Geol. Soc. Am. Bull.*, 109(5), 596–611.

Morrice, J. A., H. M. Valett, C. N. Dahm, and M. E. Campana (1997), Alluvial Characteristics, Groundwater–Surface Water Exchange and Hydrological Retention in Headwater Streams, *Hydrol. Proc.*, 11(3), 253–267.

Nakamura, F., and F. J. Swanson (1993), Effects of coarse woody debris on morphology and sediment storage of a mountain stream system in western Oregon, *Earth Surf. Proc. Land*, 18(1), 43–61, doi:10.1002/esp.3290180104.

Peterson, B. J. et al. (2001), Control of Nitrogen Export from Watersheds by Headwater Streams, *Science*, 292(5514), 86–90.

Raymond, P. A., C. J. Zappa, D. Butman, T. L. Bott, J. Potter, P. Mulholland, A. E. Laursen, W. H. McDowell, and D. Newbold (2012), Scaling the gas transfer velocity and hydraulic geometry in streams and small rivers, *Limnol. Oceanogr.: Fluids & Environments*, 2, 41–53.

Reichert, P., U. Uehlinger, and V. Acuña (2009), Estimating stream metabolism from oxygen concentrations: Effect of spatial heterogeneity, *J. Geophys. Res.*, 114(G3), doi:10.1029/2008JG000917.

Riley, A. J., and W. K. Dodds (2013), Whole-stream metabolism: strategies for measuring and modeling diel trends of dissolved oxygen, *Freshw. Sci.*, 32(1), 56–69, doi:10.1899/12-058.1.

Runkel, R. L. (2007), Toward a transport-based analysis of nutrient spiraling and uptake in streams, *Limnol. Oceanogr.: Meth.*, 5, 50–62.

Sedell, J. R., P. A. Bisson, E. J. Swanson, and S. V. Gregory (1988), What we know about large trees that fall into streams and rivers, from the forest to the sea: A story of fallen trees, General Technical Report, U.S. Forest Service.

Stanaway, D., R. Haggerty, S. Benner, A. Flores, and K. Feris (2012), persistent metal contamination limits lotic ecosystem heterotrophic metabolism after more than 100 years of exposure: A novel application of the resazurin resorufin smart tracer, *Environ. Sci. Technol.*, 46(18), 9862–9871, doi:10.1021/es3015666.

Stone, M. C., and R. H. Hotchkiss (2007), Evaluating velocity measurement techniques in shallow streams, *J. Hydraul. Res.*, 45(6), 752–762, doi:10.1080/00221686.2007.9521813.

Thome, C. R., and L. W. Zevenbergen (1985), Estimating mean velocity in mountain rivers, *J. Hydraul. Eng.-ASCE*, 111(4), 612–624, doi:10.1061/(ASCE)0733-9429(1985)111:4(612).

Tobias, C. R., J. K. Böhlke, and J. W. Harvey (2007), The oxygen-18 isotope approach for measuring aquatic metabolism in high productivity waters, *Limnol. Oceanogr.*, 52(4), 1439–1453, doi:10.4319/lo.2007.52.4.1439.

Triska, F. J., V. C. Kennedy, R. J. Avanzino, G. W. Zellweger, and K. E. Bencala (1989), Retention and transport of nutrients in a third-order stream: channel processes, *Ecology*, 1877–1892.

Vianello, A., M. Cavalli, and P. Tarolli (2009), LiDAR-derived slopes for headwater channel network analysis, *CATENA*, 76(2), 97–106, doi:10.1016/j.catena.2008.09.012.

Ward, A. S., M. Fitzgerald, M. N. Gooseff, T. J. Voltz, A. M. Binley, and K. Singha (2012), Hydrologic and geomorphic controls on hyporheic exchange during base flow recession in a headwater mountain stream, *Water Resour. Res*, 48(4), W04513.

Wechsler, S. P. (2007), Uncertainties associated with digital elevation models for hydrologic applications: a review, *Hydrol. Earth Syst. Sci.*, 11(4), 1481–1500, doi:10.5194/hess-11-1481-2007.

Wondzell, S. M. (2006), Effect of morphology and discharge on hyporheic exchange flows in two small streams in the Cascade Mountains of Oregon, USA, *Hydrol. Proc.*, 20(2), 267–287.

Wörman, A., A. I. Packman, H. Johansson, and K. Jonsson (2002), Effect of flow-induced exchange in hyporheic zones on longitudinal transport of solutes in streams and rivers, *Water Resour. Res*, 38(1), 1001.

Wörman, A., A. I. Packman, L. Marklund, J. W. Harvey, and S. H. Stone (2007), Fractal topography and subsurface water flows from fluvial bedforms to the continental shield, *Geophys. Res. Lett.*, 34(7), doi:10.1029/2007GL029426.

Young, R. G., and A. D. Huryn (1996), Interannual variation in discharge controls ecosystem metabolism along a grassland river continuum, *Can. J. Fish. Aquat. Sci.*, 53(10), 2199–2211.

Young, R. G., and A. D. Huryn (1999), Effects of land use on stream metabolism and organic matter turnover, *Ecol. Appl.*, 9(4), 1359–1376.

Young, R. G., C. D. Matthaei, and C. R. Townsend (2008), Organic matter breakdown and ecosystem metabolism: functional indicators for assessing river ecosystem health, *J. N. Am. Benthol. Soc*, 27(3), 605–625, doi:10.1899/07-121.1.

Zarnetske, J. P., R. Haggerty, S. M. Wondzell, V. A. Bokil, and R. González-Pinzón (2012), Coupled transport and reaction kinetics control the nitrate source-sink function of hyporheic zones, *Water Resour. Res*, 48(11), n/a–n/a, doi:10.1029/2012WR011894.

6. DIEL FLUCTUATIONS OF RESPIRATION IN A HEADWATER STREAM

Ricardo González-Pinzón, Marc Peipoch, Roy Haggerty, Eugènia Martí and Jan H. Fleckenstein

For submission to Environmental Science and Technology

Abstract

We investigated temperature controls on respiration rates and tested the hypothesis that community respiration is constant across nighttime and daytime. We conducted consecutive nighttime and daytime experiments in two stream reaches (with different canopy densities) using the resazurin-resorufin system to compare respiration rates. We found (1) that even though photosynthetically active radiation and stream water temperature were different across the reaches at the 95% confidence level, (2) respiration rates were not different across nighttime and daytime conditions at the 95% confidence level. This result suggests that community respiration rates in streams may not need to be "corrected" for temperature between daytime and nighttime.

6.1. Introduction

Correcting biological processing rates (e.g., respiration, decay) and chemical rates (e.g., stream-atmosphere mass transfer, hydrolysis) for temperature changes is a common practice [*Metzger and Dobbins*, 1967; *Genereux and Hemond*, 1992; *Gillooly et al.*, 2001; *Huey and Kingsolver*, 2011]. Reaction rates increase with temperature. In biological systems, reaction rates increase with temperature until some maximum value where enzymatic activity is interrupted. As a first approximation, biological reaction rates are expected to double following a 10°C increase in temperature within 0°C – 40°C, i.e., the 'biological range' [*Apple et al.*, 2006; *Chapra*, 2008]. Because streams experience diel temperature fluctuations, we would like to understand how such changes control biochemical reaction rates which, in turn, affect the cycling of major nutrients.

To account for diel temperature fluctuations in kinetic processes, ecohydrology models typically adopt chemical models developed for systems that reach a sustained net change in temperature and that have effectively negligible temperature fluctuations [*Thornton and Lessem*, 1978]. These models, including the van't Hoff equation or Q_{10} formulation, have been widely used to correct respiration rates in stream ecosystems. Commonly, diel temperature fluctuations measured above the benthic zone are used in combination with a Q_{10}-type formulation to correct respiration rates [e.g., *Tobias et al.*, 2007; *Holtgrieve et al.*, 2010; *Demars et al.*, 2011], and it has been shown that correcting respiration rates for temperature fluctuations might yield significantly different estimates of metabolic fluxes [e.g., *Riley and Dodds*, 2012]. However, correcting respiration rates with these methods in headwater streams might be incorrect because: 1) a steady-state model (Q_{10} formulation) is used to correct dynamic process with fast cycling time scales (diel temperature fluctuations), and 2) temperature fluctuations are typically measured in a compartment where the least amount of biomass is expected to live (i.e., the water column). Therefore, correcting respiration rates for diel temperature fluctuations might be misleading, and accounting for this may only add extra error to this already highly uncertain estimation.

Current methods to estimate stream metabolism are based on dissolved oxygen (DO) mass balance. These methods quantify spatial variations in DO and such variations are related to fluxes of community respiration (CR), primary production (PP), stream-atmosphere mass transfer (reaeration) and stream-groundwater mass transfer. Because PP is zero at nighttime conditions, independent estimates of DO fluxes among the atmosphere-stream-ground water interfaces are used to 'close' the system, thus allowing an estimate of CR. Once CR is estimated through a nighttime DO mass balance, CR is either assumed effectively constant for daytime conditions or temperature-corrected respiration rates are used to estimate CR at daytime conditions. Afterwards, a daytime DO mass balance is used to solve for PP. To the best of our knowledge, there have not been field experiments at the reach scale used to test the hypothesis that CR is effectively constant at nighttime and daytime conditions. This is because, to date, there is not an appropriate method available.

In this study we investigated temperature controls on respiration rates at the half-day time scale, testing the hypothesis that CR is constant at the reach scale for night and daytime conditions. We used the resazurin-resorufin system [*Haggerty et al.*, 2008; *González-Pinzón et al.*, 2012, 2013] in our experiments conducted in a headwater stream. Our experimental design considered two reaches with different canopy densities (i.e., different photosynthetically active radiation, PAR, incoming fluxes) to compare the effects of diel temperature fluctuations in shaded and open reaches. We conducted consecutive nighttime and daytime experiments in each of the two reaches to compare respiration rates. We found that even though PAR and stream water temperature were significantly different within and across the reaches, respiration rates were not significantly different at nighttime and daytime conditions.

6.2. Methodology

6.2.1. Study Sites

This study was conducted in two reaches of the stream Fuirosos, located in Catalonia (NE Spain). This headwater stream drains a 10.5 km catchment. The lithology composition is granodiorite and biotitic granodiorite (21% of total), leucogranite (51%), sericitic schists (24%), slate, mudstone, and limestone (2%), and an alluvial zone (2%) [*Bernal*, 2006]. The two stream reaches are referred to as "shaded" and "open" (Table 6.1), terms which are used as qualitative descriptors of the quantity of light reaching the stream water. The shaded reach is located in a high density forest upstream area, and the open reach is located 3 km downstream. The riparian vegetation in the open reach is sparser, primarily due to watershed management programs for agriculture.

We conducted similar experiments in both reaches. First, we conducted consecutive nighttime and daytime experiments in the downstream open reach to avoid experimental interferences. We conducted similar paired (night and day) experiments in the shaded reach four days after the nighttime injection in the open reach. The short time elapsed between the experiments, and the absence of important rainfall events, allowed us to compare the stream reaches under similar hydrological conditions. The experiments were conducted in the first 10 days of May 2012 and deciduous vegetation was at about 15% total foliage. The estimated Leaf Area Index (LAI = leaf area [L^2] / ground area [L^2]), which ranges from 0 (bare ground) to over 10 (dense conifer forests), was 4.2 ± 1.1 (mean±SD) in the shaded reach and 1.7 ± 0.7 in the open reach.

6.2.2. PAR and Stream Temperature Records

We recorded paired PAR and stream water temperature every 30 minutes with waterproof temperature and light data loggers (HOBO Pendant® UA-002-64). This information was recorded at representative sites in both reaches throughout the experiments (Table 6.2) to distinguish between night and daytime conditions, and to quantify the differences in incoming radiation reaching the shaded and open reaches at daytime conditions.

6.2.3. Stream Tracer Experiments

We coinjected the bioreactive tracer resazurin (Raz) and the conservative tracer NaCl for 3.0 h in the open reach, and for 2.0 h in the shaded reach. We attempted to increase Raz up to a maximum plateau concentration of 250 ppb, and to increase the specific conductance by ~ 70 µS/cm from its background signal (~180 µS/cm).

We took discrete Raz-Rru samples manually at stations S1-S4 in the open reach, and S2-S5 in the shaded reach (Table 6.2). These samples were filtered (0.7µm pore size GF/F) and refrigerated (iced water in the field and 4°C in the lab), and read within 48 hours with a Shimadzu RF lab spectrofluorometer. We also took semi-continuous (every 10 seconds) Raz-Rru readings with three on-line GGUN-FL30 field fluorometers [cf. *Lemke et al.*, 2013] at stations S4-S5-S6 (open reach) and S5-S6-S7 (shaded reach). The field fluorometers were calibrated immediately before the nighttime injections, and the samples at S4 (open reach) and S5 (shaded) were used as a guide to match the readings of the lab and field fluorometers.

Specific conductance was recorded with WTW (Weilheim, Germany) 3110 conductivity meters. The mean travel time τ between two sampling locations was estimated with the zeroth and first-order temporal moments (m_n) of the conservative tracer breakthrough curves (BTCs) as:

$$\tau = \frac{m_{1,cons}^{dn}}{m_{o,cons}^{dn}} - \frac{m_{1,cons}^{up}}{m_{o,cons}^{up}}, \tag{1}$$

$$m_n = \sum_{k=1}^{m} \left(0.5t_k + 0.5t_{k+1}\right)^n \left(0.5C_k + 0.5C_{k+1}\right)\left(t_{k+1} - t_k\right), \tag{2}$$

where τ [T] is the mean travel time between two sampling locations; $C(t)$ [ML^{-3}] is the measured concentration at time t [T]; j [-] is an index and m the total number of observations.

Our injections (2 x 2 h (or 3 h) continuous) and numerical analysis (temporal moments) allowed us to estimate lumped respiration patterns at the half-day time scale. With this experimental design we cannot resolve rapid metabolic responses to fluctuations in stream temperature (e.g., < 1 h). Therefore, this study provides insight into diel in-stream respiration patterns, which cannot be directly estimated at the subreach or reach scales with current methods.

6.2.4. Estimating Respiration Rates with Raz

We estimated respiration rates following the methods described by *González-Pinzón and Haggerty* [2013] and *González-Pinzón et al*. [2013]. *González-Pinzón and Haggerty* developed an efficient method to estimate transformation rates in streams. *González-Pinzón et al*. showed how this method can be used to estimate respiration rates through measurements of the zeroth temporal moments of the upstream ($m_{o,Raz}^{up}$) and downstream ($m_{o,Raz}^{dn}$) Raz BTCs (or plateau concentrations), the mean travel time in the stream reach (τ, [T]), and the molar processing ratio of DO to Raz (K_{DO}^{Raz} = [moles of DO processed / moles Raz processed]). Assuming that respiration in the water column and dispersion are negligible, the uncertainty in the estimation of volume-averaged respiration rates in the storage zone (λ_{resp}, [T^{-1}]) are [*González-Pinzón and Haggerty*, 2013]:

$$\lambda_{\theta,\, sz}^{\mathrm{Raz}} = \frac{\ln[m_{o,Raz}^{up} \big/ m_{o,Raz}^{dn}]}{\tau} \quad , \tag{3}$$

$$\lambda_{resp} = \begin{cases} [\lambda_{\theta,\, sz}^{\mathrm{Raz}}\, K_{\mathrm{DO\ min}}^{Raz},\ \ \lambda_{\theta,\, sz}^{\mathrm{Raz}}],\ \text{if}\ \ K_{\mathrm{DO}}^{Raz} = [<1,\ <1] \\ [\lambda_{\theta,\, sz}^{\mathrm{Raz}} K_{\mathrm{DO\ min}}^{Raz},\ \lambda_{\theta,\, sz}^{\mathrm{Raz}}\ K_{\mathrm{DO\ max}}^{Raz}],\ \text{if}\ \ K_{\mathrm{DO}}^{Raz} = [<1,\ >1]\,. \\ [\lambda_{\theta,\, sz}^{\mathrm{Raz}}\, ,\ \lambda_{\theta,\, sz}^{\mathrm{Raz}}\ K_{\mathrm{DO\ max}}^{Raz}],\ \text{if}\ \ K_{\mathrm{DO}}^{Raz} = [>1,\ >1] \end{cases} \tag{4}$$

6.2.5. Raz and DO Uptake Relationships in Stream Sediments

We conducted chamber experiments to calibrate the molar uptake ratio K_{DO}^{Raz} [mol O_2 / mol Raz]. For this, we incubated stream sediments collected at both reaches before each of the two experiments. Sediments were taken by hand from characteristic pools and riffles, and placed in recirculating chambers (*n* = 7) closed to the atmosphere (Table 6.3, Figure 6.1). Raz was injected instantaneously to generate a maximum concentration of about 300 ppb upon complete mixing. Oxygen consumption was measured inside the chambers with HACH HQ40D handheld meters, whereas aqueous Raz-Rru samples were collected, filtered, refrigerated at 4°C and then read within 24 h of sampling.

6.3. Results and discussion

6.3.1. Differences in Incoming PAR between Open and Shaded Reaches

We used the PAR records to quantitatively determine differences in the incoming radiation in the two reaches. Table 6.4 and Figure 6.2 show the ranges for the PAR information recorded. This information suggests that there is a 2.7:1 ratio between the average PAR in the open and shaded reaches (respectively), and a 4:1 ratio between the ranges of PAR available. Furthermore, a Fisher's least significant difference (LSD) test (STATGRAPHICS® Centurion XVI) suggests that there are statistically significant differences between the means and medians of the PAR recorded at both reaches.

6.3.2. Differences in Night and Day Time Stream Water Temperatures

We used the stream water temperature records as a proxy to determine the impacts of diel changes (within reaches) and forest coverage (across reaches) on stream metabolism. Table 6.4 and Figure 6.3 summarize the information recorded in both reaches. Results suggest that mean and median temperatures significantly change (Fisher's LSD) within consecutive (night and daytime) experiments and also across reaches.

6.3.3. Raz and DO Uptake Rates as a Function of Stream Bedforms

We investigated the variability of K_{DO}^{Raz} within and across our stream reaches with chamber experiments. We used the ratios $\Delta DO / \Delta Raz$ from each chamber experiment to analyze the variability of K_{DO}^{Raz} (Figure 6.4). $R^2 > 0.92$ in all regressions, suggesting a strong linear relationship between the transformation of Raz and respiration. Summarizing, $K_{DO}^{Raz} = [0.85, 1.40]$ for the experiments with sediments from the shaded reach and $K_{DO}^{Raz} = [0.68, 1.30]$ for the open reach. $K_{DO}^{Raz} = [0.68, 0.85]$ for the experiments with sediments from pools and $K_{DO}^{Raz} = [0.82, 1.40]$ for riffles. Finally, $K_{DO}^{Raz} = [0.68, 1.40]$ when all the experiments are considered.

From the chamber experiments we were able to define uncertainty bounds for the estimation of respiration rates, which allowed us to constrain our estimates of daytime and nighttime respiration rates. Because generally $K_{DO}^{Raz} = [<1, >1]$, the estimates of respiration rates using Raz as a proxy-tracer were bounded by the values of K_{DO}^{Raz} (cf. (4)).

A statistical analysis (Fisher's LSD) suggest that chambers 1, 4 and 6 form a homogeneous group of samples, with mean K_{DO}^{Raz} values that are not significantly different at the 95% confidence level. Chambers 4 and 6 were filled with sediments from riffles, whereas chamber 1 was filled with sediments from a pool. Chambers 2, 3, and 5 form another homogeneous group. Chambers 2 and 3 were filled with sediments from pools and chamber 5 with sediments from a riffle. Although our results suggest the presence of microbial communities with differences in the metabolism of Raz and DO, our sampling strategy was not sufficiently extensive to draw conclusions regarding spatial patterns in the arrangement of such communities (i.e., bedform type vs. light availability). Nonetheless, the differences observed in K_{DO}^{Raz} values did not affect our comparison between nighttime and daytime respiration patterns because it is unlikely that the microbial communities had changed within the timeframe of each of our experiments.

6.3.4. Differences in Respiration Rates

Current methods do not allow independent estimates of respiration rates (and fluxes) at night and day times because of the multiple and parallel pathways for oxygen production and consumption, i.e., respiration, primary production, stream-atmosphere mass transfer (reaeration) and stream-groundwater interactions [*McCutchan et al.*, 2002; *Bott*, 2007; *Reichert et al.*, 2009]. Raz might be a suitable proxy-tracer for estimating diel fluctuations of respiration because there is a nearly perfect linear relationship between oxygen consumption and Raz uptake (cf. section 6.3.3. and *González-Pinzón et al.* [2012]). Furthermore, Raz is not naturally present (or produced) in groundwater systems or in the atmosphere. However, the rate of transformation of Raz and oxygen consumption has to be found via calibration, i.e., K_{DO}^{Raz} has to be estimated.

Figure 6.5a shows the estimated respiration rates ($\lambda_{resp.}$) for the nighttime and daytime (d) consecutive experiments in the shaded reach. This figure shows the estimated rates considering the minimum and maximum K_{DO}^{Raz} values found in the chambers with sediments from the shaded reach. Figure 6.5b shows the estimated $\lambda_{resp.}$ for the consecutive experiments conducted in the open reach.

A Fisher's LSD statistical test of the results presented in Figure 6.5 indicates that the mean rates estimated at nighttime and daytime conditions in each of the open and shaded reaches are not different at the 95% confidence level. Similar results were found when the minimum and maximum K_{DO}^{Raz} values found in all chamber experiments were used to estimate $\lambda_{resp.}$. Also, respiration rates in the shaded and open reaches were in the same order of magnitude. Despite PAR and stream water temperature (above the benthic zone) are significantly different between night and daytime experiments (Table 6.4 and Figures 6.2 – 6.3), such differences did not significantly affect respiration rates (Figure 6.5). Most likely, the bulk of stream respiration took place in the hyporheic zone, where diel fluctuations of stream temperature and PAR are considerably attenuated [e.g., *Constantz*, 2008], and where temperature is not measured in routine investigations of stream metabolism. Therefore, “correcting” respiration rates (and fluxes) to compensate for the observed fluctuations in stream water temperature might be misleading and may lead to incorrect estimates of metabolism in headwater streams.

Acknowledgements

This work was funded by NSF grant EAR 08-38338 and by the Spanish Ministry of Science and Innovation through the ISONEF (ref: CGL2008-05504-C02-02/BOS) project. We thank Stephanie Merbt, Clara Romero González-Quijano, Sandra Serra, Miquel Ribot, Toraf Keller, and Eduardo Martín Sanz for lab and field assistance.

Table 6.1. Sampling locations and type of subreach bedforms.

	Shaded, Discharge = 7 Ls^{-1}			Open, Discharge = 13 Ls^{-1}		
Site	**Distance (m)**	**% Riffles – % pools**	**Width (m) – depth (cm)**	**Distance (m)**	**% Riffles – % pools**	**Width (m) – depth (cm)**
Inj.	0.0			0		
		54 – 46	2.1 – 10		77 – 23	2.7 – 7
S1	42			41		
		80 – 20	3.9 – 8		67 – 33	2.7 – 6
S2	68			61		
		38 – 62	2.3 – 6		67 – 33	2.7 – 4
S3	95			75		
		100 – 0	2.9 – 6		93 – 7	2.7 – 5
S4	123			139		
		12 – 88	3.2 – 7		64 – 36	3.6 – 7
S5	156			214		
		62 – 38	3.2 – 9		35 – 65	3.6 – 15
S6	216			293		
		67 – 33	3.6 – 12		82 – 18	2.7 – 7
S7	264			359		
Average		59 – 41	3.0 – 8.7		68 – 32	3.1 – 8.2

Table 6.2. Stream metabolism sampling scheme.

	Shaded			Open		
	Raz-Rru	**PAR/temp (# sites sampled)**	**DO station**	**Raz-Rru**	**PAR/temp (# sites sampled)**	**DO station**
S1	M-L	2 (1R, 1P)	Yes	-	2 (1R, 1P)	Yes
S2	M-L	2 (1R, 1P)	-	M-L	2 (1R, 1P)	-
S3	M-L	1R	-	M-L	3R	-
S4	M-L, F-O	1P	-	M-L	3P	Yes
S5	F-O	1R	Yes	M-L, F-O	1R (failed)	-
S6	F-O	1P	-	F-O	1R	Yes
S7	-	-	-	F-O	-	-
S8	-	1P	Yes	-	-	-

M-L: manual sampling and lab reading; F-O: field sampling, on-line reading; P: pool; R: riffle.

Table 6.3. Chamber experiments with sediments from different bedforms in open and shaded subreaches.

Chamber ID	Reach	Bedform	% Sediment > 8 mm	% Organic Matter
1	Shaded	Pool	29.8	0.6
2	Shaded	Riffle	38.3	0.5
3	Shaded	Riffle	62.0	0.6
4	Open	Pool	7.2	0.5
5	Open	Riffle	67.9	0.5
6	Open	Riffle	60.5	0.7
7	Shaded	Riffle	64.1	0.6

Table 6.4. PAR and stream water temperature values recorded during each of the experiments in both reaches.

	Reach / experiment	Mean	Standard deviation	Coeff. of variation	Range	Significant difference†	
PAR [µmol m^{-2} s^{-1}]	Shaded / day‡	119.3	91.1	76.3%	681	Yes	
	Open / day‡	323.4	403.9	124.9%	2752		
Stream water temperature [°C]	Shaded / night•	14.1	0.4	2.5%	1.8	Yes	Yes
	Shaded / day‡	15.9	0.8	5.3%	2.8		
	Open / night•	14.9	0.8	5.7%	4.3	Yes	
	Open / day‡	18.0	1.4	7.7%	6.8		

† Fisher's least significant difference (LSD) estimator was used to determine statistically significant differences in the means at the 95.0% confidence level. Mood's median test was used for the medians.

‡ Daytime information recorded is from 11 a.m. (injection) to 7 p.m., i.e., 8 h total.

• Nighttime information recorded is from 9 p.m. (injection) to 5 a.m., i.e., 8 h total.

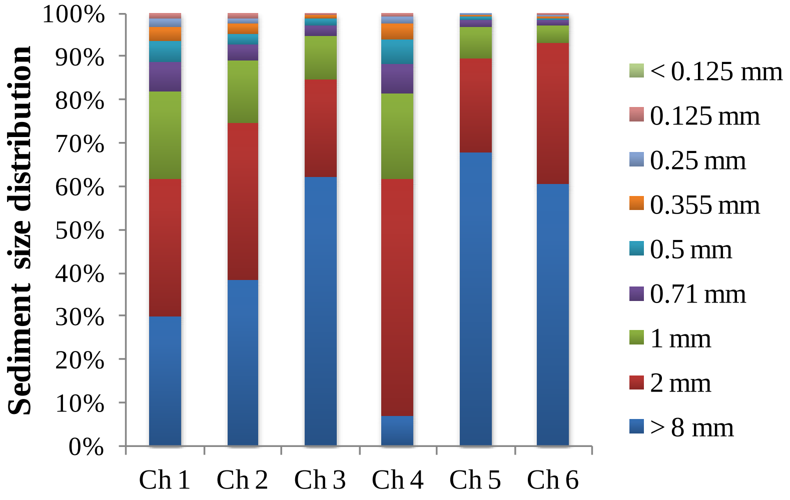

Figure 6.1. Size distribution of the sediments used in the closed chamber experiments. Colors in the bars represent different sieve diameters and percentages reflect the fraction of mass retained by the sieves.

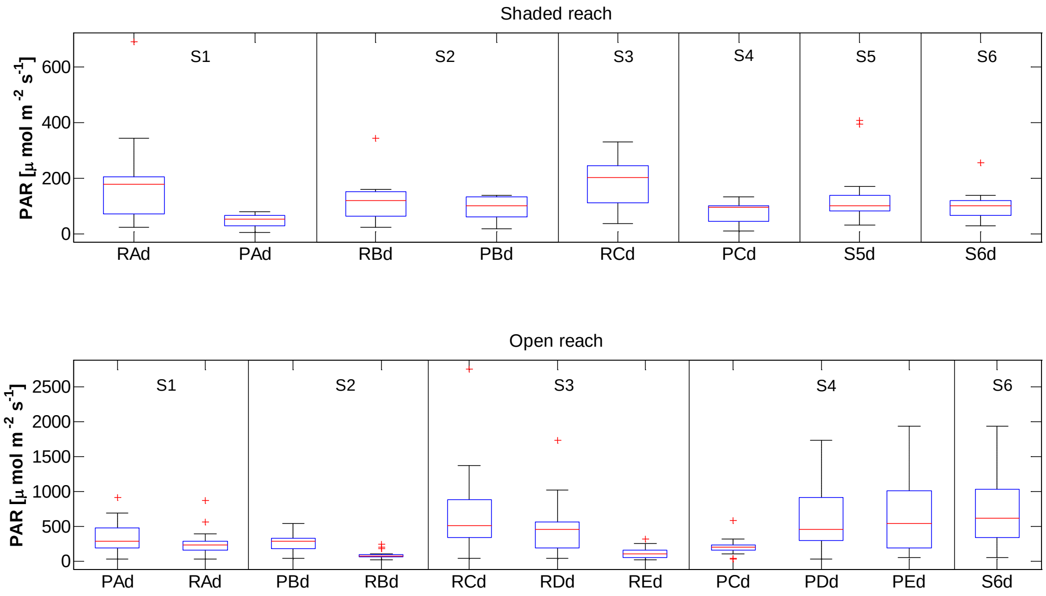

Figure 6.2. Photosynthetically active radiation (PAR) recorded at representative sites during daytime injections. Top panel shows values recorded in the shaded reach; bottom panel in the open reach. Labels in boxes (e.g., S1) indicate the nearest sampling station. Mean and median PAR values in both reaches are significantly different at the 95.0% confidence level (Fisher's LSD and Mood's median test). P: pool; R: riffle; d: day.

a) Shaded reach

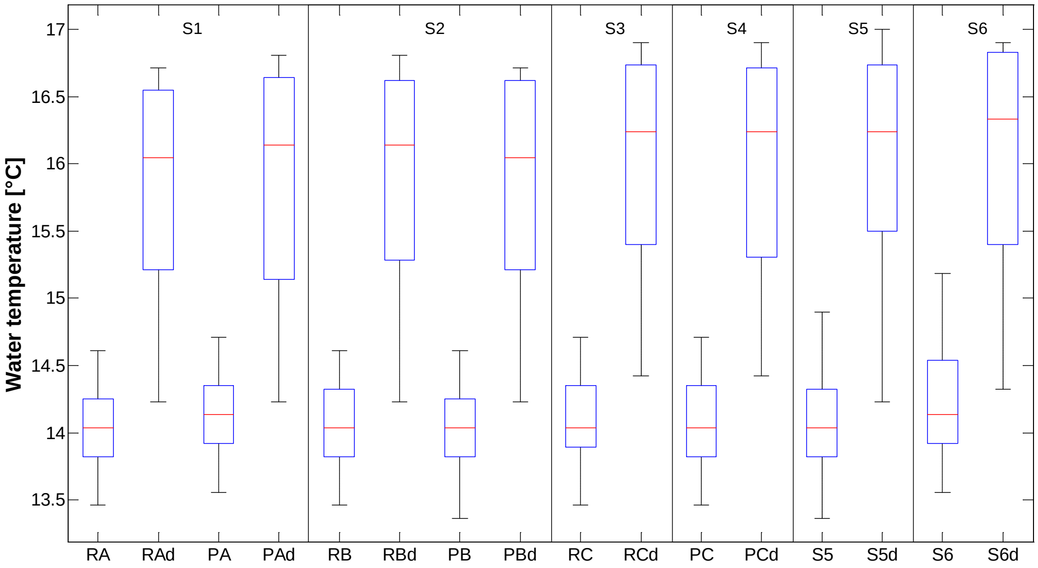

b) Open reach

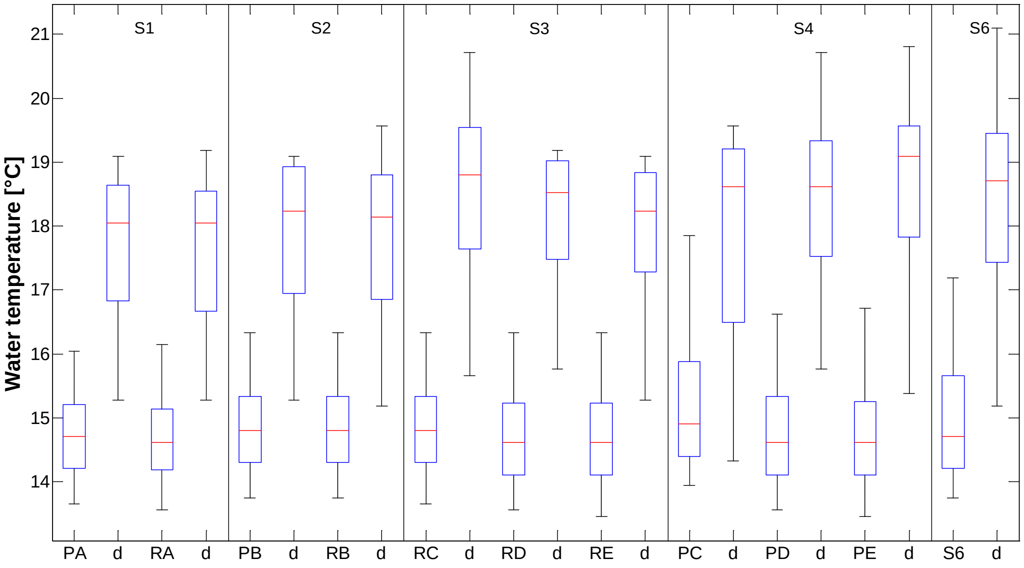

Figure 6.3. Stream water temperature recorded at representative sites during night and daytime (d) consecutive injections. Recording time spans from the beginning of the injection up to 8 h later. Day and night mean and median temperatures are significantly different at the 95.0% confidence level (Fisher's LSD and Mood's median test). P: pool; R: riffle; d: day.

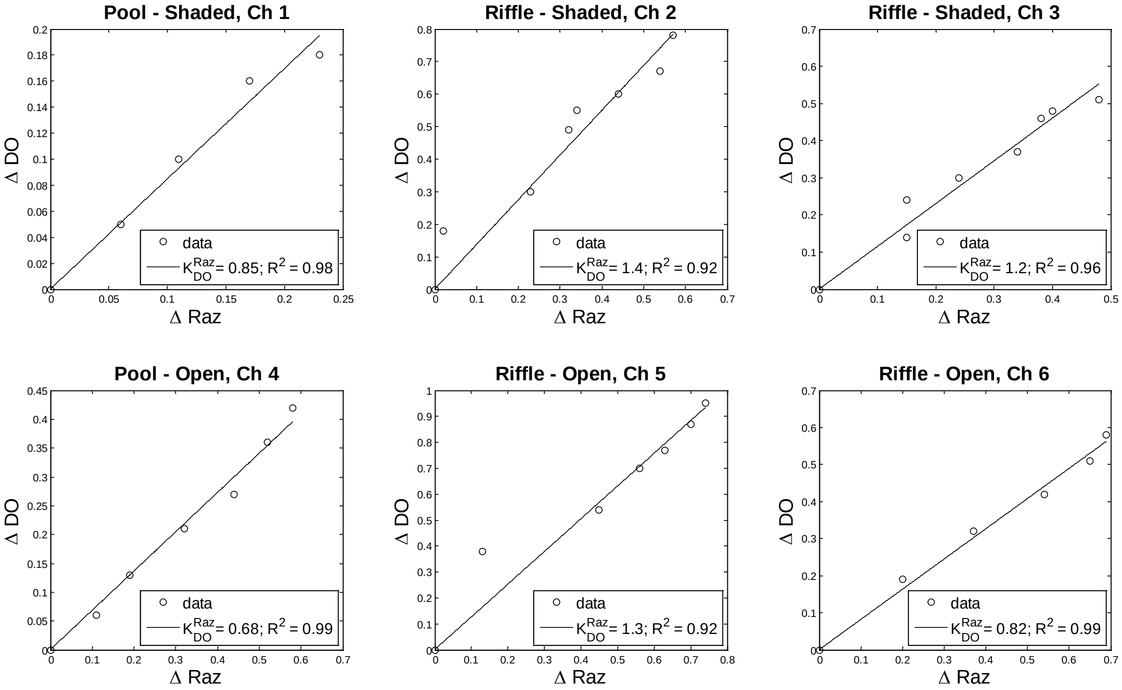

Figure 6.4. Molar uptake ratio of DO consumed to Raz consumed, K_{DO}^{Raz}. Sediment samples were taken in pools and riffles. Top panel shows results with sediments from the shaded reach; bottom panel from the open reach.

a) Shaded reach

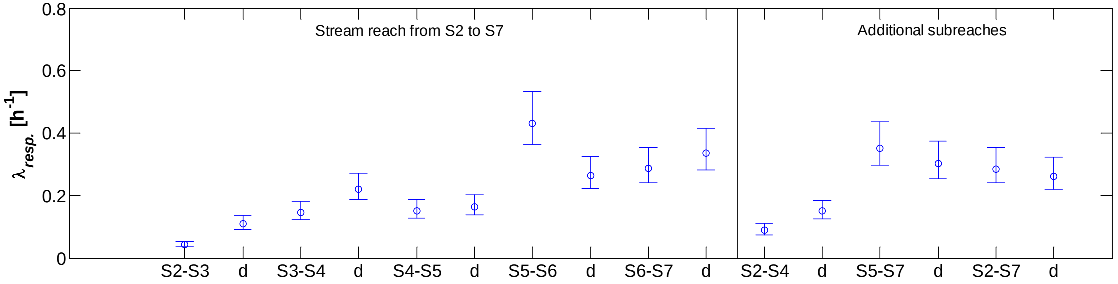

b) Open reach

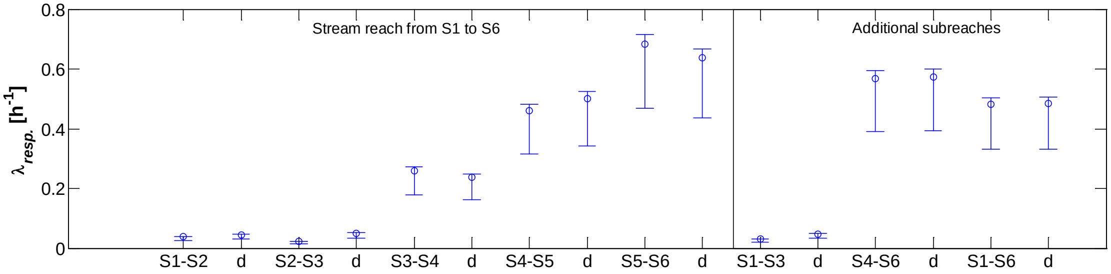

Figure 6.5. Respiration rates estimated from the Raz-Rru system. Upper and bottom whiskers represent the uncertainty in $\lambda_{resp.}$ considering only K_{DO}^{Raz} from experiments in each of the respective reaches. Circles represent $\lambda_{\theta,\,sz}^{Raz}$.

References

Apple, J. K., P. A. del Giorgio, and W. M. Kemp (2006), Temperature regulation of bacterial production, respiration, and growth efficiency in a temperate salt-marsh estuary, *Aquat. Microb. Ecol.*, 43(3), 243–254.

Bernal, S. (2006), Nitrogen storm responses in an intermittent Mediterranean stream, Ph.D. dissertation, Universitat de Barcelona.

Bott, T. L. (2007), *Primary productivity and community respiration*, in: Methods in stream ecology, pp. 663–390, Academic Press.

Chapra, S. C. (2008), *Surface Water-Quality Modeling*, Waveland Press Inc.

Constantz, J. (2008), Heat as a tracer to determine streambed water exchanges, *Water Resour. Res.*, 44, W00D10, doi:10.1029/2008WR006996.

Demars, B. O. L., J. R. Manson, J. S. Olafsson, G. M. Gislason, R. Gudmundsdottir, G. Woodward, J. Reiss, D. E. Pichler, J. J. Rasmussen, and N. Friberg (2011), Temperature and the metabolic balance of streams, *Freshw. Biol.*, 56(6), 1106–1121.

Genereux, D. P., and H. F. Hemond (1992), Determination of gas exchange rate constants for a small stream on Walker Branch Watershed, Tennessee, *Water Resour. Res.*, 28(9), 2365–2374, doi:10.1029/92WR01083.

Gillooly, J. F., J. H. Brown, G. B. West, V. M. Savage, and E. L. Charnov (2001), Effects of Size and Temperature on Metabolic Rate, *Science*, 293(5538), 2248–2251, doi:10.1126/science.1061967.

González-Pinzón, R., R. Haggerty, A. Argerich (2013), Quantifying spatial differences in metabolism in headwater streams, submitted to *Freshw. Sci.*

González-Pinzón, R., and R. Haggerty (2013), An efficient method to estimate processing rates in streams, submitted to *Water Resour. Res.*

González-Pinzón, R., R. Haggerty, and D. D. Myrold (2012), Measuring aerobic respiration in stream ecosystems using the resazurin-resorufin system, *J. Geophys. Res. Biogeosciences*, 117(G3), doi:10.1029/2012JG001965.

Haggerty, R., A. Argerich, and E. Marti (2008), Development of a "'smart'" tracer for the assessment of microbiological activity and sediment-water interaction in natural waters: The resazurin-resorufin system, *Water Resour. Res.*, 44.

Holtgrieve, G. W., D. E. Schindler, T. A. Branch, and Z. T. A'mar (2010), Simultaneous quantification of aquatic ecosystem metabolism and reaeration using a Bayesian statistical model of oxygen dynamics, *Limnol. Ocean.*, 55(3), 1047–1062, doi:10.4319/lo.2010.55.3.1047.

Huey, R. B., and J. G. Kingsolver (2011), Variation in universal temperature dependence of biological rates, *Proc. Natl. Acad. Sci.*, 108(26), 10377–10378, doi:10.1073/pnas.1107430108.

Lemke, D., P.-A. Schnegg, M. Schwientek, K. Osenbrück, and O. A. Cirpka (2013), On-line fluorometry of multiple reactive and conservative tracers in streams, *Environ. Earth Sci.*, doi:10.1007/s12665-013-2305-3.

McCutchan, J. H., J. F. Saunders, W. M. Lewis, and M. G. Hayden (2002), Effects of groundwater flux on open-channel estimates of stream metabolism, *Limnol. Ocean.*, 47(1), 321–324.

Metzger, I., and W. E. Dobbins (1967), Role of fluid properties in gas transfer, *Environ. Sci. Technol.*, 1(1), 57–65.

Reichert, P., U. Uehlinger, and V. Acuña (2009), Estimating stream metabolism from oxygen concentrations: Effect of spatial heterogeneity, *J. Geophys. Res.*, 114(G3), doi:10.1029/2008JG000917.

Riley, A. J., and W. K. Dodds (2012), Whole-stream metabolism: strategies for measuring and modeling diel trends of dissolved oxygen, *Freshw. Sci.*, 32(1), 56–69, doi:10.1899/12-058.1.

Thornton, K. W., and A. S. Lessem (1978), A Temperature Algorithm for Modifying Biological Rates, *Trans. Am. Fish. Soc.*, 107(2), 284–287.

Tobias, C. R., J. K. Böhlke, and J. W. Harvey (2007), The oxygen-18 isotope approach for measuring aquatic metabolism in high productivity waters, *Limnol. Ocean.*, 52(4), 1439–1453, doi:10.4319/lo.2007.52.4.1439.

7. GENERAL CONCLUSIONS

7.1. Solute Transport and Stream Processing

Scaling and predicting solute transport and processing can be highly uncertain. This is primarily due to the difficulties of measuring and incorporating stream hydrodynamic and geomorphic characteristics into models. Consequently, parameters cannot be obtained uniquely from physical attributes. The parameters are functions of a combination of several processes and physical attributes. Therefore, model parameters interact with each other, and the overall model response to different parameter sets might be numerically ‘equal’ and mechanistically misleading.

Because solute transport is the foundation of biogeochemical models, if transport models with unidentifiable parameters are used to investigate the coupling between transient storage and biochemical reactions across ecosystems, it is not unexpected that the relationships derived are inconclusive, as it has been extensively shown to date. Ultimately, model structural errors generate equifinal systems that can lead to biased conclusions with respect to the nature of mechanistic relationships.

The coefficient of skewness (CSK) of conservative tracer breakthrough curves is scale-invariant and equal to approximately 1.18. This result can be used to adequately predict solute transport. However, solute transport models currently used in hydrology have systematic limitations to represent the observed scaling patterns, suggesting that we need a revised solute transport theory.

A mathematical analysis of the transient storage model shows that algebraic equations can be used to estimate processing rates in streams. These equations can be easily implemented by researchers and practitioners in routine investigations of (bio)reactivity in stream ecosystems. The method only requires estimates or measurements of the zeroth temporal moments of the upstream and downstream BTCs of a reactive solute (or plateau concentrations), the mean travel time in the stream reach (which is estimated with first temporal moments of a conservative solute) and an estimate of the Peclet number. However, the Peclet number is not needed (dispersion can be assumed effectively negligible) under some common transport conditions and, therefore, no computer modeling would be needed to estimate processing rates. This method is efficient because it does not require the calibration of other intermediate transport parameters, thus reducing the uncertainty in the estimated processing rates.

7.2. Estimating Stream Metabolism with the Raz-Rru System

The transformation of Raz to Rru is nearly perfectly, positively correlated with aerobic microbial respiration. Therefore, the Raz-Rru system is an alternative approach to estimate aerobic respiration in stream ecosystems. This approach overcomes important limitations of current methods in stream ecology, particularly, the sampling disturbance of *in situ* biological and hydrodynamic conditions. The use of Raz as a bio-reactive tracer to estimate metabolic activity enables us to integrate our knowledge of solute transport and stream metabolism, thus advancing our understanding of stream ecosystem functioning.

The Raz-Rru system has several advantages: 1) Raz is not naturally present in streams, the atmosphere or groundwater; 2) Raz is a compound that allows *in vivo* and *in situ* assays without altering microbial communities and hydrodynamic conditions; 3) Raz can be used at very low concentrations (~200 ppb at plateau concentrations), thus being a cost-effective technique.

Algebraic equations can be used to estimate processing rates from one solute (proxy-tracer such as Raz, $\lambda_{\theta,\, sz}^{\mathrm{proxy}}$) to another (target solute such as dissolved oxygen, $\lambda_{\theta,\, sz}^{\mathrm{target}}$). The relationship between the two rates is a function of the molar processing ratio of the target to the proxy-tracer (K_{target}^{proxy}) and the Dahmköhler number (Da). We analyzed the coupling between solute transport and in-stream processing within the three characteristic transport conditions defined by Da and showed that the uncertainty in the estimation of $\lambda_{\theta,\, sz}^{\mathrm{target}}$ is linearly proportional to the uncertainty in the estimation of K_{target}^{proxy}. Furthermore, the uncertainty in the transport parameters is less significant than the uncertainty in

K_{target}^{proxy}. These results show that the Raz-Rru system can be directly used to estimate respiration in streams and that uncertainty of the estimates can be explicitly accounted for.

We proposed the use of the Raz-Rru system as an alternative technique to quantify metabolism in headwater streams and presented a simple modeling framework to estimate rates and fluxes of community respiration, primary production, and reaeration. Results from our field experiments in three headwater streams in OR (USA) and Spain demonstrated that the Raz-Rru system was capable of detecting spatial variations of in-stream metabolic activity. We found self-consistent relationships between Raz reactivity and (otherwise) difficult-to-quantify geomorphic and hydrodynamic conditions defining metabolic hot spots. Moreover, we found that despite PAR and stream water temperature (measured above the benthic zone) are significantly different between night and daytime experiments, such differences might not significantly affect respiration rates. Most likely, the bulk of stream respiration takes place in the hyporheic zone, where diel fluctuations of stream temperature and PAR are considerably attenuated and where temperature is not measured in routine investigations of stream metabolism. Therefore, “correcting” respiration rates (and fluxes) to compensate for the observed fluctuations in stream water temperature might be misleading and may lead to incorrect estimates of metabolism in headwater streams.